

The endothelium in COVID-19 complications and in the regulation of vascular tone

by

Alexia C. Maheux

A thesis submitted in partial fulfillment of the requirements for the degree of

Master of Science

Department of Pharmacology
University of Alberta

© Alexia C. Maheux, 2022

Abstract

Background: This thesis encompasses two distinct projects. **1)** von Willebrand factor (VWF) is a highly adhesive multimeric glycoprotein found in the Weibel-Palade bodies of endothelial cells and in α -granules of megakaryocytes and platelets. At the site of vascular injury, VWF is essential for recruitment and activation of platelets and is the key mediator of blood clot formation. SARS-CoV-2 is a respiratory virus that infects host cells by binding to angiotensin converting enzyme 2 (ACE2) on host cell surfaces. In addition to respiratory complications, inflammation and an increase in thrombotic markers (such as VWF) are also markers of severe SARS-CoV-2 infection. Since VWF is released from endothelial cells and these cells also express ACE2, I **hypothesized that engagement of ACE2 by the SARS-CoV-2 spike protein on endothelial cells induces upregulation and release of VWF.** **2)** Resistance arteries can actively regulate their diameter through endothelial and smooth muscle mechanisms that rely on signalling molecules such as calcium (Ca^{2+}) or inositol triphosphate (IP_3). Connexins (Cx) make up the gap junctions between adjacent endothelial and smooth muscle cells that allow for the spread of electrical and chemical signalling along the vessel wall via rapid transfer of ions and small molecules. Changes in gap junction function are associated with cardiovascular diseases such as hypertension but the relative importance of various Cx to vascular control is unclear. I examined vascular responses of mesenteric arteries from rats lacking Cx40 globally to test the **hypothesis that arteries from Cx40 deficient rats will show impaired responses to the endothelium-dependent vasodilator acetylcholine (ACh).**

Results: In cultured human umbilical vein endothelial cells (HUVECs), exposure to SARS-CoV-2 spike protein did not significantly change VWF mRNA expression levels but caused a significant increase in released VWF after five minutes. VWF release in cells that were treated again 72 hours

after their first treatment with spike protein was also significantly increased compared to the control and initial treatment groups. Immunofluorescence imaging confirmed the presence of ACE2 on the surface and in the cytoplasm of endothelial cells; additionally, VWF and ACE2 expression in HUVECs was detectable using western blot analysis. I used a combination of inhibitors of endothelium-dependent vasodilator pathways to investigate the impact of loss of Cx40 on responses of mesenteric resistance arteries to the endothelium-dependent vasorelaxant ACh and to the α_1 -adrenoceptor agonist phenylephrine. The effects of the inhibitors on the responses to ACh were significantly different in arteries from female rats of all genotypes and male wild type (WT) and knockout (KO) rats but not male heterozygous (HET) rats. However, in arteries from female rats, addition of the inhibitors together revealed a difference between the genotypes. A difference in the genotypes was also seen in the male control group. Phenylephrine-induced tone was enhanced in arteries from both male and female KO rats relative to responses of arteries from WT rats.

Conclusions: Exposure of endothelial cells to SARS-CoV-2 spike protein alone increases VWF release. I confirmed that HUVECs express ACE2, so it is possible that this effect is due to a spike protein-ACE2 interaction. However, more work is needed to confirm that the observed increase is due to this interaction and to elucidate the mechanism through which engagement of ACE2 leads to increased VWF release. Loss of Cx40 impacted responses to the endothelium-dependent relaxant ACh in male but not female rats but there was no obvious effect on the relative contributions of NO and EDH to ACh-evoked vasorelaxation. However, the enhancement of phenylephrine-induced tone in arteries from Cx40 KO rats of both sexes indicates that Cx40 may play a role in smooth muscle to endothelial communication in mesenteric vessels. Further work is required to explore the impact of loss of Cx40 on vascular function.

Preface

All animal care and experimental use was approved by the University of Alberta Animal Care and Use Committee for Health Sciences (AUP 312) in accordance with Canadian Council on Animal Care guidelines as described by Grundy (2015).

Acknowledgements

Firstly, I would like to thank my supervisor, Dr. Frances Plane, for her mentorship, support, and guidance throughout my four years in her lab both in my undergraduate and graduate studies. I would not be here today without all of the friendships and experiences that I gained in my time there.

I would also like to thank my co-supervisor, Dr. Nadia Jahroudi, for all her advice and support throughout this project.

I would like to thank Dr. Paul Jurasz for being on my committee and contributing his feedback and expertise to the completion of my work.

I would like to thank my examiner, Dr. Zamaneh Kassiri, for contributing her time and expertise to my thesis defence.

I would like to extend the utmost thanks to Parnian Alavi for her great help and patience as I learned new techniques in the lab. I would not have been able to do the work that I did without her.

I would like to thank my friend and former lab mate, Erika Poitras, for her endless support and encouragement throughout my studies as we both navigated grad school in the midst of a pandemic.

I would like to thank my fellow grad student, Stephen Gust, for all his help, companionship, and conversations in the lab – the days were never boring.

I would like to thank Brandon Truong, Samar Barazesh, Sufyan Malik and Caleb McInroy for their contributions to my work.

Finally, I would like to thank my friends and family for their support and encouragement. I could not have completed this degree without you.

Table of Contents

Chapter 1: Introduction	1
The role of VWF in health and disease	1
1.1 Structure of the vascular system	1
1.2 Endothelial cells and thrombosis.....	2
1.3 VWF Structure, Function, and Regulation	4
1.4 Severe acute respiratory coronavirus 2 (SARS-CoV-2).....	8
1.4.1 Origins and host entry	8
1.4.2 Spike protein structure	9
1.4.3 Angiotensin converting enzyme 2 (ACE2)	11
1.4.4 ACE2 expression and SARS-CoV-2 infection.....	13
1.5 SARS-CoV-2 and thrombosis	14
1.5.1 SARS-CoV-2 and VWF levels.....	15
1.6 Hypothesis and Research Aims	17
The role of connexins in the regulation of vascular tone.....	19
1.7 Blood pressure.....	19
1.8 Regulation of arterial diameter	19
1.8.1 Mechanisms of vasoconstriction	20
1.8.2 Endothelium-dependent vasodilation	24
1.9 Connexins and the regulation of vascular tone.....	27
1.10 Hypothesis and Research Aims	33
Chapter 2: Materials and Methods	34
2.1 Ethics Approval	34

2.2 Animal Care and Use	34
2.3 Cx40 Colony	34
2.4 Genotyping	34
2.5 Culture of HUVECs.....	36
2.6 Measurement of VWF RNA expression by real-time reverse-transcription quantitative PCR (RT-qPCR)	36
2.7 Enzyme-linked immunoassay (ELISA) for VWF	37
2.8 Immunofluorescence detection of ACE2 in HUVECs	38
2.9 Western blot analysis of ACE2 and VWF expression	39
2.10 Wire myography	40
2.11 Reagents.....	42
2.12 Statistical Analysis.....	42
Chapter 3: Results.....	44
3.1 The effects of SARS-CoV-2 spike protein on VWF release and mRNA expression in HUVECs	44
3.2 ACE2 expression in HUVECs.....	48
3.3 The impact of Cx40 genotype on responses of isolated rat mesenteric arteries.....	52
Chapter 4: Discussion	64
4.1 The effects of SARS-CoV-2 spike protein exposure on cultured HUVECs.....	64
4.2 The impact of Cx40 genotype on isolated rat mesenteric arteries.....	68
4.3 Limitations	72
4.4 Future directions.....	76
4.4.1 Further investigating the effects of SARS-CoV-2 spike protein exposure on endothelial cells.....	76
4.4.2 Further investigating the impact of Cx40 KO in the vasculature	77

4.5 Conclusions.....	78
References.....	80

List of Tables

Chapter 2: Materials and Methods

Table 2.1 Primers for PCR and genotyping.....	36
Table 2.2 Primers for RT-qPCR	37
Table 2.3 Antibodies and Stain for Immunofluorescence Imaging	39
Table 2.4 Antibodies for Western Blot Analysis	40
Table 2.5 Reagents Table.....	42

Chapter 3: Results

Table 3.1 logEC ₅₀ (M) of ACh concentration response curves in male and female rats	57
Table 3.2 Maximal relaxation induced by ACh in the presence and absence of inhibitors.....	57

List of Figures

Chapter 1: The role of VWF in health and disease

Figure 1.1 The structure of blood vessel walls	2
Figure 1.2 VWF Structure and domains	5
Figure 1.3 The physiological activities of VWF.....	7
Figure 1.4 SARS-CoV-2 spike protein structure	11
Figure 1.5 The Renin-Angiotensin-Aldosterone System.....	12
Figure 1.6 Mechanism of smooth muscle contraction.....	22
Figure 1.7 Regulation of vascular tone.....	23
Figure 1.8 A schematic representing the structure of endothelial nitric oxide synthase (eNOS).	25
Figure 1.9 Connexin assembly into gap junctions.....	29
Figure 1.10 Schematic demonstrating connexin distribution in resistance artery vascular tissue	31

Chapter 2: Materials and Methods

Figure 2.1 A third-order mesenteric artery mounted in a Mulvany-Halpern wire myograph	42
---	----

Chapter 3: Results

Figure 3.1 The effects of 1nM SARS-CoV-2 spike protein on VWF mRNA in HUVECs	46
Figure 3.2 The effects of 1nM SARS-CoV-2 spike protein on VWF release in HUVECs.....	47
Figure 3.3 Immunofluorescence imaging of ACE2 expression on permeabilized HUVECs.....	49
Figure 3.4 Immunofluorescence imaging of ACE2 expression on non-permeabilized HUVECs	50
Figure 3.5 Representative western blot analysis of ACE2 and VWF protein expression in HUVECs	51
Figure 3.6 Rehybridized western blot showing ACE2 expression in HUVECs but not HEK293 cells	51
Figure 3.7 Representative traces of control ACh concentration response curves in male and female Cx40 WT, HET, and KO rat mesenteric arteries	58
Figure 3.8 The effects of the inhibitors TRAM-34, apamin, and L-NAME on ACh concentration response curves in female WT, HET, and KO rat mesenteric arteries	59
Figure 3.9 The effects of the inhibitors TRAM-34, apamin, and L-NAME on ACh concentration response curves in male WT, HET, and KO rat mesenteric arteries	60
Figure 3.10 The influence of Cx40 genotype in ACh concentration response curves in female WT, HET, and KO rat mesenteric arteries	61
Figure 3.11 The influence of Cx40 genotype in ACh concentration response curves in male WT, HET, and KO rat mesenteric arteries	62
Figure 3.12 Contractile force of isolated rat mesenteric arteries in response to PE	63

Chapter 1: Introduction

This thesis is comprised of two distinct projects. The first investigates the effects the SARS-CoV-2 spike protein on VWF release and upregulation in cultured endothelial cells while the second investigates the role of Cx40 in endothelium-dependent relaxation using isolated mesenteric arteries from Cx40 KO rats.

The role of VWF in health and disease

1.1 Structure of the vascular system

The purpose of blood vessels is to transport nutrients and oxygen to tissues and to remove waste. All blood vessels share a similar structure whereby they are composed of three layers: the *tunica intima*, the *tunica media*, and the *tunica adventitia* also known as the *tunica externa* (**Figure 1.1**).¹ The *tunica intima* is primarily composed of the endothelial cells that line the lumen of the blood vessel. The middle layer, the *tunica media*, is composed of smooth muscle cells and the *tunica adventitia* is composed of connective tissue and collagen.¹ This outer layer is also the site of autonomic innervation. Arteries and veins share the same structure; however, the *tunica media* of veins is thinner and contains less smooth muscle cells. Capillaries are single cell layer blood vessels, composed of only the *tunica intima* layer as well as external support cells called pericytes. This topic is reviewed by Pugsley and Tabrizchi (2000).¹

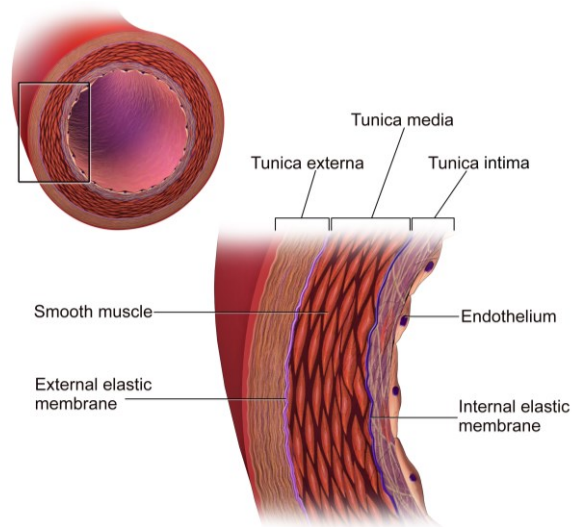


Figure 1.1 The structure of blood vessels. Image reproduced from Blausen.com staff (2014).²

1.2 Endothelial cells and thrombosis

Endothelial cells play many important roles in the cardiovascular system. Most importantly they play a role in blood pressure control as well as in the regulation of platelet activation and coagulation.³ The intact endothelium expresses and releases molecules that prevent inappropriate coagulation and thrombosis. Surface expression of negatively charged heparan sulfate proteoglycans and ecto-nucleotidases (such as CD39) that convert adenosine diphosphate (ADP; a platelet agonist) to adenosine, prevent platelet adhesion and activation.^{4,5} The release of prostacyclin I₂ (PGI₂) and prostaglandin E₂ as well as nitric oxide (NO) from endothelial cells contributes to their protective role by also preventing platelet adhesion.⁶⁻⁸ The endothelium also plays a role in inhibiting the formation of thrombin, which normally promotes fibrin formation from fibrinogen and stabilizes clots.⁹ Endothelial surface heparan sulfates in the glycocalyx, which consists of luminal membrane proteoglycans and glycoproteins, bind antithrombin, a potent thrombin inhibitor.¹⁰ Endothelial cells also express receptors that can bind thrombin to promote anticoagulant properties. These receptors, such as thrombomodulin and endothelial cell protein C

receptor can contribute to the thrombin-catalyzed formation of activated protein C (APC).^{11,12} APC is a serine protease with anticoagulant activities that causes irreversible inactivation of factor Va and VIIIa, both implicated in coagulation. A loss of thrombomodulin has been linked to increased thrombosis and coagulation.¹³ Finally, endothelial cells also express tissue factor pathway inhibitor which prevents the initiation of the extrinsic coagulation pathway by inhibiting the formation of the factor VIIa/tissue factor complex.¹⁴

Conversely, endothelial cells play an important role in the preservation of blood volume in the face of vascular injury. After stimulation with thrombin, histamine, or bradykinin, endothelial cells release endothelin-1 which causes rapid local vasoconstriction to prevent blood loss.¹⁵ In response to injury, endothelial cells also release hemostatic proteins such as von Willebrand factor (VWF) that binds to factor VIII, platelets, and extracellular matrix proteins and is essential to clot formation.¹⁶

This balance in the regulation of thrombosis and hemostasis by endothelial cells can be disrupted by a shift in endothelial cell phenotype from healthy to proadhesive, proinflammatory, and prothrombotic, which contributes to endothelial dysfunction (ED).¹⁷ This can be linked to risk factors such as hyperlipidemia, diabetes, smoking, and hypoxia to name a few, and results in increased thrombosis and decreased thrombus resolution. Endothelial stimulation with inflammatory cytokines such as tumor necrosis factor (TNF)- α and interleukin (IL)-1 can lead to an increase in tissue factor and VWF release accompanied with a decrease in NO and PGI₂ production.³ Hypoxia can also induce VWF upregulation and release leading to increased platelet binding.¹⁸ Endothelial cells may additionally be activated to increase the surface expression of adhesion receptors leading to the increased recruitment of immune and inflammatory cells.³ The

consequences of ED highlight the importance of appropriate regulation of thrombotic mediators such as platelets, thrombin, and VWF.

1.3 VWF Structure, Function, and Regulation

VWF is a multimeric glycoprotein that is exclusively made in endothelial cells and megakaryocytes (platelet precursors).¹⁶ Additionally, it is found circulating in the plasma as well as deposited in the sub-endothelial matrix, and plays an important role in hemostasis and thrombosis.¹⁹⁻²¹ The gene for VWF is located on chromosome 12, is 180kb in length, and contains 52 exons.^{22,23} VWF is synthesized as a pre-propolypeptide of 2813 amino acids (22 in signal peptide, 741 in propeptide, 2050 in mature protein) with repeating domain structures.^{16,19,24} The sequence of these domain structures is D1-D2-D'-D3-A1-A2-A3-D4-C1-C2-C3-C4-C5-C6-CK (see **Figure 1.2**). VWF contains many cysteine residues (8.3% of the protein).¹⁶ These allow for the formation of many disulfide bonds that are important for protein folding and secretion as well as the formation of VWF dimers and multimers.^{25,26} Dimerization occurs due to disulfide bonds at the C-terminal domains, while multimerization is due to disulfide bonds at the D1, D2, and D3 domains.^{27,28} VWF undergoes many post-translational modifications including dimerization, multimerization, cleavage of the propeptide (D1, D2 domains), and glycosylation.¹⁹ N- and O-linked glycans can undergo further modification such as sialylation, sulfation, and the addition of ABO(H) blood group determinants.^{29,30}

The domains of VWF contain many binding sites that play an important role in its hemostatic activities. The A1 domain is primarily responsible for binding to glycoprotein (Gp) Iba receptors on the platelet surface as well as binding to extracellular membrane protein collagen type I, III, and VI.³¹⁻³³ The A2 domain is the site of cleavage for ADAMTS13, a metalloprotease responsible for the cleavage of VWF multimers.³⁴ The A3 domain is the main binding site of

collagen to VWF.^{35,36} C1 is the binding site for GpIIb/IIIa receptors on activated platelets. The D'D3 domain is the binding site for factor VIII (FVIII), a protein involved in the intrinsic clotting pathway that is carried and stabilized in circulation by VWF.³⁷ The C-terminal cysteine knot (CK) is responsible for the dimerization of VWF monomers.²⁸

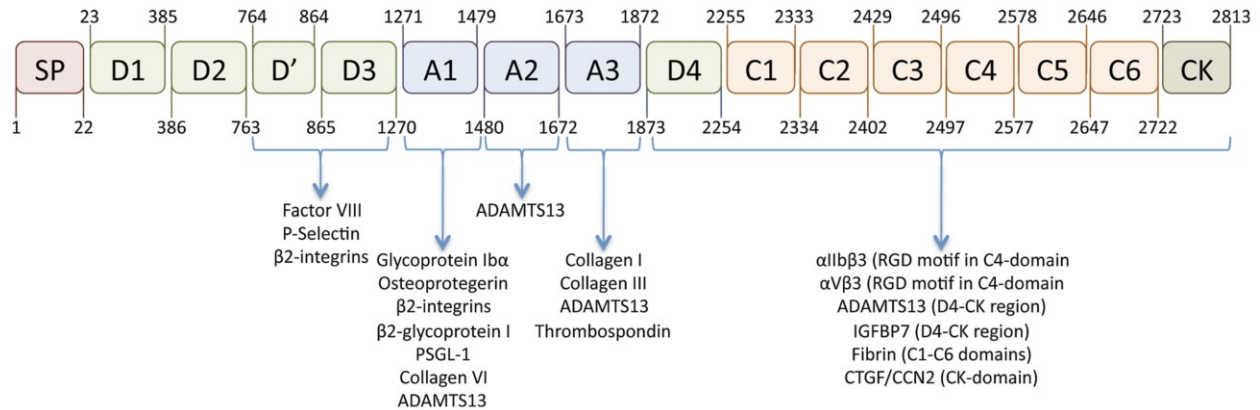


Figure 1.2 VWF structure and domains. A schematic of a VWF monomer indicating its domains and binding sites. The signal peptide (SP) is removed along with the D1-D2 propeptide in mature VWF. VWF monomers will interact at the C-terminal cysteine knot (CK) and dimerize. Image reproduced from Bryckaert *et al* (2015).³⁸

Multimerized VWF is stored in Weibel-Palade bodies (WPB) in endothelial cells and α-granules in megakaryocytes.^{21,39} VWF multimers range in size from 500kDa to over 10,000 kDa.⁴⁰ Unlike α-granules, WPB formation is dependent on the presence of VWF in the cell.⁴¹ During storage, VWF multimers need to be in a helicoidal structure that allows for 100-fold compaction of the protein.¹⁹ VWF release from platelets requires stimulation while VWF release from WPB is both basal and subject to regulation.^{42,43} Basal release occurs when random movement of WPBs in the cell drives them to the membrane where they can fuse and release their contents into the blood or sub-endothelium.⁴⁴ There also exists a pool of VWF in endothelial cells that is not stored in WPB and is released constitutively. This constitutively released VWF usually consists of small multimers and dimers and does not elicit a thrombotic response; rather, it is either deposited in the

extracellular matrix, or its role is primarily to act as a carrier for FVIII, increasing its half-life by protecting it from clearance.⁴⁵⁻⁴⁸ Endothelial stimulation due to injury or other inducers will result in the release of ultra-long (UL) VWF. Regulated release happens through the localization of the WPBs to the perinuclear area, followed by the fusion of many WPBs to form a secretory pod and subsequent release of VWF multimers.^{44,49} These released UL-VWF multimers are highly adhesive, binding to the extracellular matrix (ECM) and endothelial cell surface, as well as to platelets. These associations occur through VWF interactions with their target receptors including platelet glycoprotein receptors, making UL-VWF the most hemostatically active form of VWF.^{42,50,51} VWF release can be triggered by many stimuli including adrenaline, ADP, collagen, fibrin, histamine, thrombin, complement protein, DDAVP (1-deamino-8-D-arginine vasopressin), hypoxia and inflammation among many others.⁵²⁻⁵⁷

Once VWF is released it can be found in the subluminal ECM as small dimers/multimers or circulating as globular UL-VWF. Since it is a highly adhesive protein it can also associate with other ECM proteins such as collagen that become exposed upon injury of the vessel wall and mediate platelet aggregation and thrombosis.⁴⁵ VWF is sensitive to changes in hydrodynamic forces, and in the presence of shear stress, globular UL-VWF anchored to the ECM or the endothelial luminal surface membrane unravels and exposes its binding sites (**Figure 1.3**).^{58,59} UL-VWF is the most susceptible to unfolding since it is bigger and therefore experiences the greatest shear stress.

Platelet adhesion occurs when GpIb α binds to the A1 domain on tethered, unfolded VWF leading to a transient interaction which slows down the platelet.^{60,61} Stable platelet aggregation occurs through platelet adhesion interactions to collagen through the receptors GpVI and $\alpha_2\beta_1$ integrin (GpIa/IIa) and activation of platelet GpIIb/IIIa receptors which bind fibrinogen and

contribute to interplatelet interactions.⁶²⁻⁶⁴ High shear stress can also cause VWF self-association where VWF multimers bind to each other to create fibres that form web-like structures.^{58,65,66} These structures allow for even greater platelet adhesion during hemostasis. Activated platelets release UL-VWF (from α -granules), thromboxane A₂, ADP, and serotonin all of which lead to the recruitment of other platelets.^{67,68} Platelets contribute to secondary hemostasis through thrombin release and subsequent three-dimensional clot formation.

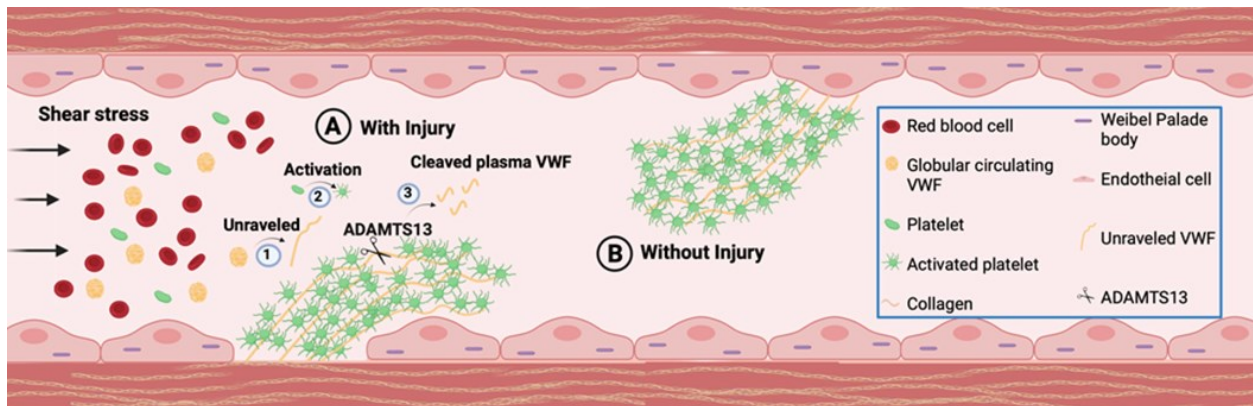


Figure 1.3 The physiological activities of VWF. **A)** In the presence of injury and/or shear stress, globular VWF in blood will unravel and expose its binding sites. It can bind to collagen in the exposed sub-endothelial layer as well as bind and activate platelets, initiating thrombus formation. VWF activity is regulated by ADAMTS13 that cleaves VWF multimers to reduce their hemostatic activity. **B)** VWF release by external stimuli leads to binding to the surface of endothelial cells and unravelling to bind platelets and form aggregates in a similar way to those seen in injury. Image reproduced from Alavi *et al* (2021).⁴⁵

VWF activity is regulated by ADAMTS13 (a disintegrin and metalloproteinase with a thrombospondin type 1 motif, member 13). This protease cleaves unfolded VWF on the A2 domain at Tyr1605-Met1606 to limit the pro-thrombotic and pro-hemostatic activities of UL-VWF.⁶⁹ VWF multimer size is related to its biological and hemostatic function, and therefore regulation is important. VWF cleavage is enhanced by shear stress, and binding to both FVIII and platelet GpIb suggesting a further destabilization of the A2 domain through altered domain-domain

interactions.⁷⁰⁻⁷² Disruptions in the ratio of VWF to ADAMTS13 levels, in favour of VWF can lead to coagulopathies.

Decreased VWF in von Willebrand's disease (VWD) is the most common inherited bleeding disease of which there are four subtypes.⁷³ Decreased VWF levels (quantitative) are characteristic of both type 1 (mild deficit) and type 3 (severe deficit) VWD while in type 2 VWD, there is impaired VWF function (qualitative).^{74,75} Platelet-type VWD is characterized by a gain of function mutation in platelet GpIb α that causes greater than is appropriate VWF-platelet binding leading to thrombocytopenia.⁷⁶ Conversely, increased VWF levels and activity are risk factors for thrombosis that in large vessels could lead to stroke or heart attack and in small vessels could lead to thrombotic microangiopathy.⁷⁷ Decreased ADAMTS13 activity, leading to increased VWF can cause thrombotic thrombocytopenic purpura.⁷⁸ Increased levels of VWF have also been found in other disease states such as vascular dementia, Alzheimer's, traumatic brain injury, acute respiratory distress syndrome, kidney failure, and COVID-19.⁷⁹⁻⁸³ Other factors such as age can affect VWF levels as well.⁴⁵

1.4 Severe acute respiratory coronavirus 2 (SARS-CoV-2)

1.4.1 Origins and host entry

Severe acute respiratory syndrome coronavirus 2 (SARS-CoV-2), which causes coronavirus disease 2019 (COVID-19), is a viral respiratory virus that first emerged in Wuhan, China in 2019 and has since become a global pandemic.⁸⁴ SARS-CoV-2 belongs to the genus Betacoronavirus and is an enveloped, positive sense, single stranded RNA virus.⁸⁴ Other viruses that belong to this genus include SARS-CoV (responsible for the 2002-2004 SARS epidemic), Middle East respiratory syndrome (MERS-CoV), and the human coronaviruses (HCoV) HCoV-OC43 and HCoV-HKU1.⁸⁵ SARS-CoV-2 enters cells through initial interactions with the receptor

angiotensin converting enzyme 2 (ACE2).⁸⁶⁻⁸⁸ ACE2 is also the receptor for SARS-CoV and alphacoronavirus HCoV-NL63 entry into cells.^{89,90}

The SARS-CoV-2 virion consists of the nucleocapsid, membrane, envelope, and spike (S) proteins. Spike proteins form a homotrimer of which there are multiple copies on the membrane; it is through this protein that the virus attaches to the host membrane and viral fusion is achieved.^{85,91} During viral maturation, the SARS-CoV-2 spike protein gets cleaved into the S1 and S2 subunits by furin (a proprotein convertase) in the Golgi apparatus of virus producing cells.⁹² In the mature virion, S1 and S2 form non-covalent bonds with each other.⁸⁵ The role of S1 is to bind to ACE2 and S2 contains the fusion peptide and interacts with other proteins that are involved in membrane fusion.⁹³

SARS-CoV-2 infection is dependent on the insertion of viral RNA into the host cytoplasm to allow for viral replication. Formation of a fusion pore occurs through host receptor engagement with viral glycoproteins and other triggers that induce a conformational change in the spike protein subunits and allows the membranes to come together.⁹³ In SARS-CoV-2, binding to ACE2 by S1 exposes another site in the S2 unit called S2' which can be cleaved by transmembrane protease, serine 2 (TMPRSS2) on the host cell surface or by cathepsin L after clathrin-mediated endocytosis envelops the ACE2 bound virus in an endolysosome.⁹⁴⁻⁹⁸ This releases the fusion peptide and initiates the formation of the fusion pore with either the cell membrane or endosomal membrane allowing viral RNA into the host cell cytoplasm.

1.4.2 Spike protein structure

Spike monomers are classified as type 1 membrane proteins and each trimer contains 66 N-linked glycans (22 per monomer).⁹⁹ In the prefusion conformation, the S1 subunit has four domains: N-terminal domain (NTD), receptor binding domain (RBD), and C-terminal domain

(CTD) 1 and 2 (**Figure 1.4**).¹⁰⁰ The role of the NTD is unclear, however, it is the target of some neutralizing antibodies, and mutations and deletions in the NTD have rendered these antibodies ineffective.¹⁰¹⁻¹⁰⁴ This suggests that the NTD has a functional role or is near other important functional domains such as the RBD. The RBD, specifically the receptor binding motif (RBM), is responsible for SARS-CoV-2 interactions with ACE2.^{86,87} This domain is also the primary target for antibodies from immune response or vaccination and three antigenic sites in this region have been identified.¹⁰⁵ The CTDs play a role in stabilizing the spike protein structure and mediating the conformational changes needed for fusion. CTD1 appears to act as a structural relay between RBD and the fusion peptide proximal region (FPPR) on S2 which helps stabilize the closed conformation of the S trimer.^{100,106} CTD2 contains the '630 loop' that helps stabilize the S trimer as well as containing the furin cleavage site.¹⁰⁶ In the prefusion conformation, most of the S2 subunit peptide forms a nine-helix bundle made up of a central coiled coil containing heptad repeat 1 (HR1) and other helices that stabilizes the spike protein.¹⁰⁷ S2 contains the fusion peptide adjacent to the FPPR. Post-fusion, the S2 subunit elongates into a stable structure.¹⁰⁰ It is likely that the HR1 conformational change inserts the fusion peptide into the cell membrane which is similar to the mechanism proposed in other coronaviruses.^{108,109} SARS-CoV-2 structure and mechanism of entry is well reviewed by Jackson *et al* (2022).⁸⁵

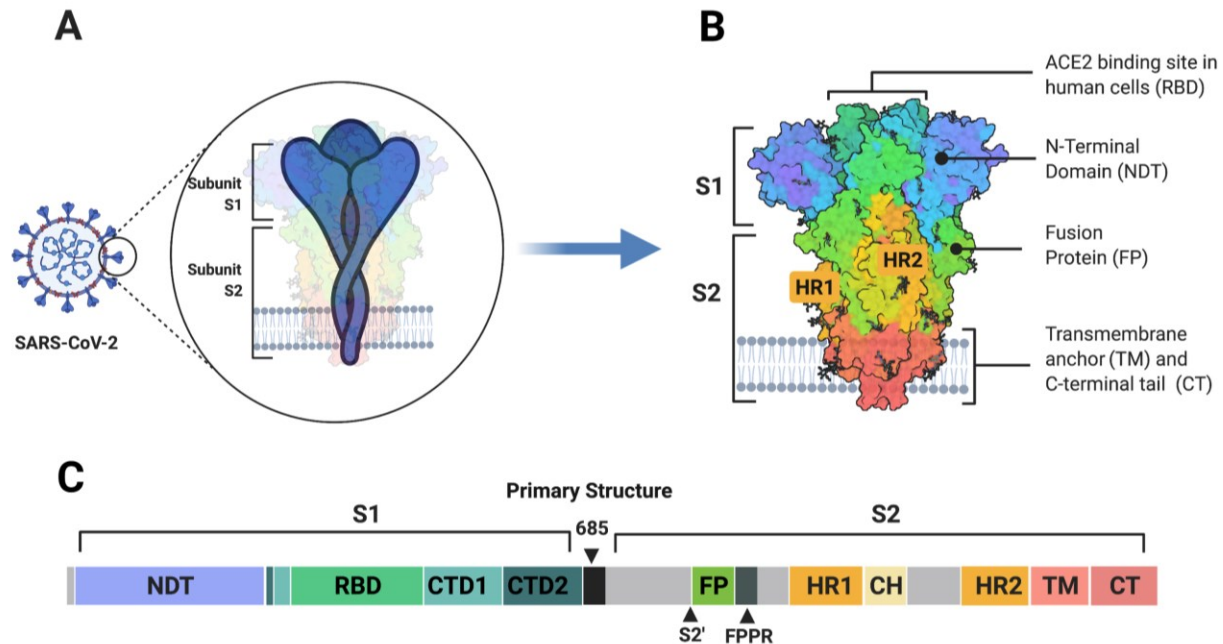


Figure 1.4 SARS-CoV-2 spike protein structure. **A)** Schematic of the SARS-CoV-2 virus and its spike protein with two subunits (S1 and S2). **B)** Spike protein structure as seen by X-ray crystallography. **C)** Primary structure of SARS-CoV-2 spike protein. Angiotensin converting enzyme 2 (ACE2); N-terminal domain (NTD); receptor binding domain (RBD); C-terminal domain (CTD); fusion protein (FP); fusion peptide proximal region (FPPR); heptad repeat 1/2 (HR1/2); central helix (CH); transmembrane anchor (TM); C-terminal tail (CT). Adapted from “An In-depth Look into the Structure of the SARS-CoV2 Spike”, by BioRender.com (2022) using information from Jackson *et al* (2022).⁸⁵ Retrieved from <https://app.biorender.com/biorender-templates>.

1.4.3 Angiotensin converting enzyme 2 (ACE2)

ACE2 is an 805 amino acid zinc carboxypeptidase found on the surface of some cells.^{110,111} It is part of the renin-angiotensin-aldosterone system (RAAS) that regulates sodium retention, proliferation, blood vessel diameter, and cell growth (**Figure 1.3**).¹¹² The ACE2 gene is located on chromosome Xp22 and has 18 exons and the resulting protein is 40% homologous to angiotensin converting enzyme (ACE).¹¹⁰ ACE2 is an integral membrane protein with its N-terminus and catalytic domain exposed in the extracellular space making it an ectoenzyme. The catalytic domain

includes the HEMGH zinc-binding motif that is conserved from ACE.^{111,113} The intracellular C-terminus contains a membrane anchor.^{110,111}

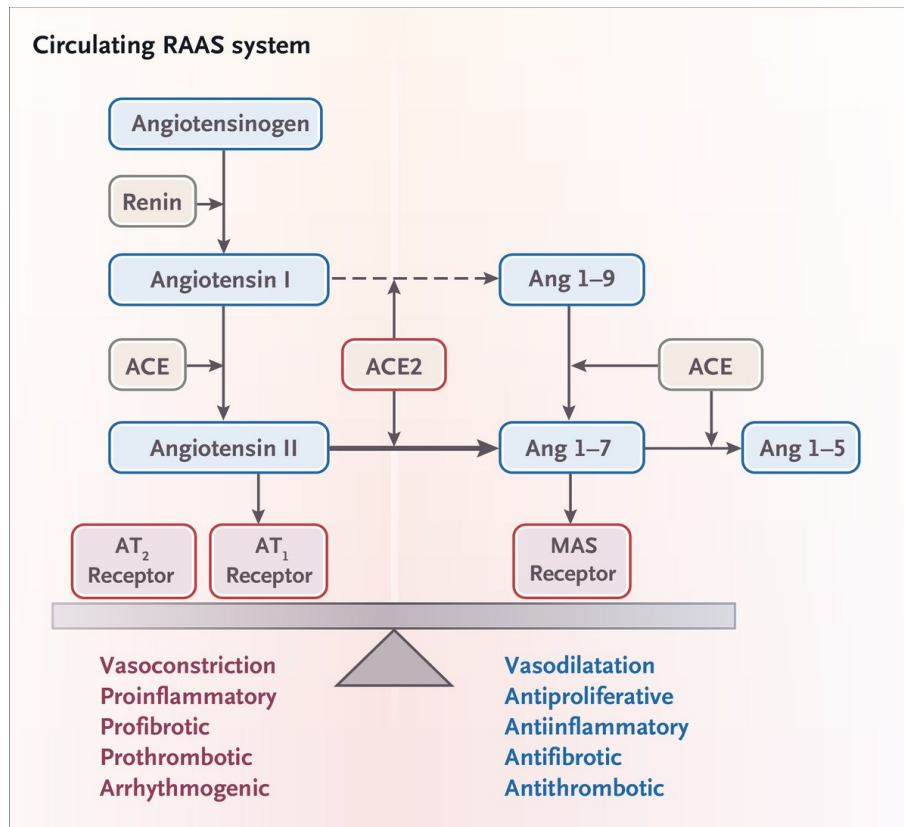


Figure 1.5 The Renin-Angiotensin-Aldosterone System (RAAS). Angiotensin converting enzyme (ACE) converts angiotensin I into angiotensin II. ACE2 primarily converts angiotensin II into angiotensin (1-7) (Ang 1-7) and converts angiotensin I into angiotensin (1-9) (Ang 1-9). Angiotensin II acts on angiotensin II type 1 and 2 receptors (AT₁ and AT₂). Ang 1-7 acts on MAS (mitochondrial assembly)-related G-protein-coupled receptor (MAS). Reproduced with permission from Renin-Angiotensin-Aldosterone System Inhibitors in Covid-19, New England Journal of Medicine (2020), Copyright Massachusetts Medical Society.¹¹⁴

ACE2, like ACE is a C-terminus carboxypeptidase; however, it only cleaves a single peptide, whereas ACE cleaves a dipeptide. Its main substrates are angiotensin (Ang) I and II that get converted to Ang(1-9) and Ang(1-7) respectively (**Figure 1.3**).¹¹¹ Of both AngI and AngII, the latter is hydrolyzed more efficiently by two orders of magnitude than AngI, suggesting that the major physiological role of ACE2 is to make Ang(1-7) rather than Ang(1-9).¹¹⁵ ACE2 can also act

on other substrates such as apelin-13, neurotensin (1-11), dynorphin A-(1-13), β -casomorphin-(1-7), and ghrelin.¹¹⁶ As stated earlier, ACE2 is also a receptor for human coronaviruses such as SARS-CoV, HCoV-NL63, and SARS-CoV-2.⁸⁸⁻⁹⁰

1.4.4 ACE2 expression and SARS-CoV-2 infection

The ACE2-RBD interface, which mediates the association of SARS-CoV-2 with a target cell, is formed by the concave outer surface of the SARS-CoV-2 S1 RBM and the ACE2 N-terminal helix.^{86,87} Twenty residues from ACE2 and 17 from the S1 RBD form hydrophilic side-chain interactions. Mutations in the RBD at residues such as Lys417, Leu452, Glu484, and Asn501 occur in SARS-CoV-2 variants and may increase receptor binding and/or antibody resistance.⁸⁵ As with SARS-CoV RBD binding, the SARS-CoV-2 spike protein trimer interacts with monomeric ACE2 when the spike RBD is in its up conformation.¹¹⁷ Upon binding, the NTD shifts slightly outwards while the conformation of the S2 subunit remains unchanged.

ACE2 expression throughout the body is variable both in organ and cell type. Hikmet *et al* recently conducted a thorough study in which immunohistochemical analysis of ACE2 was examined in multiple cell types and found consistent ACE2 expression in enterocytes, renal tubules, gallbladder, cardiomyocytes, male reproductive cells, placental trophoblasts, ductal cells, and vascular endothelial cells.¹¹⁸ However, they did not find consistent ACE2 expression in the respiratory system, which differs from what other groups have found,¹¹⁹⁻¹²² and this could be due to differences in detection protocol used. ACE2 expression can be tied to SARS-CoV-2 comorbidities.¹²² Later studies found that ACE2 expression in the respiratory tract aligns with the infection gradient seen.¹²³ The nasal epithelium (especially ciliated cells) and the upper bronchial epithelium have higher ACE2 expression compared to the limited expression seen in type II alveolar cells in the lower lung.^{122,124-126} In early infection, the ciliated nasal cells are the primary

targets for SARS-CoV-2 replication.¹²⁴ Autopsies have revealed cardiac infection, and it has been suggested that gastrointestinal and renal complications are due to ACE2 expression in colon (enterocytes) and kidney (proximal tubule cells and in the Bowman's capsule) cells.^{118,126,127} Upregulation of ACE2 expression due to inflammatory cytokines such as IL-1 β and type I and type III interferons from SARS-CoV-2 infection can lead to a positive-feedback loop for increased viral replication.^{121,128,129}

1.5 SARS-CoV-2 and thrombosis

Most patients with viral infection due to SARS-CoV-2 do not experience severe symptoms; however, severe disease is associated with inflammation and thrombosis, which can lead to multi-organ failure, as well as respiratory failure, and increased morbidity and mortality.¹³⁰⁻¹³⁴ Both arterial and venous thrombosis in the lung, kidney, heart, and brain are seen in severe SARS-CoV-2 infection. These thrombotic events are seen despite the use of anticoagulant prophylaxis in patients with severe COVID-19.^{132,134} Venous thromboembolic events (VTE) are most common, such as pulmonary embolism (PE), deep vein thrombosis (DVT), and cerebral venous sinus thrombosis.^{134,135} Microvascular thrombosis was discovered in organ microvessels after autopsy in lung, heart, kidney, and liver.¹³⁰ This can affect organ perfusion and can lead to multi-organ failure. Thrombosis has been correlated with patient death in severe COVID-19. Autopsy reports have revealed DVT and PE in patients where PE was the cause of death.¹³⁶ Another autopsy report found alveolar-capillary microthrombi in the lungs of afflicted patients.¹³⁷ Another group reported a procoagulant state in 50% of non-survivors compared to 7% in survivors.¹³⁵ These findings highlight the significant contribution of coagulation along with increased platelet activation and lack of fibrinolysis to disease severity and patient morbidity and mortality.

In severe COVID-19, there is a hypercoagulable state where high levels of D-dimer (fibrin degradation product), VWF, and FVIII as well as increased thrombosis and lack of fibrinolysis have been observed.¹³⁸⁻¹⁴¹ The presence of other markers of thrombosis such as prothrombin time, platelet count, decreased ADAMTS13, IL-6, fibrinogen, and antiphospholipid antibodies have also been reported in severely ill patients.^{140,142-144} In addition, a ‘cytokine storm’ involving the release of many inflammatory markers such as interleukins, interferons, tumor necrosis factor, and chemokines is characteristic of the hyperinflammatory state in severe SARS-CoV-2 infection.¹⁴⁵ Increased neutrophils and neutrophil extracellular traps are also associated with increased risk of thrombosis although the mechanism is unclear.^{146,147} Inflammation can damage endothelial cells and leads to ED, resulting in a shift in endothelial cell phenotype to a procoagulant state.¹⁴⁷ This leads to the release of procoagulant molecules such as VWF. These factors along with underlying comorbidities and hospitalization contribute to the increased coagulopathy seen in patients with severe COVID-19.

1.5.1 SARS-CoV-2 and VWF levels

As previously mentioned, thrombosis is usually triggered by an insult to the endothelium. The role of the endothelium in regulating this process has led to the hypothesis that SARS-CoV-2 is an endothelial disease in addition to being a respiratory disease.¹⁴⁸ As mentioned in **Section 1.4.3**, ACE2 is expressed on endothelial cells, and plays an important role in the RAAS to maintain hemostasis.¹¹² Endothelial damage and subsequent activation and release of large quantities of VWF can arise as a result of inflammation from viral infection.^{149,150} Released VWF will activate platelets and initiates the coagulation cascade resulting in clot formation.⁶¹ Hemodynamic changes can also contribute to thrombosis and stimulate VWF release. Shear stress is another inducer of VWF release and causes the unfolding of globular VWF into hemostatically active VWF strings

that can bind collagen and platelets.^{58,59} Inflammation may result in vasoconstriction as the body reduces blood flow at the site of injury.¹⁵¹ In small vessels and capillaries, such as alveolar capillaries, the effects of vasoconstriction are more pronounced and there is an increase in resistance to blood flow.^{1,151} Consequently, shear stress could potentially induce VWF release. The high incidence of thrombosis in COVID-19 patients in addition to the development of pathophysiological conditions that result in VWF release highlight the importance of VWF in SARS-CoV-2 pathology.

Whether ED and the release of procoagulant molecules is due to inflammation because of epithelial cell infection alone or also due to direct endothelial cell infection has been debated. A study by Monteil *et al* in engineered capillary organoids found evidence of SARS-CoV-2 infection in these cells.¹⁵² Liu *et al* observed SARS-CoV-2 infection of lung endothelial cells in a mouse model expressing human ACE2 as well as in autopsied lung tissue and in aortic mouse endothelial cells.¹⁵³ The contrasting view that SARS-CoV-2 does not infect endothelial cells is guided by the principle that endothelial cells do not express high enough levels of ACE2 or TMPRSS2 for infection.¹⁵⁴ Experiments done by Schimmel *et al* support this hypothesis since they observed endothelial cell infection only when ACE2 was upregulated or the cells were exposed to high levels of SARS-CoV-2.¹⁵⁵ Another group only saw infection of primary human endothelial cells, which exhibited low levels of endogenous ACE2 expression, when modified to exogenously express recombinant ACE2.¹⁵⁶ Many of the experiments that found endothelial cell infection were done *in vitro*, or in models that do not accurately represent human physiology, and this may explain the differences in the observed results. Other groups have confirmed that the inflammatory responses in endothelial cells were not due to direct infection but rather through epithelial cell infection that affected the surrounding cells.^{157,158} Overall, it seems that ACE2 may not mediate

endothelial cell infection; however, this does not rule out the possibility that SARS-CoV-2 may bind to, but not enter endothelial cells through ACE2.

It is well established that there is an increase in VWF levels in critically ill patients. Increased VWF has been associated with disease severity, admittance to the ICU, mortality, increased risk of PE, and severe acute respiratory distress syndrome.¹⁴⁰ In some cases, VWF levels were observed to be elevated up to six times higher than its upper limit.^{159,160} This can also be associated with a decrease in ADAMTS13 that enhances the VWF elevation in the blood, however this is not always seen. The effects of SARS-CoV-2 can range beyond increased plasma VWF; the enhancement of some qualities of VWF have been reported.¹⁶¹ Ward *et al* reported that patients with severe COVID-19 exhibited enhanced collagen binding activity of VWF compared to control.¹⁶¹ This enhanced activity means that VWF is more likely to bind subendothelial collagen, unravel, and mediate platelet activation and clot formation. In those with comorbidities such as age, diabetes, and hypertension where there are already increased plasma VWF levels, a subsequent increase due to SARS-CoV-2 could result in severe disease with increase thrombosis-associated morbidity and mortality.

1.6 Hypothesis and Research Aims

VWF plays a key role in thrombosis and in SARS-CoV-2 thrombotic coagulopathy. The lack of SARS-CoV-2 virus within endothelial cells has led to the hypothesis that systemic inflammation is the main contributing factor to the release of procoagulant molecules such as VWF. However, the presence of ACE2 on endothelial cell surface has led us to hypothesize that ACE2 engagement on endothelial cells, but not viral infection of these cells may trigger upregulation and/or degranulation of WPB and the release of VWF. Therefore, the aim of my research is to test **the hypothesis that engagement of ACE2 by the SARS-CoV-2 spike protein**

on endothelial cells induces upregulation and release of VWF. To address this, I examined the consequences of adding SARS-CoV-2 spike protein to cultured endothelial cells using ELISA and RT-qPCR to measure expression and release of VWF and to examine the localization and expression of ACE2 on these cells.

The role of connexins in the regulation of vascular tone

1.7 Blood pressure

Maintenance of blood pressure is critical for the distribution of nutrients and oxygen to tissues around the body. The major determinants of blood pressure are cardiac output (volume of blood ejected by the heart) and peripheral vascular resistance.^{162,163} Resistance arteries are pre-capillary arteries with a diameter less than 500µm. These include arterioles (defined as having one complete layer of smooth muscle) and small arteries proximal to arterioles. Resistance arteries can regulate their own diameter, which in turn affects blood pressure. The effect of changes in arterial diameter on blood pressure can be described by Poiseuille's Law:

$$R = \frac{8L\eta}{\pi r^4}$$

where R=resistance, L=vessel length, η = blood viscosity, and r = arterial radius.

Resistance is inversely proportional to the radius of the vessel to the power of 4 (r^4); therefore, small changes in arterial diameter have a great impact on vascular resistance and therefore blood pressure.^{1,164}

1.8 Regulation of arterial diameter

The structure of the vascular system is described in **Section 1.1**. Of the described components, endothelial and smooth muscle cells play the major role in regulating resistance artery diameter. Vasoconstriction is primarily driven by autonomic innervation from the sympathetic system. Noradrenaline (NA) released from sympathetic nerves acts on smooth muscle α_1 -adrenoreceptors to increase cytosolic calcium (Ca^{2+}) and stimulate contraction. Vasodilation is stimulated by endogenous ligands such as acetylcholine (ACh) and adenosine triphosphate (ATP) as well as by mechanical stimulation of the endothelium by changes in blood flow over the surface

and relies on endothelium-dependent mechanisms such as the release of NO and endothelium-dependent hyperpolarization (EDH). Appropriate blood pressure regulation is dependent on a balance between vasoconstriction and vasodilation.

1.8.1 Mechanisms of vasoconstriction

Vasoconstriction is primarily mediated by sympathetic output of autonomic nerves onto vascular smooth muscle cells. Muscle contraction depends on membrane depolarization and increased intracellular Ca^{2+} levels which allows actin-myosin cross bridge cycling. Increased intracellular Ca^{2+} can be achieved through Ca^{2+} influx through cell surface ion channels and the release of stored Ca^{2+} .¹⁶⁵ Ca^{2+} enters the cell through long lasting (L) type and transient (T) type voltage gated Ca^{2+} channels (VGCCs)^{165–168} as well as transient receptor potential vanilloid 1 (TRPV1) channels.^{169,170} Depolarization increases the open probability of VGCC channels and allows more Ca^{2+} to enter the cell. The stimulation of inositol triphosphate receptors (IP₃R) on the sarcoplasmic reticulum leads to a release of stored Ca^{2+} from this organelle and contributes to the increased intracellular Ca^{2+} levels.^{171,172}

Sympathetic nerves innervate smooth muscle cells through varicosities which are bulb-like formations along the axon capable of releasing neurotransmitters such as NA, ATP, and neuropeptide Y (NPY).^{173,174} These neurotransmitters act on smooth muscle cell surface receptors α_1 -adrenoreceptors, purinergic receptor P2X 1 (P2X₁), and NPY receptors respectively. The effects of NA are mediated through binding to α_1 -adrenoreceptors, which are G-protein coupled receptors (GPCRs) coupled to G_{q/11}.^{175,176} Some helpful reviews on GPCR activation and downstream signalling include those by Kobilka (2007) and Mahoney and Sunahara (2016).^{177,178} The binding of NA induces a conformational change in the receptor and allows GTP to bind to the α -subunit which dissociates and activates and phosphorylates phospholipase C (PLC).^{179,180} Activated PLC

cleaves phosphatidylinositol 4,5-bisphosphate (PIP₂) into the second messengers diacylglycerol (DAG) and inositol triphosphate (IP₃). IP₃ can act on its receptors on the sarcoplasmic reticulum to release stored Ca²⁺,^{172,179,181} while DAG activates protein kinase C (PKC) which subsequently activates a tyrosine protein kinase that increases L-VGCC open probability to allow more Ca²⁺ into the cell.¹⁸²⁻¹⁸⁴ Ligands such as ATP binding to P2X₁, leads directly to Ca²⁺ entry into the cell followed by smooth muscle depolarization and IP₃-mediated Ca²⁺ release.^{185,186} NPY binding to its receptor potentiates the effects of both NA and ATP.¹⁸⁷

Increased intracellular Ca²⁺ binds to calmodulin (CaM), forming a Ca²⁺-CaM complex that activates myosin light chain kinase (MLCK) (**Figures 1.6 & 1.7**).^{188,189} Activated MLCK will phosphorylate myosin light chain (MLC) at Ser19 which increases its actin-activated MgATPase activity.^{190,191} In addition, MLC can be phosphorylated at Thr18 by a Ca²⁺ independent kinase theorized to be an integrin linked kinase or zipper-protein interacting kinase.¹⁹²⁻¹⁹⁴ This diphosphorylation can lead to a reduction in the rate of relaxation, i.e. sustained contraction.¹⁹⁵ However, it is the phosphorylation at Ser19 that determines the contractile force and characteristics. MLC phosphorylation is essential for actin-myosin interactions to potentiate muscle contraction through ATP-dependent cross-bridge cycling of the myosin heads along the actin filaments.^{188,189,196,197} The mechanisms and regulation of smooth muscle contraction have been thoroughly reviewed.^{164,188,189,198}

As the initial Ca²⁺ signal fades, Ca²⁺ sensitization occurs to maintain muscle contraction.¹⁹⁹ Ca²⁺ sensitization maintains the phosphorylated state of myosin without Ca²⁺-CaM signalling. This can occur through DAG-PLC-PKC activation of kinases and the RhoA-Rho kinase pathway.²⁰⁰ PLC activates two kinases: PKC maintains the phosphorylated state of MLCK and phosphorylates C-kinase potentiated protein Phosphatase 1 inhibitor, molecular mass 17 kDa (CPI-17) which

inhibits myosin light chain phosphatase (MLCP), responsible for dephosphorylating MLC. These allow for the prolonged activity of MLCK and actin-myosin interaction. The RhoA-Rho kinase pathway is stimulated when agonist-induced $G_{12/13}$ signalling leads to the activation of the small GTPase RhoA which activates ROCK which phosphorylates (or leads to the phosphorylation of) myosin phosphatase target subunit 1 (MYPT1; an MLCP inhibitor) and CPI-17.^{201–203}

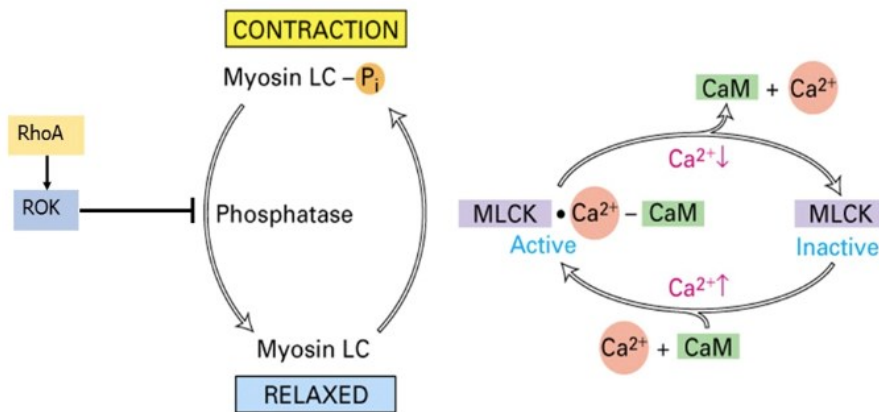


Figure 1.6 Mechanism of smooth muscle contraction. Smooth muscle contraction depends on increased Ca^{2+} associating with calmodulin (CaM) and activating myosin light chain kinase (MLCK) which phosphorylates myosin light chain (LC). In the case of Ca^{2+} sensitization, other kinases can also phosphorylate MLC and the activation of the RhoA-Rho kinase (ROK) can inhibit phosphatase activity to maintain contraction. Image reproduced from Wei (2018).²⁰⁴

Smooth muscle relaxation is mediated by a decrease in smooth muscle intracellular Ca^{2+} through the inactivation of L-VGCCs, activation of the plasma membrane Ca^{2+} -ATP pump and the sodium- Ca^{2+} exchanger to increase Ca^{2+} efflux, and activation of the sarcoplasmic/endoplasmic reticulum Ca^{2+} ATPase (SERCA) to take Ca^{2+} up into the sarcoplasmic reticulum (**Figure 1.7**).^{164,205} Ca^{2+} dissociation from CaM results in the inactivation of MLCK and the dephosphorylation of MLC by the serine/threonine phosphatase, MLCP. Dephosphorylation prevents actin-myosin interactions and, therefore, contraction. MLCP activity can also be increased by endothelial-derived NO which will be further discussed in the following sections.

Contraction is dependent on the relative activities of MLCK and MLCP which determines the phosphorylated state of MLC and actin-myosin interactions. However, the phosphorylation state of MLC ultimately depends on Ca^{2+} concentrations inside the cell, making it the key modulator of vasoconstriction.

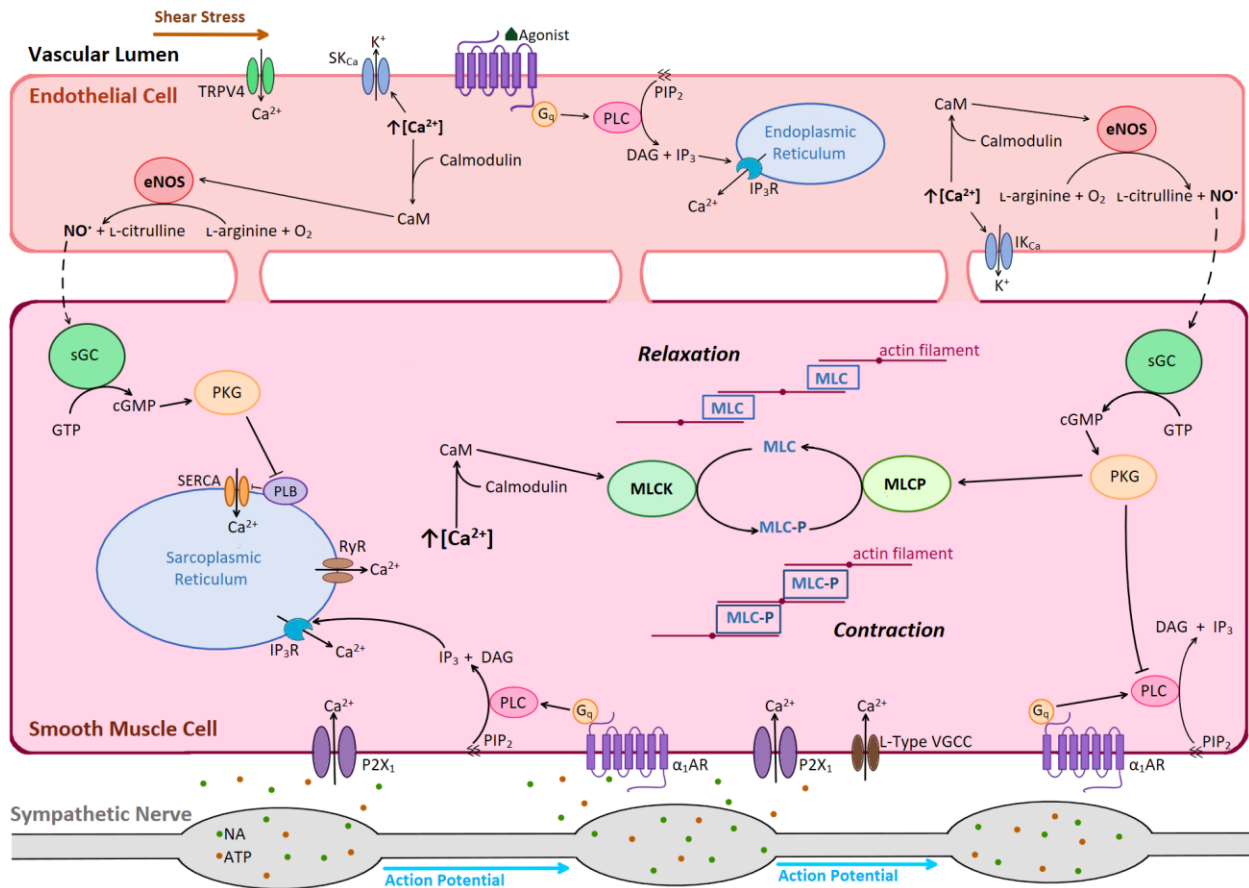


Figure 1.7 Regulation of vascular tone. Smooth muscle contraction is mediated through neurotransmitters such as noradrenaline (NA) and adenosine triphosphate (ATP) binding to their respective receptors: α_1 -adrenoreceptors ($\alpha_1\text{AR}$) and purinergic receptor P2X 1 (P2X₁) to elicit depolarization and increased intracellular Ca^{2+} , Ca^{2+} will bind to CaM and form a Ca^{2+} -CaM complex which activates myosin light chain kinase (MLCK) and results in the phosphorylation (P) of myosin light chain (MLC). MLC-P allows for the interaction of actin and myosin to elicit muscle contraction. This is regulated through the de-phosphorylation of MLC-P by myosin light chain phosphatase (MLCP). Image created by Erika Poitras.

1.8.2 Endothelium-dependent vasodilation

Vasodilation is achieved through two different pathways originating in the endothelium: endothelial NO synthase (eNOS) activation and subsequent NO generation and EDH.²⁰⁶ As with vasoconstriction, vasodilation is also dependent on intracellular Ca^{2+} concentrations but in the endothelial rather than smooth muscle cells. Increased endothelial intracellular Ca^{2+} can be stimulated by signals in the blood stream such as bradykinin, ACh, histamine, thrombin, and vascular endothelial growth factor. For example, bradykinin binding to the bradykinin type 2 receptor, a $G_{q/11}$ coupled GPCR initiates the signalling cascade previously described in **Section 1.8.1** which leads to the production of IP_3 and subsequent release of stored Ca^{2+} from the endoplasmic reticulum.^{207,208} Shear stress, the parallel force exerted on endothelial cells as blood flows in the vessel, can also stimulate the production of NO and PGI_2 release as well as the opening of apical ion channels such as TRPV4.^{209–212} These channels can also be stimulated by agonists such as arachidonic acid, and their opening results in Ca^{2+} influx into the endothelial cell.^{213–215} The increased endothelial intracellular Ca^{2+} allows for vasodilation, a process which is key to balance vasoconstriction.

NO-dependent vasodilation

NO is formed by NOS, a protein which forms a functional homodimer with each monomer containing an N-terminal oxygenase domain and C-terminal reductase domain that is connected by a sequence able to bind CaM.^{216–218} There are three types of NOS: inducible NOS, neuronal NOS and eNOS. The dimer is stabilized by both the co-factor (6R-)5,6,7,8-tetrahydrobiopterin (BH_4) and zinc bound to the oxygenase domain in addition to the prosthetic heme group.^{219–221} The reductase domain binds nicotinamide-adenine-dinucleotide phosphate (NADPH), flavin adenine dinucleotide (FAD), and flavin mononucleotide (FMN).^{222,223} The formation of NO is dependent

on electron transfer which starts from the reduced NADPH and then flows to FAD followed by FMN until it reaches and reduces the heme group on the oxygenase domain of the opposite monomer which catalyzes the formation of NO and L-citrulline from L-arginine and oxygen (Figure 1.8).²²⁴ eNOS activity is dependent on activators such as the Ca²⁺-CaM complex that forms when high concentrations of intracellular Ca²⁺ facilitate binding to CaM.^{216,225} The role of the Ca²⁺-CaM is to stabilize eNOS structural intermediates as well as to activate and position FMN so that it can pivot and reach the opposite monomer oxygenase domain.²²⁶ Other endogenous modulators of eNOS include the inhibitors calveolin-1 (which sterically prevents CaM binding), NOS interacting protein, and α -globulin (from the α -subunit of hemoglobin) and the activators β -actin and heat shock protein 90 (which reverses the effects of calveolin-1).²²⁷⁻²³¹ Additional compounds that can inhibit eNOS activity include L-arginine analogues such as L-N^G-nitroarginine (L-NOARG) and N^G-nitro-L-arginine methyl ester (L-NAME) that compete with L-arginine for the substrate binding site.^{232,233}

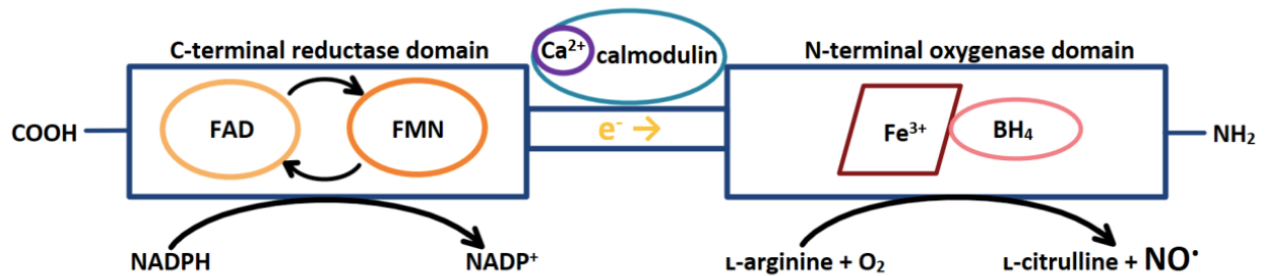


Figure 1.8 A schematic representing the structure of endothelial nitric oxide synthase (eNOS). Two monomers come together to form the functional form of eNOS. Reduced nicotinamide-adenine-dinucleotide phosphate (NADPH) donates an electron (e⁻) to the flavin cofactors: flavin adenine dinucleotide (FAD) and flavin mononucleotide (FMN). The electron passes to the heme group which catalyzes the conversion of L-arginine and molecular oxygen (O₂) to L-citrulline and NO. Image created by Erika Poitras.

The discovery that NO was identical in function to endothelium-derived relaxing factor, led Palmer *et al* to postulate that they were the same.²³⁴ NO synthesis by eNOS can be activated by physical stimuli as well as other endothelial mediators.²⁰⁹ It exerts its vasodilatory effects by diffusing from the endothelial cell to smooth muscle cell (**Figure 1.7**). Once in the smooth muscle cell, it activates soluble guanylyl cyclase by binding to the regulatory subunit to increase cyclic guanosine monophosphate (cGMP) production from guanosine triphosphate (GTP).^{235–237} cGMP activates protein kinase G (PKG) which phosphorylates targets such as MLCP, phospholamban (a SERCA inhibitor whose phosphorylation attenuates its inhibitory effect), large conductance calcium-activated potassium channels (BK_{Ca}) channels, and IP₃R as well as inhibits the formation of IP₃ to decrease intracellular Ca²⁺ and prevent vasoconstriction via the pathways discussed in **Section 1.8.1**.^{237–242}

Endothelium dependent hyperpolarization (EDH)

EDH-mediated relaxation occurs independently of NO-mediated vasodilation and is dependent on the activation of endothelial cell surface Ca²⁺ activated potassium (K_{Ca}) channels.²⁴³ These channels form homotetramers with each monomer containing six transmembrane domains, and they bind CaM at the C-terminal end.²⁴⁴ Ca²⁺ binding to CaM induces a conformational change in the channel that stabilizes it in its open conformation and allows potassium into the cell.^{245,246} The two channel subtypes found in endothelial cells are SK_{Ca} (small conductance) and IK_{Ca} (intermediate conductance) channels which are voltage-independent, Ca²⁺-dependent K⁺ channels that allow for movement of K⁺ out of endothelial cells with different conductances.^{244,247} The locations of these channels differ; SK_{Ca} are localized to endothelial gap junctions (GJs) and colocalized to caveolae with TRP channels on the endothelial cell surface while IK_{Ca} are localized to the abluminal side at the endothelial cell-smooth muscle interface near myoendothelial gap

junctions (MEGJs) (**Figure 1.7**).²⁴⁸⁻²⁵⁰ Their location governs which source of Ca^{2+} and pathway they are dependent on for activation. SK_{Ca} channels depend on shear mediated Ca^{2+} influx from activation of TRPV4 channels.²⁵¹ Meanwhile, IK_{Ca} channels are stimulated by smooth muscle derived IP_3 diffusing across the MEGJs and stimulating Ca^{2+} release from endothelial endoplasmic reticulum.^{249,252} The efflux of K^+ from the cell via these channels hyperpolarizes the endothelial cell membrane potential and the charge spreads to the smooth muscle via MEGJs.²⁴³ Hyperpolarization decreases the open probability of L-type VGCCs which reduces Ca^{2+} influx into the smooth muscle cell that would be able to elicit smooth muscle contraction. These SK_{Ca} and IK_{Ca} channels can be blocked by selective blockers such as apamin, found in bee venom, that allosterically inhibits SK_{Ca} channels and 1-[(2-chlorophenyl) diphenyl-methyl]1H pyrazole (TRAM-34) which binds the IK_{Ca} inner pore.^{253,254}

1.9 Connexins and the regulation of vascular tone

GJs were first reported in the 1960s as low resistance intercellular channels that formed between adjacent cells and allowed the exchange of large molecules.^{255,256} It was only twenty years later that it was discovered that connexins were the proteins that made up these channels. Connexins (Cxs) are important for intercellular communication. They are ubiquitous transmembrane proteins that form hemichannels when they are uncoupled on the plasma membrane and GJs formed between coupled hemichannels of adjacent cells.²⁵⁷⁻²⁵⁹ Cxs are expressed in almost all tissues and cells including endothelial cells and vascular smooth muscle cells. There are 21 Cx genes in the human genome ranging in molecular weights from 20-62 kDa.^{260,261} Their structure consists of four transmembrane domains, two extracellular loops, a cytoplasmic loop, and a cytoplasmic N- and C-terminal (**Figure 1.9**). Once formed, Cxs oligomerize into hexameric connexons that localize to the plasma membrane to form

hemichannels. These hemichannels have a finite, low open probability in physiological conditions, and their open probability can be increased due to pathological stimuli.²⁵⁷

Most cell types express two or more Cxs; this adds a further layer of complexity to the oligomerization and formation of connexons.²⁶² Connexons can be homomeric (made up of only one Cx) or heteromeric (made up of multiple Cxs).^{263–265} When the plasma membranes of two cells are close to each other, two connexons can dock to form a GJ. These GJs may be homotypic (where identical Cxs dock with each other) or heterotypic (where different Cxs dock with each other).²⁶⁶ The formation of these mixed channels by cells allows for the production of a greater variety of channels with a variety of permeability and gating characteristics than between those formed with just one Cx.^{267,268} Most Cxs will selectively oligomerize with the Cxs of another connexon that are within their subgroup.²⁶⁹ It is the channel composition rather than the pore size that determines which molecules may pass through a GJ.²⁷⁰ Differences in channel permeability to ions, dyes, and signalling molecules such as cAMP and cGMP in channels composed of different connexins have been reported.^{267,268,271,272} GJs are very dynamic with a short half-life of a few hours.^{266,273} They will cluster together and form plaques of up to 2,000 GJs. New GJs are added to the periphery of these plaques while channels in the middle are pulled out and recycled.²⁷⁴ GJs allow for the direct exchange of ions and metabolites of up to 1,000 Da between the cells allowing for a rapid transduction of a signal/effector and a unified response in the tissue.

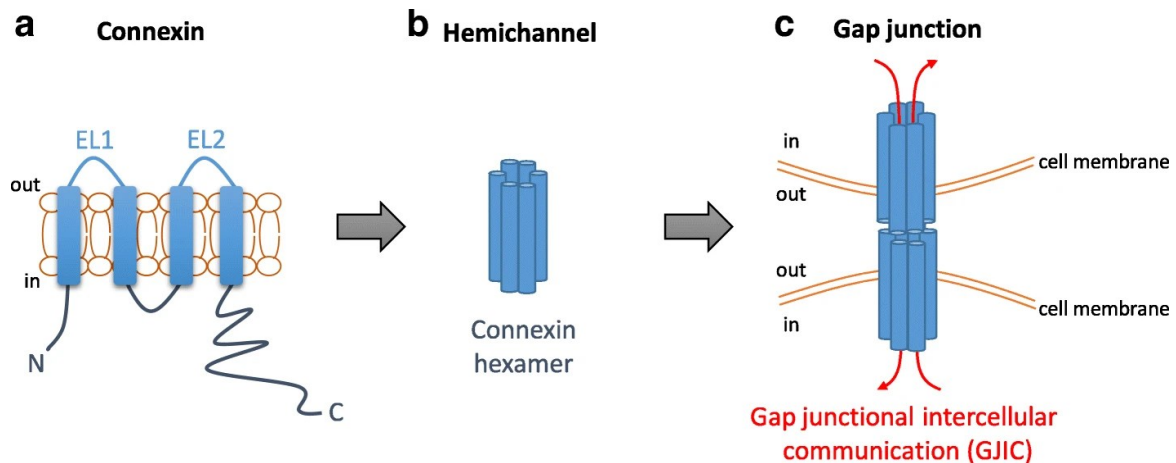


Figure 1.9 Connexin assembly into gap junctions. A) Topology of a connexin with four transmembrane domains, two extracellular loops (EL) EL1 and EL2, and intracellular loop and cytoplasmic N- and C-termini. **B)** Cxs will oligomerize into hexameric connexons that form hemichannels. **C)** The cell membranes of two cells can come together and dock to form a GJ that allows for direct and rapid cell-cell communication. Image reproduced from Wu and Wang (2019).²⁷⁵

Post translational modification of Cxs in GJs allows for the control of their life cycle, permeability, and interactions with other proteins.²⁷⁶ Modification of the extracellular loops has not been extensively studied; however, it has been established that some cysteines in these loops undergo redox regulation.²⁷⁷ This is thought to regulate the joining of two hemichannels. The N-terminal domain of GJs can be modified to regulate channel closure,²⁷⁸ channel size and charge selectivity,^{279,280} and membrane insertion.²⁸¹ Modification of the intracellular loop has been reported in some connexins. For example, Cx43 contains a CaM binding site and Cx35 has a PKA dependent phosphorylation site.^{282,283} These modifications are thought to contribute to channel opening and closing. The C-terminal domain is the most widely modified site in Cxs and these modifications can change the tail structure of the C-terminal domain.^{284,285} These modifications are involved in the regulation of channel conduction, permeability, selectivity, and voltage gating as well as open probability.^{286–288} Such modifications include the phosphorylation of serine,

threonine, and tyrosine residues,^{289,290} nitrosylation,^{284,291,292} acetylation,^{293,294} and ubiquitination.²⁹⁵ Many of these modifications have most extensively been studied in Cx43 – this is perhaps due to the fact that it is the most ubiquitously expressed Cx. The most studied modification is phosphorylation, particularly in Cx43; however, other studies have also examined this in other Cxs.^{284,290,296} Many protein kinases such as PKA, PKC, mitogen-activated kinases, protein kinase B (AKT), and Src kinases have been shown to phosphorylate the Cx C-terminal.^{284,289,297–300} Phosphorylation also affects GJs turnover and interactions with other proteins.

Cxs are found in almost all cell types, with expression varying depending on the cell and tissue type. In the vascular system, the Cxs forming GJs found in endothelial and smooth muscle cells are Cx37, Cx40, Cx43, and Cx45 (**Figure 1.10**).^{257,276} The size and abundance of these GJs varies depending on the region in the vascular tree and disease states such as atherosclerosis and hypertension.^{301,302} In resistance arteries, the vessels responsible for regulating blood pressure, GJs between endothelial cells, smooth muscle cells and endothelial-smooth muscle cells allow for the intercellular distribution of signals during vasoconstriction and vasodilation to allow for a synchronized response along a vessel length. Endothelial cells express Cx37, Cx40, and Cx43 while smooth muscle cells express mainly Cx43 and Cx45, and the GJs that form longitudinally between these cell types are formed by these Cxs.^{303,304} MEGJs, which are formed between endothelial cell projections into the internal elastic lamina, separating smooth muscle and endothelial cells, generally consist of connexons made of Cx43 and Cx37 or Cx40.³⁰⁵ The structure, function, and role of Cxs in vascular function is well reviewed by Pogoda *et al* (2019).²⁷⁶

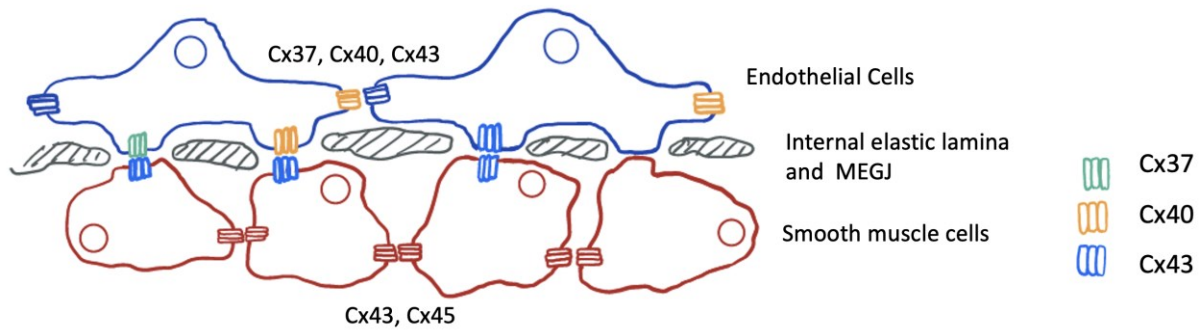


Figure 1.10 Schematic demonstrating connexin distribution in resistance artery vascular tissue. Endothelial cells express Cx37, Cx40, and Cx43 while smooth muscle cells express Cx43 and Cx45. GJs form between endothelial cells and between smooth muscle cells. They also form between endothelial projections and smooth muscle cells to form myoendothelial GJs (MEGJs). These GJs allow for rapid intercellular signalling.

GJs are essential for the radial and longitudinal conduction of signals in blood vessels. Radial transmission happens through MEGJs and allows for the exchange of Ca^{2+} , signalling molecules such as IP_3 , and current.²⁷⁰ GJs are essential to allow the electrotonic transmission of hyperpolarizing current from endothelial cells to elicit vasodilation through the pathways described **Section 1.8.2**. This is supported by the findings that Cx-mimetic blocking peptides against Cx43, Cx40, and Cx37 attenuates EDH signalling.³⁰⁶ There is also evidence that deletion of Cx40 from endothelial cells leads to reduced signalling of EDH.³⁰⁷ NO normally diffuses through the membrane to reach the smooth muscle cell; however, it has been reported that NO may pass through MEGJs and that this plays a role in ACh-mediated vasodilation.³⁰⁸ Longitudinal conduction of signals within resistance arteries allows for the coordinated responses to stimuli along the vessel length. The electrotonic spread of charge creates a conducted vasomotor response to a stimulus from the origin to up and downstream locations along the vessel.^{257,309}

The role of each Cx in the conduction of this longitudinal response has not yet been elucidated; however, there is evidence that Cx40 plays a major role. Irregular vasomotion is

observed with deletion of Cx40 in mice.³¹⁰ Experiments examining the conduction of endothelium-dependent signals due to ACh or bradykinin in Cx40 knockout (KO) mouse arterioles demonstrate an attenuation in conducted hyperpolarizing responses.^{311,312} This model also demonstrated sustained hypertension. While investigating this phenomenon, Jobs *et al* noted that Cx37 did not seem to be able to make up for the lack of functional Cx40 in this model.³¹² In mice where Cx37 was knocked out, the conducted vasodilatory responses remained intact.^{312,313} In a model that targeted the replacement of Cx40 by Cx45, Wölfle *et al* also found that Cx45 could not replace the function of Cx40 in the transmission of endothelium-dependent dilations in mouse arterioles.³¹⁴

Cx expression can be altered by disease state in addition to physiological stimuli such as shear stress. In experiments done in spontaneously hypertensive rats, consistent reduction of both Cx37 and Cx40 was observed, with varying modifications of Cx43 expression.^{302,315} Yeh *et al* found reduced expression of both Cx37 and Cx43 but no change in Cx40 expression in induced hypertension in rats.³⁰² Altered Cx expression has also been implicated in atherosclerosis.³¹⁶ Changes in expression vary with plaque progression as well as with disturbed flow and increased shear stress that results from plaque formation and the narrowing of the blood vessel lumen. In early plaque formation, intimal smooth muscle cell Cx43 is initially upregulated followed by a loss in developed plaques.^{317,318} Endothelial cell Cx37 and Cx40 expression is only decreased in advanced plaques in the surface endothelial cells.^{301,316} Shear stress has been shown to increase expression and disorganization of Cx43 in endothelial cells.^{319,320} GJ communication in the presence of shear stress was found to be increased and primarily mediated by Cx40 with some contributions by Cx37.³²¹ In addition, it was found that shear stress could lead to a long term induction in Cx40 protein expression.³²² The importance of GJs in vascular signalling and their modulation in disease states implicates connexins as essential to proper vascular function.

1.10 Hypothesis and Research Aims

The aim of my research was to assess the role of Cx40 in endothelium-dependent vasodilation in rat mesenteric arteries by testing the **hypothesis that arteries from Cx40 deficient rats will show an impaired response to ACh-induced vasodilation**. To address this, I investigated the effects of ACh-induced vasodilation in isolated mesenteric arteries of male and female Cx40 wild type (WT), heterozygous (HET), and knockout (KO) rats mounted in a wire myograph. I used pharmacological tools that modulate both EDH and NO synthesis to examine the impact of each pathway in each group's response. In doing this, I will be characterizing the vascular responses of this novel rat knockout model *in vitro* to elucidate the impact of Cx40 deficiency.

Chapter 2: Materials and Methods

2.1 Ethics Approval

All animal care and experimental use was approved by the University of Alberta Animal Care and Use Committee for Health Sciences (AUP 312) in accordance with Canadian Council on Animal Care guidelines. Description of care and use is described by Grundy (2015).³²³

2.2 Animal Care and Use

Male and female Wistar Kyoto (WKY) rats (Cx40 WT, HET, KO) were housed by the University of Alberta Health Sciences Laboratory Animal Services (HSLAS). These animals were provided with an enriched environment with water and chow available *ad libitum*. These animals were kept in rooms with a 12:12h light-dark cycle at 23°C average temperature. Euthanasia was performed via isoflurane inhalation followed by decapitation. The gut and other relevant tissues were removed from the animal and kept in ice-cold Krebs buffer until use.

2.3 Cx40 Colony

The knockout WKY Cx40 KO strain was produced by injecting a CRISPR plasmid targeting the sequence CGATGACCGTAGAGTGCTTG on the *Gja5* gene into WKY rat embryos. The resulting mutation is a one base pair substitution that creates a stop codon. These rats were a gift from Dr. William Cupples who had them made as part of a competition funded by the National Institute of Health.

The colony was bred in-house using HET x HET crossings. Ear notch samples of each rat were collected by HSLAS staff.

2.4 Genotyping

The genotype of each litter of rats was determined prior to being used in any of the experimental setups described below.

DNA extraction: DNA was extracted from ear notch samples collected by HSLAS staff. Samples were placed in an alkaline lysis reagent (25mM NaOH, 0.2 mM Na₂EDTA-2H₂O, pH ~12) and heated at 95°C for one hour. An equal volume of neutralization reagent (40mM Tris-HCl, pH ~5) was added and the samples were cooled to 4°C. DNA concentrations were measured in a spectrophotometer (NanoDrop ND-10000) and recorded.

Polymerase chain reaction (PCR): Reactions were performed at a 25µl reaction volume in a Bio-Rad ICycler thermocycler. Each reaction contained: PCR grade water (6.5µl; FroggaBio), 2X Taq FroggaMix (12.5µl; FroggaBio), Gja5 forward and reverse primer (0.5µM; Integrated DNA Technologies), and extracted DNA (1µl). The cycling conditions were: 94°C for 15 minutes; 30 cycles of 94°C for 1 minute, 68°C for 30 seconds, 72°C for 1 minute; 72°C for 10 minutes; and 4°C hold.

Gel electrophoresis: To confirm that the PCR yielded the desired product, all PCR reactions were run on a 1.5% agarose gel with ethidium bromide by electrophoresis and visualized under UV light.

PCR product extraction: The PCR product was purified using a PCR cleanup kit (TruIn Science) and manufacturer's protocol was followed. The final DNA concentration was measured using a spectrophotometer as described above.

Sequencing and analysis: All sequencing reactions were run on a 3730 Genetic Analyzer (Applied Biosystems) at the University of Alberta's Molecular Biology Services Unit. Samples were prepared as 10µl samples containing 15ng/µl DNA from the PCR product and 0.25µM Gja5 forward primer (Integrated DNA Technologies). Data files were analyzed in SnapGene.

Table 2.1 Primers for PCR and genotyping		
Gene	Sequence	Manufacturer
WKY-Gja5 (connexin 40)	F 5'-TGGATCAGTGGTCCAGAGCATGATG-3' R 5'-GCGTGGCCCATGTACACCAGAGAT-3'	Integrated DNA Technologies

2.5 Culture of HUVECs

Human umbilical vein endothelial cells (HUVECs) were isolated directly from individual sources and obtained from our collaborator, Dr. Barbara Ballermann, were cultured in cell culture plates (Sarstedt) covered in gelatin-based coating solution (Cell Biologics) and Media 199 (Gibco) supplemented with 20% fetal bovine serum (FBS; Gibco), 200mM L-Glutamine (Gibco), 100IU/ml Penicillin-Streptomycin (Gibco), and 100µg/ml endothelial cell growth serum contents (Corning) and grown at 37°C/5% CO₂ as previously described.³²⁴

Confluent HUVEC cultures were treated with 1nM SARS-CoV-2 (2019-nCoV) Spike S1+S2 ECD-His Recombinant Protein (Sino Biological, #40589-V08B1-B) and samples were collected at various timepoints ranging from 5 mins to 72 hours. At each timepoint, media was collected, and the cells were washed with PBS and lysed on ice with QIAzol® Lysis Reagent (Qiagen) for RNA preparation or RIPA buffer (ThermoFischer) for protein isolation as described below.

2.6 Measurement of VWF RNA expression by real-time reverse-transcription quantitative PCR (RT-qPCR)

Expression levels of VWF RNA in cell lysate at different time points were evaluated using real-time reverse-transcription quantitative PCR (RT-qPCR).

RNA extraction and cDNA synthesis: RNA extraction was performed using the RNeasy Micro Kit (Qiagen) following a protocol modified from the manufacturer's recommendations. Chloroform (100µl; Sigma Aldrich) was added to each tube containing the lysed cells. The samples

were mixed and centrifuged at 8,000rpm at 4°C for 15 minutes. The top clear layer of the supernatant was collected and pipetted into the spin columns provided in the RNeasy kit; then 1:1 volume of 70% ethanol was also added to the column. The samples were centrifuged at 8,000rpm for 15 seconds, and the flow-through was discarded. Buffer RW1 (from RNeasy kit; 500µl) was added to each column and centrifuged at 8,000rpm for 15 seconds. The RNeasy kit protocol was followed from step 6 onwards. The concentration of extracted RNA was measured on a spectrophotometer (NanoDrop ND-10000) and recorded. Complementary DNA (cDNA) was synthesized from the RNA using a QuantiTect Reverse Transcription Kit (Qiagen) following the manufacturer's protocol. Samples were stored at -20°C.

Quantitative real-time PCR was performed using the SYBRGreen kit (Applied Biosystems). cDNA samples were diluted 1:5 and 1µl of diluted cDNA was analyzed in a total 20µl reaction mixture that contained: 10µl SYBRGreen PCR Master Mix (Applied Biosystems), 1µl VWF or HPRT primer, and 8µl PCR-grade water. Reactions were carried out in an ABI 7900 Genome Analyzer System (Applied Biosystems). Data for each sample was analyzed by first normalizing VWF to the internal control HPRT using experimental Ct (threshold cycle) values for each triplicate sample ($\Delta Ct = Ct(VWF) - Ct(HPRT)$) and then averaging these values. The VWF mRNA levels were calculated using $2^{-\Delta Ct}$.

Table 2.2 Primers for RT-qPCR	
Gene	Company and Cat #
VWF	QIAGEN-QT00051975
HPRT	QIAGEN-QT00059066

2.7 Enzyme-linked immunoassay (ELISA) for VWF

VWF concentrations in cell culture media (that was collected at each time point and stored at -80°C) were analyzed using a Human Von Willebrand Factor ELISA Kit (Abcam, #ab108918)

following the manufacturer's protocol. The sample plate was read in a Synergy H4 Hybrid Reader (BioTek) at 450nm and 570nm absorbance.

2.8 Immunofluorescence detection of ACE2 in HUVECs

HUVECs were cultured as described above on glass coverslips (Fisher Scientific) in a 24-well plate. Once fully confluent, the cells were fixed with 4% paraformaldehyde (Santa Cruz Biotechnology) for 20 minutes. Some coverslips were treated with 0.2% TritonX-100 (Sigma) on ice for 5 minutes to permeabilize the cells, while the remaining cells were left unpermeabilized. All cells were blocked with a solution made with 10% donkey serum (Sigma) and 2.5% fish gelatin (Sigma) in phosphate-buffered saline (PBS; Gibco) for one hour at room temperature. Cells were incubated overnight with anti-ACE2 (Abcam) and anti-Human VE-cadherin PE-conjugated (R&D Systems) primary antibodies in a humid chamber at 4°C. Antibodies were diluted at 1:100 and 1:150 respectively in 5% BSA. Cells were washed with 0.3% BSA. Secondary antibodies diluted at 1:500 in 5% BSA were added to the samples and incubated in the dark at room temperature for one hour. Samples were washed then incubated with 4',6-diamidino-2-phenylindole (DAPI; Sigma) diluted 1:1000 for 5 minutes at room temperature. Samples were washed with 0.3% BSA. Cover slips were mounted on microscope slides using ProLong Gold antifade mountant (Invitrogen).

Negative used controls included for blocking solution without antibodies, only primary antibodies, and only secondary antibodies. Immunofluorescence images were taken on with Leica DM IRB fluorescence microscope (Leica; Germany) at 630x magnification in the Open Lab software, version 4.0.2.

Table 2.3 Antibodies and Stain for Immunofluorescence Imaging			
Primary Antibodies	Source	Dilution	Company and Cat #
Anti-ACE2	Rabbit polyclonal	1:100	Abcam, #ab15348
Anti-VE-cadherin PE-conjugated	Mouse monoclonal	1:150	R&D Systems, #FAB9381P
Secondary Antibodies			
Alexa Fluor 488 Anti-rabbit IgG (H+L)	Donkey polyclonal	1:1000	Invitrogen, #A32790
Stain			
4', 6-diamidino-2-phenylindole (DAPI)	N/A	1:1000	Sigma, #32670-5MG-F

2.9 Western blot analysis of ACE2 and VWF expression

Cultured HUVEC and HEK293 cells were lysed with RIPA buffer (ThermoFischer) and placed in a rotator at 4°C for 1-2 hours. Samples were vortexed for 1-2 minutes and then centrifuged at 12,000rpm for 20 minutes at 4°C. The supernatant was collected, and sample protein concentration was determined using DC Protein Assay reagents (Bio-Rad). A microplate was loaded with the following reagents in this order: 25µl Reagent A, 5µl supernatant, 200µl Reagent B and incubated in the dark for 15 minutes. The microplate was read in a Synergy H4 Hybrid Reader (BioTek) at 750 nm absorbance. Western blot analyses were performed by diluting samples containing 25µg protein in 4X Laemmli buffer containing 10% β-mercaptoethanol. Samples with total volume 400µl containing 1X Laemmli buffer and water were denatured at 95°C for 7-8 minutes and run on an 8% SDS-PAGE at 120V for 2h. The proteins on the gels were then transferred to a polyvinylidene difluoride (PVDF) membrane and maintained overnight at 4°C.

The membranes were blocked with 5% skim milk (ThermoFischer) diluted in Tris-Buffered Saline-Tween (TBS-T) for one hour and washed with TBS-T three times at room temperature. VWF, ACE2, and α-tubulin proteins were detected by incubating the PVDF membrane with primary antibodies against target proteins which were diluted in Western Blot

blocker solution (Sigma). Membranes were incubated with primary antibodies at 4°C overnight, followed by washes with TBS-T three times at room temperature and incubated with the appropriate secondary antibodies for one hour at room temperature.

The membranes were developed using Amersham™ ECL™ Prime Western Blotting Detection Reagent (GE Healthcare) and sandwiched between two thin clear plastic sheets. The membranes were exposed in a ImageQuant LAS 500 imager (GE Healthcare).

Primary Antibodies	Source	Dilution	Company and Cat #
Anti-ACE2	Rabbit polyclonal	1:500	Abcam, #ab15348
Anti- α -tubulin	Mouse monoclonal	1:15,000	Sigma-Aldrich, #05-829
Anti-VWF	Rabbit polyclonal	1:5,000	Dako, #A0082
Secondary Antibodies			
Goat anti-rabbit IgG	Goat polyclonal	1:10,000	Abcam, #ab97051
Goat anti-mouse IgG	Goat polyclonal	1:10,000	Sigma-Aldrich, #12-349

2.10 Wire myography

See **Section 2.11** for the list of reagents used.

A 2nd or 3rd order branch isolated from the rat mesenteric bed was pinned in a petri dish filled with ice-cold Krebs buffer and visualized under a dissecting microscope. The adhering fat and the vein were cut away with care not to stretch or pierce the arterial wall. The artery was cut into four segments approximately 2mm wide that were then threaded with 25 μ m diameter gold plated tungsten wire (Goodfellows, U.K.), taking care not to damage the endothelium by having the end of the wire scrape the inner vessel wall. Segments were then mounted on a four-channel Mulvany-Halpern 610M wire myograph (Danish Myo Technology, Aarhus, Denmark) to record changes in isometric wire tension. The volume of each bath was 7mls of Krebs and was maintained at 37°C and bubbled continuously with 5% CO₂/95% O₂.

Once mounted, the vessels were equilibrated to a resting baseline tension of 5mN for 20 minutes. Vessel endothelial function was then tested using phenylephrine (PE; 3 μ M), an agonist at α_1 -adrenoreceptors, to constrict the vessels followed by ACh (3 μ M), an agonist at muscarinic receptors, to cause vasodilation. Vessels exhibiting a >90% reduction in PE-induced tone were considered to have an intact endothelium.

To examine the contribution of Cx40 on endothelium-dependent vasodilation, cumulative concentration response curves to ACh were constructed in the absence and presence of a combination of inhibitors: TRAM-34 (1 μ M), apamin (50 nM), and L-NAME (100 μ M). Vessel tone was increased with PE (3 μ M), then a control ACh concentration response curve (1nM to 10 μ M) was constructed in each vessel segment by addition of increasing cumulative half logarithmic concentrations. Then, each of the four baths was incubated with an inhibitor for twenty minutes as follows: 1) time control, 2) TRAM-34 + apamin, 3) L-NAME, and 4) TRAM-34 + apamin + L-NAME. Once the incubation period had passed, a second concentration response curve with ACh was constructed as described above. Data were recorded in the software LabChart 8 (ADInstruments) through a PowerLab 4/25 (ADInstruments).



Figure 3.1 A third-order mesenteric artery mounted in a Mulvany-Halpern wire myograph. The yellow arrow denotes an artery threaded with gold-plated tungsten wire; one foot is connected to an isometric force transducer.

2.11 Reagents

The physiological buffer used was Krebs buffer which contains 118mM NaCl, 3.6mM KCl, 25mM NaHCO₃, 1.2mM NaH₂PO₄, 11mM glucose, 1.2mM MgSO₄•7H₂O, and 2.5mM CaCl₂.

Table 2.5 Reagents Table			
Reagent	Manufacturer	Mechanism of Action	Solvent
ACh	Sigma-Aldrich	Muscarinic receptor agonist	Distilled water
Apamin	Tocris	SK _{Ca} channel inhibitor	Distilled water
L-NAME	Sigma-Aldrich	NO synthase inhibitor	Distilled water
L-phenylephrine hydrochloride (PE)	Sigma-Aldrich	α ₁ -adrenoreceptor agonist	Distilled water
TRAM-34	Cayman	IK _{Ca} channel inhibitor	Dimethyl sulfoxide

2.12 Statistical Analysis

Each experiment (n=1) used HUVECs from a different source and for each experiment biological duplicates were completed. For animal experiments, each data point represents tissue

taken from one rat (n=1). All data is represented as mean \pm standard error of the mean (SEM). Analysis with two-way, repeated measures analysis of variance (ANOVA) was done to compare multiple experimental groups with two independent variables. Tukey's multiple comparisons test was done to compare multiple points with each other. One-way ANOVA was completed to compare three or more groups with one independent variable. Unpaired two-tailed t-tests were performed on comparisons between two groups. A p-value < 0.05 was considered significant. All data analysis was done in Microsoft Excel and GraphPad Prism 9.

Chapter 3: Results

3.1 The effects of SARS-CoV-2 spike protein on VWF release and mRNA expression in HUVECs

To determine the effects of SARS-CoV-2 exposure on both released VWF and VWF mRNA levels in cultured HUVECs from two sources, I examined both parameters over a time course designed to evaluate both immediate effects (5 mins) as well as longer term effects (72h). The time course design was as follows: 5min, 1h, 4h, 6h, 12h, 24h, 48h, and 72h. Prior to the start of the experiment, cells were given full fresh medium followed by administration of 1nM SARS-CoV-2 spike protein at t=0. This concentration of spike protein was used based on the effects of spike protein in previous studies.^{325,326} At each time point, media was collected, and cells were lysed to collect RNA in both the control and treated groups.

Evaluation of VWF mRNA levels at each timepoint revealed no statistically significant differences between the control and spike treated groups (**Figure 3.1**), although an increasing trend of VWF mRNA in spike protein treated cells at 48 and 72 hours was indicated.

The effect of SARS-CoV-2 spike protein exposure on VWF release was evaluated using ELISA for measuring the concentration of VWF in the media of both the control and spike treated groups (**Figure 3.2**). The results demonstrated that the levels of secreted VWF in cells exposed to spike protein was significantly higher compared to control at 5 minutes post exposure. An approximately 2-fold increase in the VWF levels in media of spike protein treated vs control cells was observed (**Figure 3.2B**). This increased level of VWF was only significant at the 5-minute time interval (**Figure 3.2A**). A higher concentration of VWF in the media after 5 minutes of exposure to spike protein suggests immediate release of VWF from WPB and is consistent with

previous reports demonstrating similar response pattern to other inducers of WPB degranulation.³²⁷

In a separate experiment, the effect of re-stimulating a group of cells at 72h after initial treatment with spike protein was examined. Cells were stimulated once with spike protein at t=0 and again at t=72h, and the media was collected 5 mins after the second treatment since this is where we had seen effects of VWF release from WPB (**Figure 3.2A-B**). Comparison of the VWF concentrations in the media of control (-), cells treated at t=0 only (+), and cells treated at both t=0 and t=72h (++) revealed a significant difference between the groups (**Figure 3.2C**). The group treated twice was significantly greater (~2 fold) than either the control or cells treated once at t=0. As expected, based on results shown in **Figure 3.2A**, cells treated with spike protein only at t=0, after 72 hours exhibited similar levels of VWF to control (approximately 40 ng/ μ l), however this level was significantly higher in absolute value from the VWF levels where media from cells were analyzed at the first 5 mins after exposure at t=0 (<1.5 ng). These results indicates that VWF accumulation increases within cells with time in culture and could translate into significantly higher levels of stored VWF. Thus, exposure to spike protein leading to immediate release under these circumstances may translate into a significantly higher absolute levels of released VWF (i.e., 80 ng/ μ l compared to 40ng/ μ l as shown in **Figure 3.2C**).

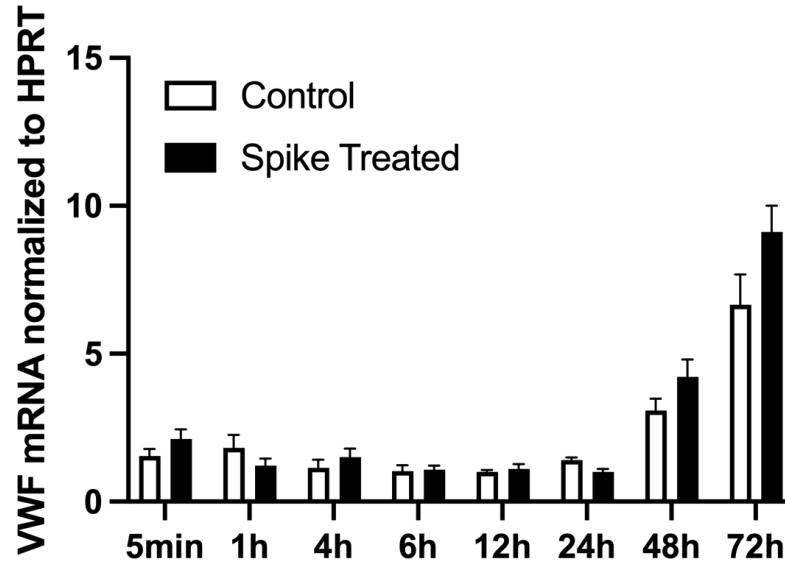
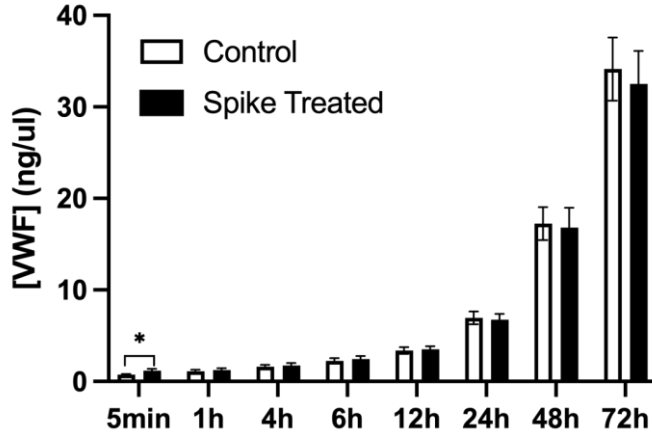
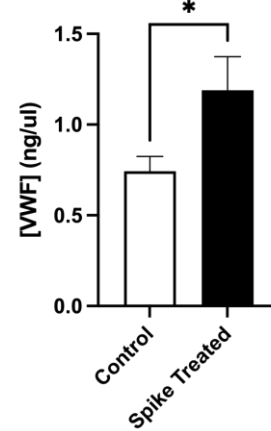
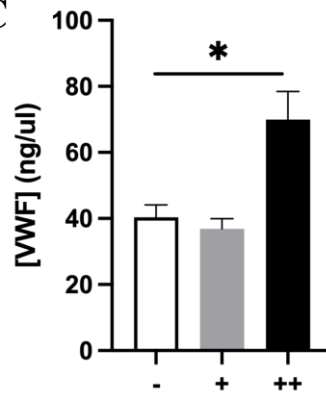


Figure 3.1 The effects of 1nM SARS-CoV-2 spike protein on VWF mRNA in HUVECs. Human umbilical vein endothelial cells (HUVECs) were cultured until confluent and were treated with 1nM SARS-CoV-2 spike protein at t=0. At each timepoint, cells were lysed, the RNA was extracted, and cDNA was made and analyzed in real-time quantitative PCR. All data is represented as mean \pm SEM (n=2), with $p < 0.05$ considered significant.

A**B****C**

Stimulation with SARS-CoV-2 spike protein at 72h

Figure 3.2 The effects of 1nM SARS-CoV-2 spike protein on VWF release in HUVECs. Human umbilical vein endothelial cells (HUVECs) were cultured until confluent and media was replaced with fresh media containing 1nM SARS-CoV-2 or vehicle (control). At each timepoint, media was collected and VWF protein concentrations were analyzed using ELISA. **A)** VWF concentration at each timepoint after addition of spike protein at t=0 (n=2). **B)** VWF concentrations at 5mins in control vs spike treated groups (n=2). **C)** VWF concentrations at 72h without spike treatment (-), with spike treatment at t=0 (+), and two spike treatments at both t=0, t=72 (++) (n=1). All data is represented as mean \pm SEM with *p<0.05 considered significant.

3.2 ACE2 expression in HUVECs

To evaluate whether the effects of adding spike protein to cultured HUVECs could be due to its interaction with ACE2 on endothelial cell surfaces, first, we evaluated ACE2 expression in un-treated HUVECs using both immunofluorescence imaging and western blot analysis.

Immunofluorescence imaging was done on both permeabilized and non-permeabilized HUVECs to determine ACE2 expression, both in the cytoplasm and on the cell surface. Cell boundaries were visualized using VE-cadherin, a protein present at endothelial cell junctions. In the permeabilized cells, ACE2 (green) can be seen throughout the cytoplasm of all cells (**Figure 3.3**). ACE2 expression on the surface of non-permeabilized cells exhibits clumps of ACE2 in some but not all cells (**Figure 3.4**). This suggests that surface ACE2 expression can be variable; however, there is ACE2 present on the cell surface.

ACE2 expression in HUVECs was confirmed with western blot analysis in duplicate samples (**Figure 3.5**). The presence of a band at around 97kDa was expected and seen in the blot. However, there were also other bands of higher molecular weight, which may represent nonspecific and/or degradation/cleavage products. VWF expression in HUVECs was confirmed with the presence of a strong band at around 250kDa. HEK293 cells were used as a negative control for VWF. Tubulin was used as a loading control for each sample. The VWF blot was cut and stripped and rehybridized to demonstrate the lack of ACE2 in HEK293 (**Figure 3.6**). There is an ACE2 band at ~97kDa in the HUVEC sample, and there does not appear to be ACE2 in the HEK293 sample.

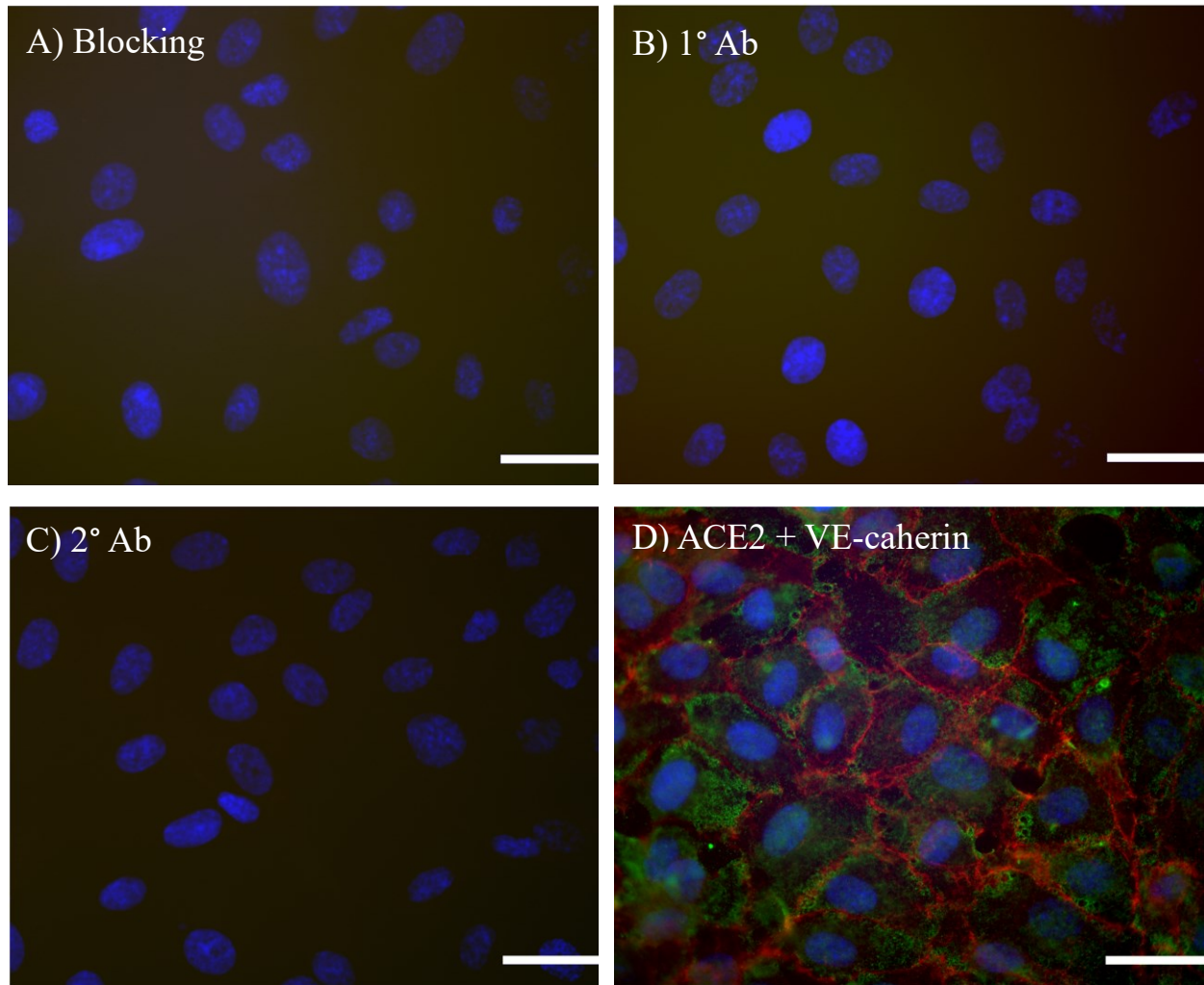


Figure 3.3 Immunofluorescence imaging of ACE2 expression on permeabilized HUVECs. A) Blocking control. **B)** Primary (1°) antibody (Ab) control. **C)** Secondary (2°) antibody control. **D)** ACE2 (green) and VE-cadherin (red) staining. Blue staining represents DAPI. The scale bar represents 95 μm (n=1).

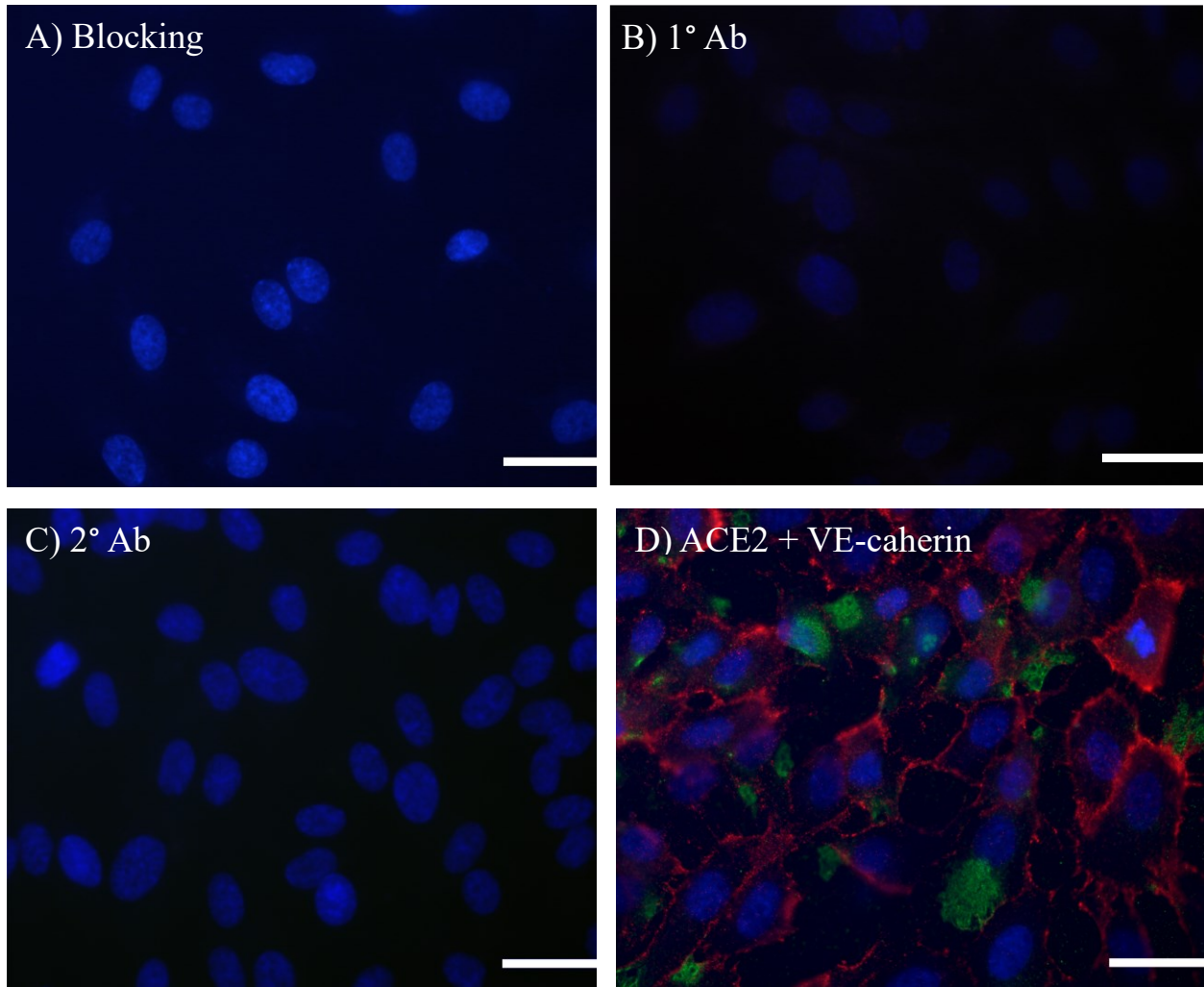


Figure 3.4 Immunofluorescence imaging of ACE2 expression on non-permeabilized HUVECs. A) Blocking control. **B)** Primary (1°) antibody (Ab) control. **C)** Secondary (2°) antibody control. **D)** ACE2 (green) and VE-cadherin (red) staining. Blue staining represents DAPI. The scale bar represents 95 μm (n=1).

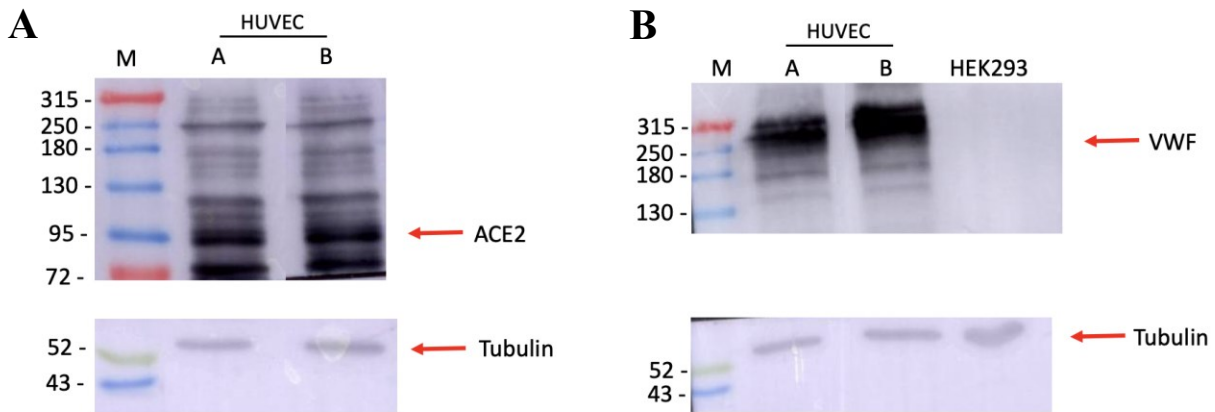


Figure 3.5 Representative western blot analysis of ACE2 and VWF protein expression in HUVECs. Duplicate HUVEC samples (A & B) were analyzed on the same blot. **A)** ACE2 protein expression and **B)** VWF protein expression with a HEK293 cell lysate used as a negative control. Tubulin was used as a loading control for both blots. The red arrow indicates the expected band for each ACE2, VWF and tubulin. The ladder is indicated by the marker “M” and all units are in kDa (n=1).

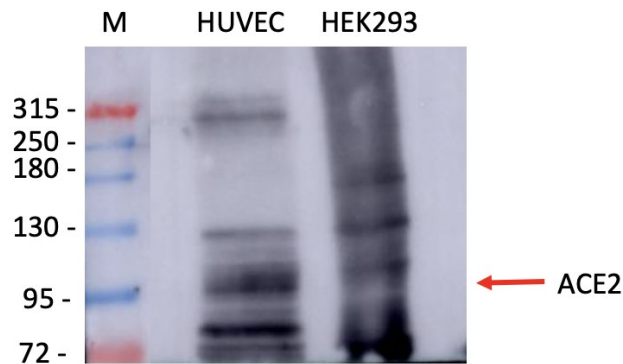


Figure 3.6 Rehybridized western blot showing ACE2 expression in HUVECs but not HEK293 cells. The blot from Figure 3.5B was stripped and rehybridized to show ACE2 expression. The band for ACE2 is indicated with an arrow. The ladder is indicated by the marker “M” and all units are in kDa (n=1).

3.3 The impact of Cx40 genotype on responses of isolated rat mesenteric arteries

Male and female 5–6-month-old WKY rats were used in all experiments. Cumulative ACh concentration response curves were constructed in the absence and presence of a combination inhibitors of endothelium-dependent vasodilation. Both TRAM-34 and apamin block endothelial K_{Ca} channels to inhibit EDH, while L-NAME blocks NO synthesis. These inhibitors were incubated with the arterial segments for twenty minutes prior to construction of a second ACh concentration response curve as described in **Section 2.10**. The log of the half-maximal effective concentration (EC_{50}) for ACh was calculated for each concentration-response curve (**Table 3.1**). Representative traces for control curves in all genotypes in both female and male animals are provided (**Figure 3.7**).

For each sex and genotype group, the effects of the inhibitors were compared. In the female group, each of the WT, HET and KO groups had significant overall differences between the experimental treatment groups ($p < 0.01$ for all groups). This can be seen as differences in the $\log EC_{50}$ of each curve (**Table 3.1**) as well as the mean data (**Figure 3.8**). In all groups the control curve had the lowest $\log EC_{50}$ followed by similar TRAM-34 and apamin and L-NAME curve $\log EC_{50}$ s and with the combination of all three inhibitors having the highest EC_{50} (**Table 3.1**). In the female group, in each of the control, TRAM-34 and apamin, and L-NAME groups within each genotype the maximum relaxation seen was $>90\%$ even in the presence of inhibitors (**Table 3.2**). The combination of TRAM-34, apamin, and L-NAME had the greatest inhibitory effect overall since the maximum relaxations in this group are all below 90%. The greatest inhibition of ACh-induced vasodilation was seen in the KO group ($64.9 \pm 13.9\%$).

When comparing the effects of the inhibitors in the male groups, there are more differences between the WT, HET, and KO groups. In the male WT group, the difference between the control

and treatment groups was significant ($p < 0.05$; **Figure 3.9A**), and 100 μM L-NAME alone caused the greatest inhibition of vasodilation where the maximum relaxation was reduced to $68.5\% \pm 8.3\%$ (**Table 3.2**). The control group had the lowest $\log EC_{50}$ while the other groups had similar and slightly higher $\log EC_{50}$ s than control (**Table 3.1**). The male HET group, the effect of the inhibitors was not overall significant (**Figure 3.9B**). The $\log EC_{50}$ values were very similar for the control, TRAM-34 and apamin, and L-NAME groups, while the group with all three inhibitors combined had the highest $\log EC_{50}$ (-6.7 ± 0.2) in the HET group (**Table 3.1**). Despite not being significant, the maximum relaxations observed for this group ranged from $78.2 \pm 11.4\%$ to $82.0 \pm 15.8\%$ in the groups with the inhibitors compared to the $95.9 \pm 1.0\%$ relaxation seen in the control group (**Table 3.2**). In the male KO group, the effects of the inhibitors were overall significant ($p < 0.01$; **Figure 3.9C**). The control group had the lowest $\log EC_{50}$ (-8.1 ± 0.1), while the group treated with TRAM-34 and apamin and L-NAME had the highest $\log EC_{50}$ (-6.6 ± 0.1) (**Table 3.1**). The maximum relaxations were above 90% in all groups except the group treated with TRAM-34, apamin, and L-NAME which exhibited the greatest inhibitory effect and relaxed to $75.2 \pm 4.2\%$ of PE-induced tone (**Table 3.2**).

Since I was interested in the difference between the genotypes and their responses, I also compared the effects of genotype in each group (control, TRAM-34 and apamin, L-NAME, and TRAM-34, apamin, and L-NAME combined).

In females, there was no significant difference between genotypes in the control, TRAM-34 and apamin, and L-NAME groups (**Figure 3.10A-C**). The $\log EC_{50}$ values for these groups are very similar (**Table 3.1**) as well as the maximum relaxation observed (**Table 3.2**). The only group that had a significant difference between the genotypes was the group with all three inhibitors (**Figure 3.10D**). The WT and HET curves are very similar, but the greatest difference between the

curves is seen in the KO group. Compared to the other genotypes, the KO group had the lowest maximum relaxation ($64.9 \pm 13.9\%$ vs $89.5 \pm 2.7\%$ and $84.8 \pm 5.6\%$ for WT and HET respectively; **Table 3.2**) as well as the highest $\log EC_{50}$ (-6.4 ± 0.2 vs -6.6 ± 0.1 and -6.7 ± 0.1 for WT and HET respectively; **Table 3.1**).

In males, the only significant difference between the genotypes was seen in the control group ($p < 0.05$; **Figure 3.11A**). The $\log EC_{50}$ values for this group vary (WT: -7.7 ± 0.1 , HET: -7.4 ± 0.1 , and KO: -8.1 ± 0.1 ; **Table 3.1**); however, the maximum relaxations are very similar (**Table 3.2**). There was no significant difference between the genotypes in any of the groups with inhibitors (**Figure 3.11B-D**). Despite this, there is a difference in the maximum relaxation induced by ACh for each of these groups (**Table 3.2**). In the TRAM-34 and apamin group, both the WT and KO groups relaxed $> 95\%$, while the HET group demonstrated $82.0 \pm 15.8\%$ relaxation. In the L-NAME group, there was a great variation between each genotype; WT vessels exhibited the least amount of relaxation ($66.9 \pm 17.1\%$) followed by a higher relaxation in the HET group ($80.3 \pm 14.7\%$), and an almost complete relaxation achieved in the KO group ($90.2 \pm 0.6\%$). In the group containing all the inhibitors, the highest relaxation was seen in the WT group ($90.4 \pm 1.9\%$), while both the HET and KO groups relaxed to $78.2 \pm 11.4\%$ and $75.2 \pm 4.2\%$ of the maximum respectively.

The effects of the inhibitors differed slightly between female and male groups. All the groups except for the male HET group had a significant difference between the experimental groups using inhibitors (**Figures 3.8 & 3.9**). In the control group for both female and male rats of all genotypes, the maximum relaxations were all greater than 95% (**Table 3.2**). The $\log EC_{50}$ s of the WT and HET female and male groups were virtually identical (**Table 3.1**). The male KO group

had a slightly lower logEC₅₀ than the female KO group (-8.1 ± 0.1 vs -7.7 ± 0.1). However, the effect of genotype was significant in the males but not the females (**Figures 3.10A & 3.11A**).

In the TRAM-34 and apamin group, the logEC₅₀s ranged from -7.5 to -7.2; between female and male groups of the same genotype the logEC₅₀s were very similar (**Table 3.1**). The maximum relaxation was greater than 94% in all groups except the male HET group that only had a maximum relaxation of $82.0 \pm 15.8\%$ (**Table 3.2**). The effects of genotype were not significant for either the females or males in this group (**Figures 3.10B & 3.11B**).

The L-NAME group also had similar logEC₅₀s (between -7.4 to -7.2) between the female and male groups of the same genotype (**Table 3.1**). The maximum relaxation was quite variable between female and male genotypes. In all female genotypes, the maximum relaxation was greater than 94%, but in the male genotypes differed greatly both among each other and from the female values for the same genotype (**Table 3.2**). The male WT group had the lowest maximum relaxation followed by the HET and KO groups ($66.9 \pm 17.1\%$, $80.3 \pm 14.7\%$, and $90.2 \pm 0.6\%$ respectively; **Table 3.2**). The effects of genotype were not significant for either the females or males in this group (**Figures 3.10C & 3.11C**).

The group containing TRAM-34, apamin, and L-NAME, had the highest logEC₅₀ and lowest maximum relaxations for both the male and female groups. The female WT group had a slightly higher logEC₅₀ than the male group (-6.6 ± 0.1 vs -7.0 ± 0.1), while in the HET group there was virtually no difference between the female and male groups (-6.7 ± 0.1 vs -6.7 ± 0.2) (**Table 3.1**). The female KO group had a slightly higher logEC₅₀ than the male KO group (-6.4 ± 0.2 vs -6.6 ± 0.1). The maximum relaxations in the female and male WT group were almost identical ($89.5 \pm 2.7\%$ vs $90.4 \pm 1.9\%$), while the female and male HET group were lower than WT and the female HET group had a higher maximum relaxation compared to the male HET (84.8

$\pm 5.6\%$ vs $78.2 \pm 11.4\%$) (**Table 3.2**). The KO group had the smallest maximum relaxation in both males and females in this group, however, the difference between these was much greater ($64.9 \pm 13.9\%$ vs $75.2 \pm 4.2\%$). The female genotypes were significantly different in their response to TRAM-34, apamin, and L-NAME, while the male genotypes were not (**Figures 3.10D & 3.11D**).

To determine if Cx40 genotype influenced vessel contraction, the contractile force (mN) elicited by $3 \mu\text{M}$ phenylephrine prior to application of ACh were measured (**Figure 3.12**). In the female group there was a significant difference between WT and KO ($5.6 \pm 0.7\text{mN}$ vs $8.7 \pm 1.3\text{mN}$ respectively; $p < 0.05$), but not between WT and HET ($5.6 \pm 0.7\text{mN}$ vs $7.1 \pm 1.1\text{mN}$) or between HET and KO ($7.1 \pm 1.1\text{mN}$ vs $8.7 \pm 1.3\text{mN}$) (**Figure 3.12A**). In the male group there was a significant difference between both WT and KO ($5.9 \pm 0.6\text{mN}$ vs $9.7 \pm 0.8\text{mN}$; $p < 0.01$) and between HET and KO ($5.9 \pm 1.2\text{mN}$ vs $9.7 \pm 0.8\text{mN}$; $p < 0.05$), but not between WT and HET ($5.9 \pm 0.6\text{mN}$ vs $5.9 \pm 1.2\text{mN}$) (**Figure 3.12B**). In both sexes, the WT and KO groups were significantly different from each other. The WT contractions in the female vs male group are similar ($5.6 \pm 0.7\text{mN}$ vs $5.9 \pm 0.6\text{mN}$), while in the HET group, the females exhibit higher average contraction than the males ($7.1 \pm 1.1\text{mN}$ vs $5.9 \pm 1.2\text{mN}$). The male KO group exhibited slightly higher contractile force than the female group ($9.7 \pm 0.8\text{mN}$ vs $8.7 \pm 1.3\text{mN}$).

Overall, the effects of the inhibitors TRAM-34, apamin, and L-NAME on ACh-induced vasodilation in male and female WT, HET, and KO isolated mesenteric arteries was significant except in the male HET group. When the effect of genotype was compared in each treatment group, the only significant differences due to genotype were seen in the female group containing TRAM-34, apamin, and L-NAME and the male control group. There was a significant difference between the WT and KO contractile force in both the female and male groups. In addition, the contractile force values between the male HET and KO groups were also significantly different.

Table 3.1 logEC₅₀ (M) of ACh concentration response curves in male and female rats				
	Control	TRAM-34 + apamin	L-NAME	TRAM-34 + apamin + L-NAME
Female				
WT	-7.7 ± 0.1	-7.2 ± 0.1	-7.3 ± 0.1	-6.6 ± 0.1
HET	-7.4 ± 0.1	-7.2 ± 0.1	-7.2 ± 0.1	-6.7 ± 0.1
KO	-7.9 ± 0.2	-7.4 ± 0.1	-7.3 ± 0.2	-6.4 ± 0.2
Male				
WT	-7.7 ± 0.1	-7.1 ± 0.1	-7.3 ± 0.3	-7.0 ± 0.1
HET	-7.4 ± 0.1	-7.2 ± 0.2	-7.4 ± 0.2	-6.7 ± 0.2
KO	-8.1 ± 0.1	-7.5 ± 0.1	-7.4 ± 0.1	-6.6 ± 0.1

Table 3.1 logEC₅₀ of ACh concentration response curves in male and female rats. Each data point is represented as mean ± SEM (n=4-7).

Table 3.2 Maximal relaxation induced by ACh				
	Control	TRAM-34 + apamin	L-NAME	TRAM-34 + apamin + L-NAME
Female				
WT	99.0 ± 0.2%	94.1 ± 3.1%	95.7 ± 0.8%	89.5 ± 2.7%
HET	97.4 ± 1.1%	97.6 ± 0.9%	97.6 ± 1.2%	84.8 ± 5.6%
KO	98.9 ± 0.2%	97.2 ± 0.5%	94.2 ± 1.4%	64.9 ± 13.9%
Male				
WT	98.1 ± 0.7%	95.6 ± 1.3%	66.9 ± 17.1%	90.4 ± 1.9%
HET	95.9 ± 1.0%	82.0 ± 15.8%	80.3 ± 14.7%	78.2 ± 11.4%
KO	97.9 ± 0.6%	95.6 ± 0.7%	90.2 ± 0.6%	75.2 ± 4.2%

Table 3.2 Maximum relaxation induced by ACh in the presence and absence of inhibitors. These values are expressed as % relaxation of phenylephrine-induced tone. Data is presented as mean ± SEM (n=4-7).

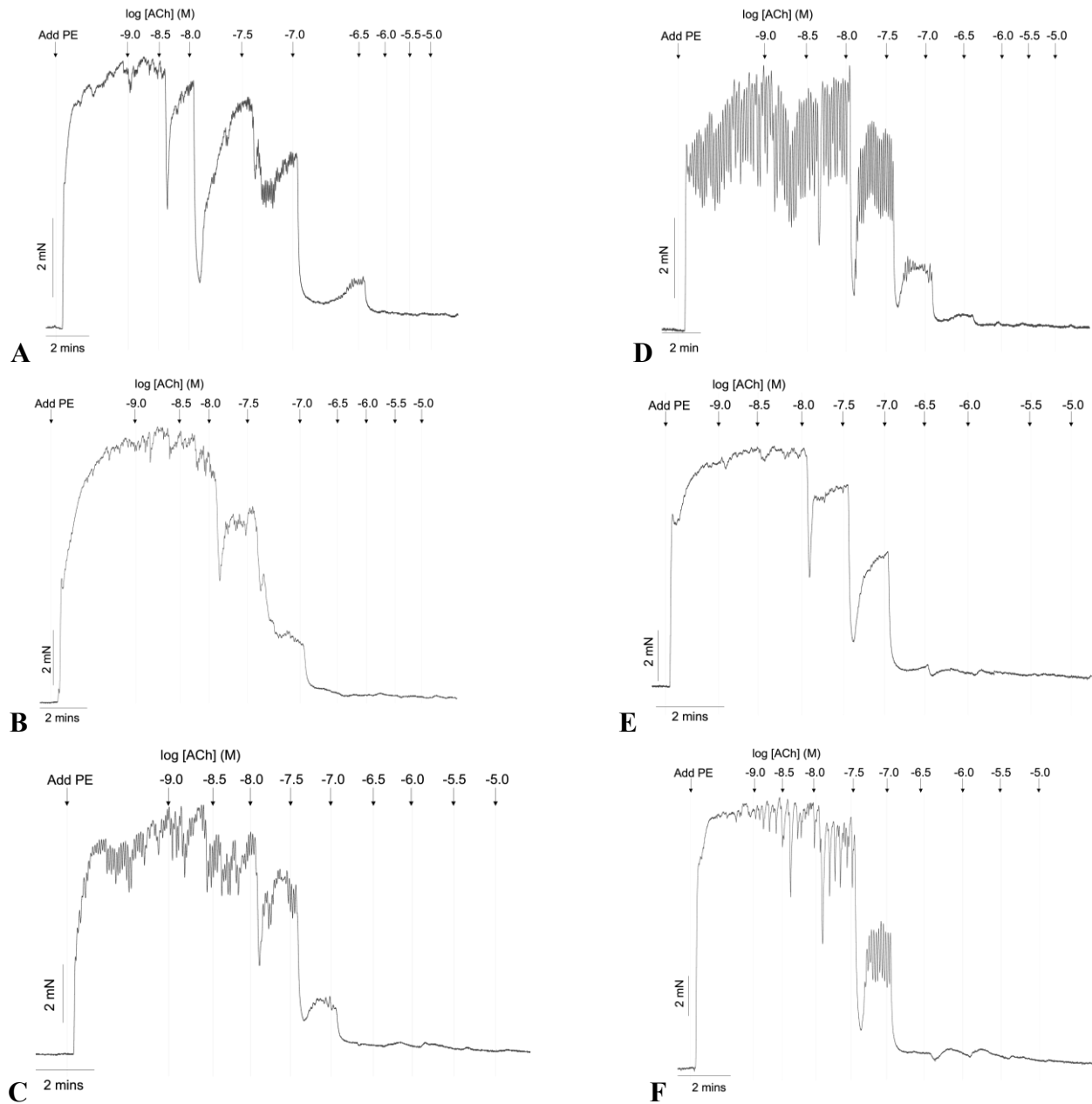


Figure 3.7 Representative traces of control ACh concentration response curves in male and female Cx40 WT, HET, and KO rat mesenteric arteries. A) Female WT B) Female HET C) Female KO D) Male WT E) Male HET F) Male KO. Vascular tone was increased with 3 μ M PE and increasing cumulative concentrations of ACh from 1nM to 10 μ M were added to the vessel baths in a wire myograph. Isometric force was measured in mN vs time.

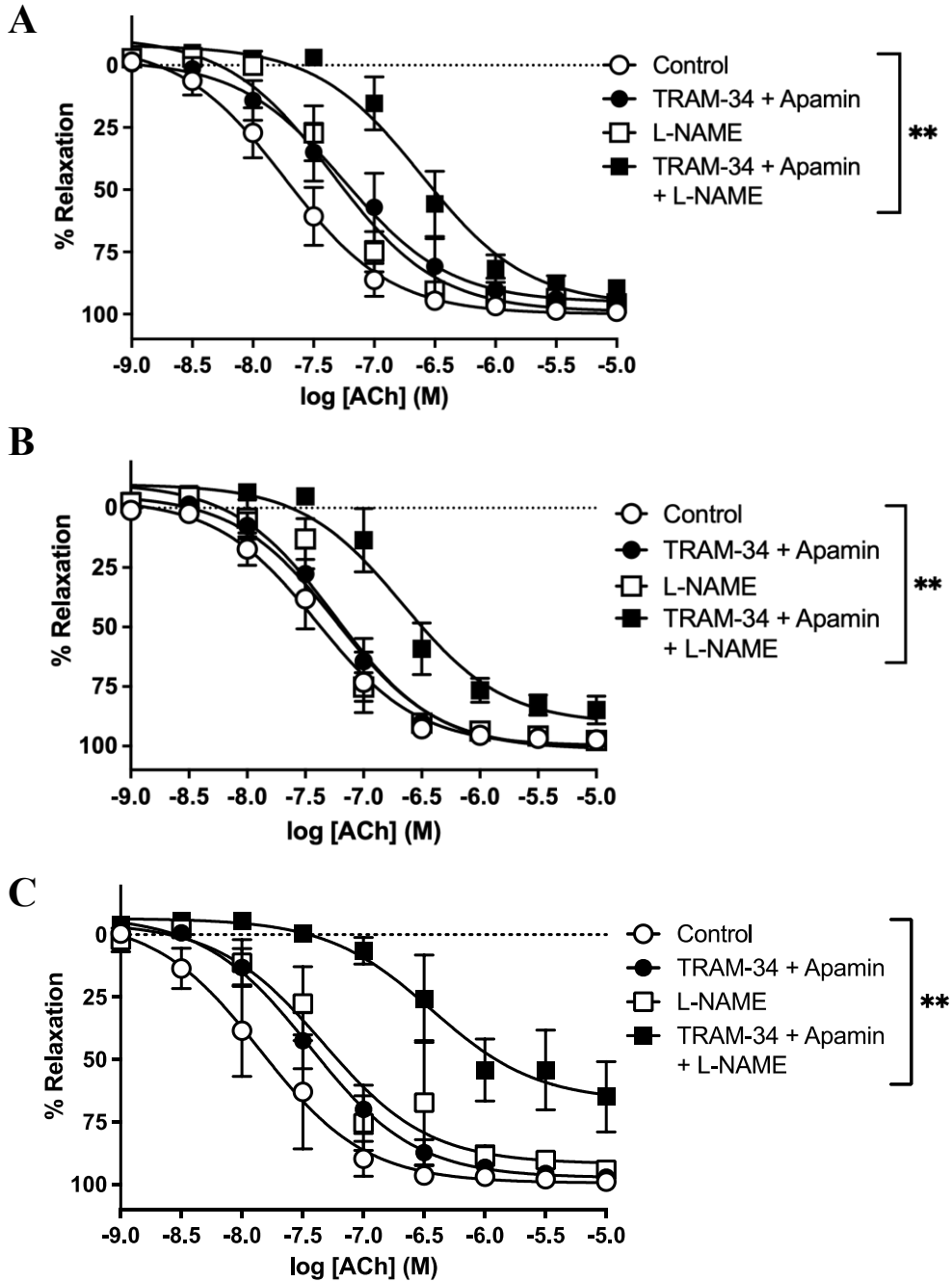


Figure 3.8 The effects of the inhibitors TRAM-34, apamin, and L-NAME on ACh concentration response curves in female WT, HET, and KO rat mesenteric arteries. Each ACh cumulative concentration response curve was completed after a 20 min incubation with various combinations of TRAM-34 (1 μ M), apamin (50 nM), and L-NAME (100 μ M). Vessel tone was elevated with 3 μ M PE before each curve. **A)** Female WT **B)** Female HET **C)** Female KO. Each data point represents the mean \pm SEM (n=4-7) with a p-value < 0.05 being considered significant. ** denotes p<0.01. *Note: some data contributed by Brandon Truong and Sufyan Malik.*

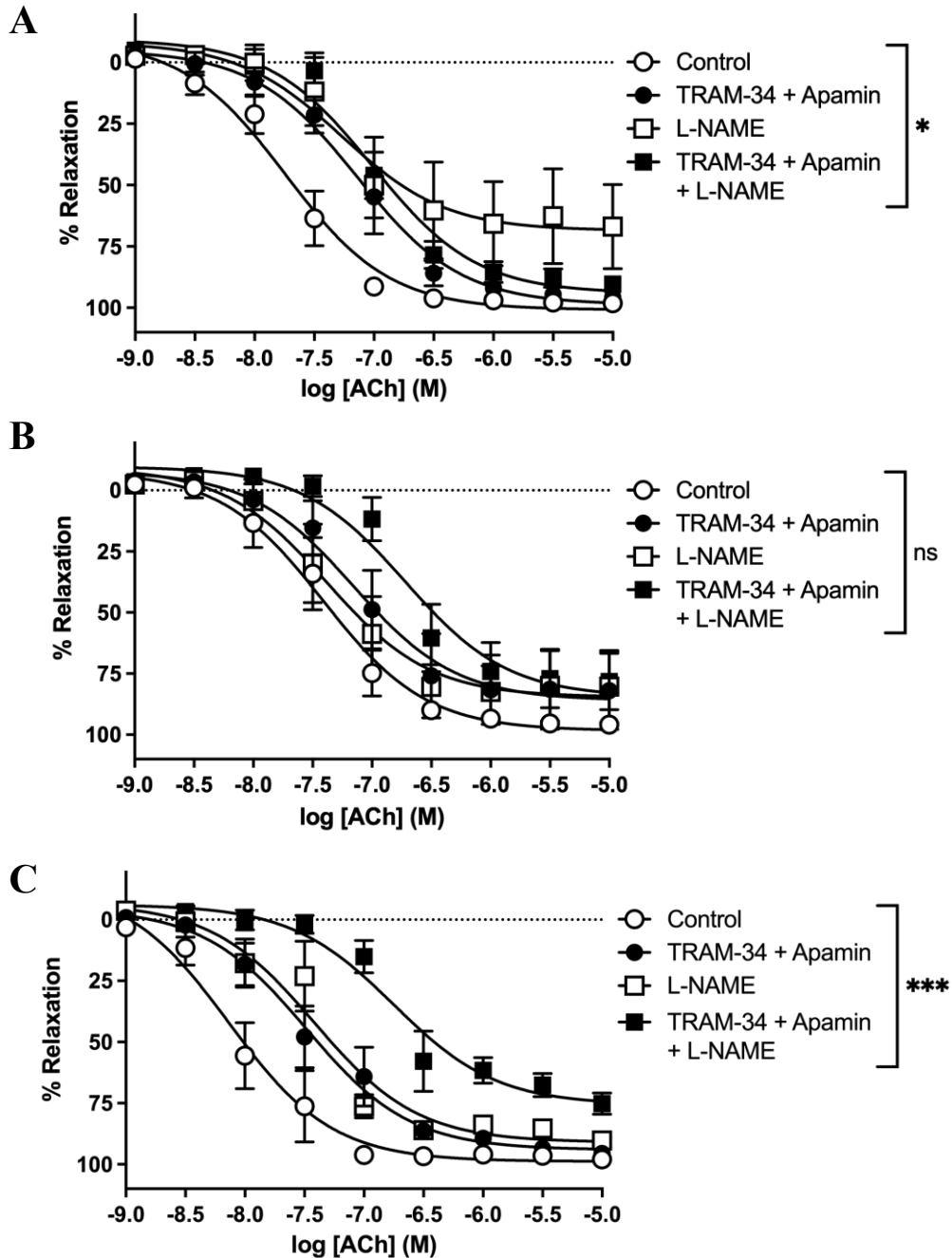


Figure 3.9 The effects of the inhibitors TRAM-34, apamin, and L-NAME on ACh concentration response curves in male WT, HET, and KO rat mesenteric arteries. Each ACh cumulative concentration response curve was completed after a 20 min incubation with various combinations of TRAM-34 (1 μ M), apamin (50 nM), and L-NAME (100 μ M). Vessel tone was elevated with 3 μ M PE before each curve. **A)** Male WT **B)** Male HET **C)** Male KO. Each data point represents the mean \pm SEM (n=4-7) with a p-value < 0.05 being considered significant. *denotes p<0.05; ***denotes p<0.001. *Note: some data contributed by Brandon Truong and Sufyan Malik.*

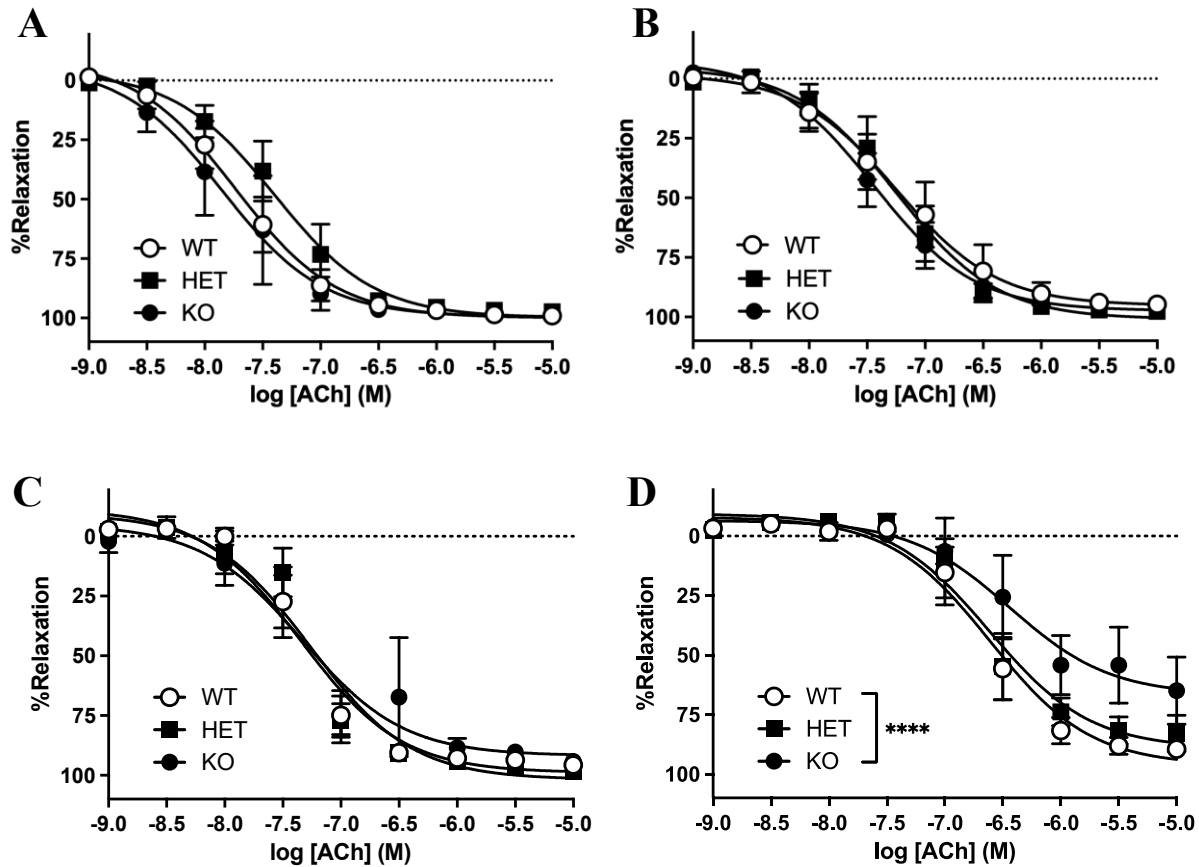


Figure 3.10 The influence of Cx40 genotype in ACh concentration response curves in female WT, HET, and KO rat mesenteric arteries. **A)** Control **B)** TRAM-34 (1 μ M) + apamin (50 nM) **C)** L-NAME (100 μ M) **D)** TRAM-34 + apamin + L-NAME. Each data point represents the mean \pm SEM (n=4-7) with a p-value < 0.05 considered significant. ****denotes p<0.0001.

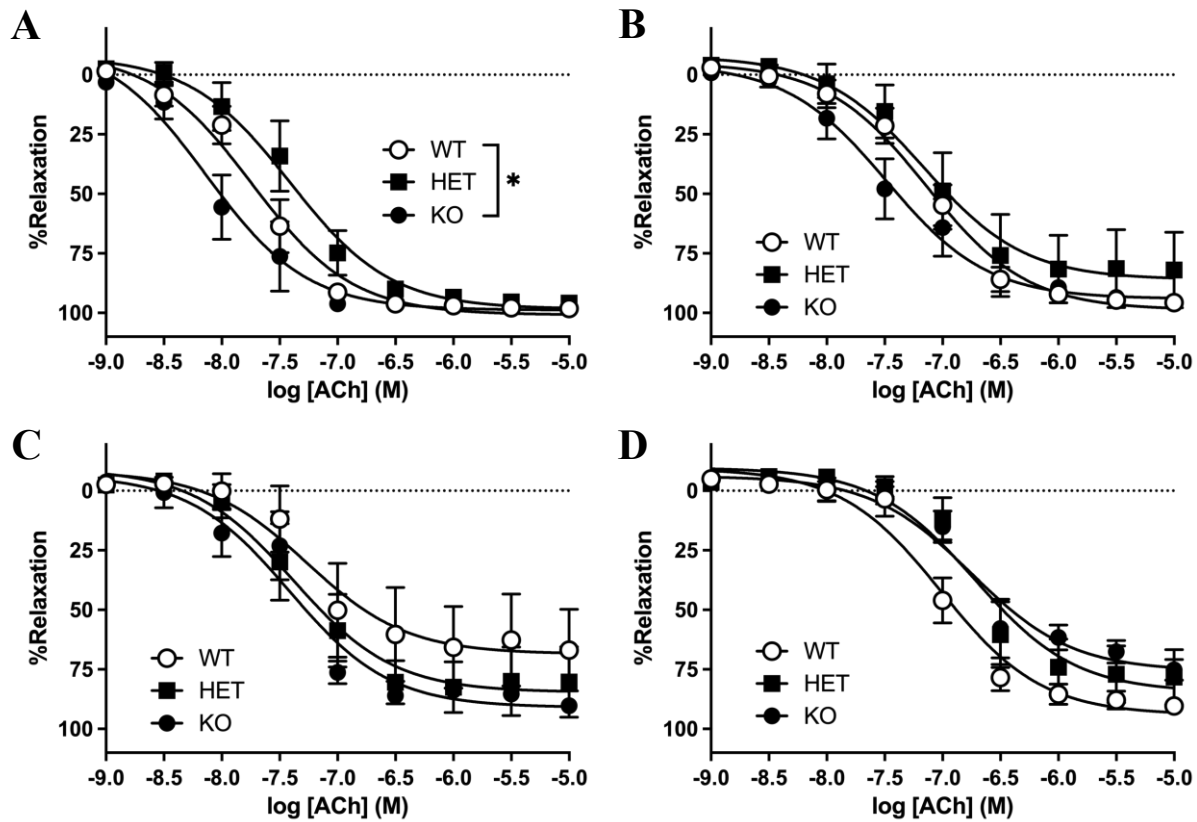


Figure 3.11 The influence of Cx40 genotype in ACh concentration response curves in male WT, HET, and KO rat mesenteric arteries. **A)** Control **B)** TRAM-34 (1 μ M) + apamin (50 nM) **C)** L-NAME (100 μ M) **D)** TRAM-34 + apamin + L-NAME. Each data point represents the mean \pm SEM (n=4-7) with a p-value < 0.05 considered significant. *denotes p<0.05.

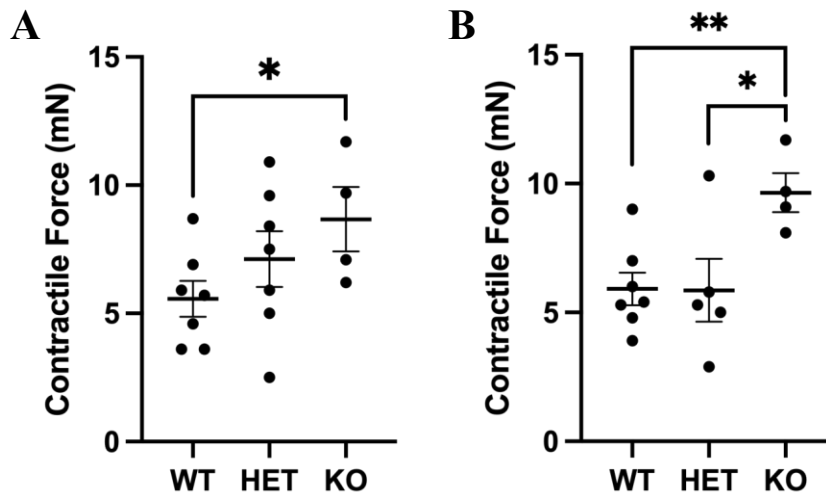


Figure 3.12 Contractile force of isolated rat mesenteric arteries in response to PE. The contractile force in both **A**) female and **B**) male Cx40 WT, HET and KO intact isolated mesenteric arteries was measured prior to performing ACh concentration response curves. The difference between baseline tension before and after the addition of 3 μ M PE to the bath was calculated and graphed. Data is represented as the mean \pm SEM (n=4-7) with a p-value<0.05 considered significant. *denotes p<0.05; **denotes p<0.01.

Chapter 4: Discussion

4.1 The effects of SARS-CoV-2 spike protein exposure on cultured HUVECs

It is well established that severe infection with SARS-CoV-2 leads to inflammation and thrombotic complications that arise from the release of many procoagulant molecules such as VWF from endothelial cells.^{45,140} Whether this is due to inflammation of surrounding tissues and/or due to viral interactions with endothelial cells is not known. Although it is not yet fully established whether or not endothelial cells are infected with SARS-CoV-2, electron microscopy has shown the presence of SARS-CoV-2 in endothelial cells in autopsy tissues; however, this does not mean that the virus is able to replicate in these cells.³²⁸ Despite conflicting evidence, this does not preclude the spike protein from interacting with ACE2 receptors on the surface of endothelial cells and triggering a response. My goal was to begin establishing the impact of endothelial cell exposure to SARS-CoV-2 spike protein to lay the ground for further research in order to determine whether the spike protein interacts with ACE2 on endothelial cells and whether such interaction could trigger an endothelial response consistent with increased VWF levels, and if so to elucidate the mechanism through which this happens.

From my results, it is evident that exposure of HUVECs to spike protein has a significant effect on VWF release, if not VWF transcription. Induction within in the first hour such as what is seen at the 5-minute mark is similar to what has been reported for other inducers of VWF release, including hypoxia.³²⁹ In addition, our results demonstrated that magnitude of induction remained at approximately 2-fold, irrespective of starting basal levels of VWF. This suggests that spike protein exposure of endothelial cells with high basal levels of VWF may translate to sufficiently high levels of VWF that can significantly alter VWF/ADAMTS13 ratio to invoke procoagulant and thrombogenic activity. While the VWF mRNA levels were not significantly altered at the 48h

or 72h post exposure to spike protein, an increasing trend was observed in treated cells compared to control at these time points. These results were combined analyses from two independent sources of HUVECs, and it may be possible that with inclusion of data from additional HUVEC sources, such an increasing trend could reach statistical significance. A challenge with assessing VWF mRNA levels in primary cell cultures is that these cells originate from individual human donors, and there may be significant heterogeneity in potential transcriptional response of VWF to inducers; this highlights the value of completing more replicate experiments. Furthermore, there is heterogeneity of endothelial cells from various organs regarding structure, function, and molecular signature. Thus, it is not unlikely that endothelial cells from distinct organs may respond differently. In our analyses of VWF response to hypoxia, our group had also originally explored HUVECs, and our analyses had demonstrated that while VWF release from WPB occurred within 5 min of hypoxia exposure of HUVECs, increased mRNA levels were not significantly altered at any time points, although an increasing trend at 72 hours were observed (data not shown). However, when endothelial cells from lung and heart vasculature were exposed to hypoxia, a significant increase in VWF mRNA at 48-72 hours were observed.^{18,329} Thus, we propose that using endothelial cells from other organs for determining VWF response to spike protein exposure is necessary to obtain a clearer picture of a potential VWF response at the transcriptional level. In addition, to gain more insight into whether VWF mRNA levels are altered, we can explore whether cellular protein levels are altered after cell exposure to spike protein. While any such alterations may be indicative of increased translational efficiencies or protein stability, it may also reflect increased levels of template VWF mRNA available for translation. Cellular VWF protein levels may be determined and compared by Western blot analyses as shown in **Figure 3.5** in control and spike treated endothelial cells over time at the beginning (t=0), 5 minutes, and 72h post spike

treatment. Cellular protein levels are important to determine even if VWF mRNA levels were to be increased in response to spike treatment, because changes in mRNA levels do not always translate to changes in protein expression.

The notion that ACE2 engagement by the SARS-CoV-2 can modulate endothelial cell phenotype, including VWF levels, is supported by recent findings by Perico *et al.*³³⁰ This group studied the ability of the S1 spike protein to change the phenotype of human microvascular endothelial cells (HMEC-1). Their focus was mostly on the complement system as well as thrombotic markers, including VWF and intercellular adhesion molecule 1 (ICAM-1), an adhesion glycoprotein on the surface of endothelial cells. Results from this work that are relevant to this project are the fact that treatment of HMECs with S1 spike protein had a dose dependent effect on VWF deposition in the extracellular matrix using immunofluorescence imaging quantification. This group also demonstrated that these effects were attenuated by treatment of the cells with anti-ACE2 antibody in conjunction with S1 but not when the cells were treated with an irrelevant antibody. They also repeated these experiments in lung endothelial cells and found similar results. When this is taken into consideration, it is consistent with our observations, suggesting that effects that I observed could be due to the spike protein binding to ACE2. However, similar ACE2 blocking experiments in my investigations would be needed to support this.

I did demonstrate ACE2 expression on the surface of HUVECs but beyond this, investigating the effects of HUVEC treatment with ACE2 antibody is a first step in determining the role of ACE2 engagement in inducing VWF release and/or upregulation of expression. This will help us to determine if ACE2 engagement alone causes VWF release (i.e., antibody elicits similar responses as the spike protein) or if ACE2 antibody treatment in conjunction with spike protein is successful in attenuating the responses seen with cell exposure to the spike protein. This

would suggest that the antibody is blocking the effects of spike protein-ACE2 interactions. Based on the results from Perico *et al*, we would expect that ACE2 antibody would attenuate responses seen with the treatment of cells with the spike protein.

I have established that SARS-CoV-2 treatment of endothelial cells results in an increase in VWF release. It is likely that my results are due to spike protein-ACE2 interactions, but the mechanism for this response is currently unknown and is part of what this project eventually aims to determine. Acute VWF release due to thrombin and histamine is due to an increase in intracellular calcium.^{53,331} Other agonists such as adenosine, prostacyclin, and DDAVP have been shown to cause VWF release from WPB through a cyclic adenosine monophosphate (cAMP)-dependent manner.³³²⁻³³⁴ Similarly, it is possible that the increase in VWF that I reported is due to similar increases in second messenger signaling in endothelial cells.

It is also important to consider tissue specificity in thrombogenic responses. Unpublished data from our lab has shown organ specific changes in VWF expression in response to aging and published results show differences in responses to hypoxia.¹⁸ In addition, SARS-CoV-2 infection does not only affect the vascular system, but the greatest effects are also seen in the lungs since the respiratory tract is the viral point of entry in the body.¹³⁹ It is well established that lung epithelial cells are infected by the virus, but these are also adjacent to lung endothelial cells.^{123,124} Therefore, investigating the impacts of SARS-CoV-2 spike protein through similar experiments in lung endothelial cells would be valuable. Our lab has previously demonstrated that hypoxia causes *de novo* activation of VWF in lung microvascular endothelial cells; based on these findings it is possible that other activators of VWF expression may elicit a similar response.³²⁹ In addition, investigating the effects of spike protein exposure on endothelial cells of other organs known to be affected by severe infection could reveal whether there is a contribution of VWF to their

dysfunction. Such cells would primarily include brain microvascular endothelial cells, as well as cardiac, kidney, and liver endothelial cells.

The elevation of thrombotic markers such as VWF is well established in severe infection with SARS-CoV-2 and understanding the mechanisms through which this occurs is valuable. Investigating the effects of SARS-CoV-2 spike protein beyond viral infection is significant because spike protein in the circulation has been detected in serum from some hospitalized patients.³³⁰ While these levels may not be as high as those seen after initial infection, it is possible that even low levels of the spike protein can have detrimental effects and contribute to disease severity. Considering that patients with comorbidities that are shown to elicit high levels of VWF, such as diabetes and aging, are more susceptible to thrombotic consequences and that my results demonstrated an approximately two fold increase in secreted VWF in response to spike exposure regardless of basal levels, this suggests that these patient population may be specifically susceptible to the consequences of SARS-CoV-2 infection with regard to elevated levels of VWF and its thrombogenic consequences.³³⁵ This project is part of an effort to understand the effects and mechanism of SARS-CoV-2 infection that are associated with an observed increase in VWF levels.

4.2 The impact of Cx40 genotype on isolated rat mesenteric arteries

Previous studies examining the effects of Cx40 KO in animal models have usually been in mice – there has not been an established Cx40 KO rat model. These previous studies have indicated that Cx40 plays an important role in the transduction of signals both longitudinally through endothelial and smooth muscle cell GJs, and also radially through MEGJs. Therefore, one of the main goals of my project was to contribute to the characterization of this Cx40 to endothelium-dependent vasorelaxation in the rat KO model. In addition, most of the previous studies involved

other resistance vessels such as cremaster arterioles and also involved the study of conducted responses.

The actions of the inhibitors TRAM-34, apamin, and L-NAME as inhibitors of endothelium-dependent vasodilation are well established with the three blockers together causing significant reductions in ACh-evoked relaxation in isolated arteries. This matches what was seen in the present study in all female genotypes and the WT and KO male groups, but not the male HET group. The responses to ACh-induced vasodilation were not identical between groups; however, they were not different enough to be significant.

When comparing the impact of genotype in each experimental treatment group, there were few differences. The only statistically significant differences seen were in the female group treated with TRAM-34 and apamin and L-NAME, where the KO response was quite different. In the male group, the only significant difference was seen in the control group. The lack of greater significant differences between the genotypes is not surprising. Cxs are largely implicated in the conduction of responses along a vessel through the spread of signaling molecules from an origin point. However, the wire myograph is not an apparatus in which conducted responses along a vessel can be measured, rather the vessel is submerged in a bath where the desired compounds/reagents are added. This means that the vessel is stimulated along its entire length, removing the need for conducted responses to elicit a response to whichever stimulus the vessel is subjected to. The significant differences seen in this data are interesting, but not consistent between sex or genotype.

This supports the study of rat resistance arteries in other experimental setups that examine the impact of Cx40 KO on physiological stimuli. ACh was used in these experiments as an example of receptor-mediated stimulus on endothelial cells. ACh receptors are widely present on endothelial cells however the source of this ACh is not clear. Wilson *et al* demonstrated that

endothelial cells can release ACh in response to flow.³³⁶ It has also been suggested that platelets are able to release ACh and may be a source of ACh that is able to affect endothelial cells.³³⁷ Shear stress and pressure have been shown to influence Cx expression, and thus using an apparatus in which the pressure can be manipulated such as a pressure myograph would be of interest. In addition, the effects of flow and shear stress can be examined in the perfused mesenteric bed where the effects of nerve-evoked vasoconstriction in the presence of flow can be elucidated. Most importantly, the study of conducted responses in rat resistance artery preparations would allow us to further examine the impact of Cx40 KO and the importance of Cx40 in conducted responses in endothelium-dependent vasodilation.

In mouse Cx40 KO models, hypertension has been reported, but there is no evidence of increased blood pressure in these our rat Cx40 KO model.^{310,338} This could be due to the compensatory increase in expression of other Cxs in the vasculature to make up for the loss of Cx40. Since modified Cx40 expression has been reported in disease states such as hypertension and atherosclerosis and their consequences such as increased vessel wall shear stress, the effects of Cx40 knockout may become more pronounced when these animals undergo physiological stress. For example, animals fed a high fat diet, which is consistent with worsening control of vascular diameter, could exhibit a greater impairment of endothelium-dependent vasodilation. In this case it is possible that Cx40 KO rats would have a greater impairment compared to WT animals.

The need for a Cx40 KO model is highlighted by the complexity of Cx oligomerization. Multiple different Cxs can come together to form a GJ. This makes the study of the contribution of each Cx very complicated since the inhibitors that exist are not very specific for a single connexin. Most Cx inhibitors act on both hemichannels and GJ and completely block the effects

of both.³³⁹ Challenges in using GJ inhibitors include the need for very high doses and long incubation time required to guarantee full channel blockade. In addition, many inhibitors also do not display any Cx selectivity adding another layer of complexity. These inhibitors may also elicit other effects that are not related to GJ inhibition. For example, carbenoxolone, a non-specific GJ inhibitor, also blocks Ca^{2+} channels, pannexin channels, and P_2X_7 receptors at concentrations lower than those that elicit GJ blockade.³³⁹ These issues emphasize the need for a KO model to study the effects of various Cxs. Many experiments have been done in mouse Cx40 KO models; however, rats are considered to be a closer model to humans than mice. Therefore, our rat KO model is valuable tool to study the effects of Cx40 KO.

The difference between PE-evoked contractile force in both the female and male groups was of interest. While Cx40 is implicated in the formation of GJs between endothelial cells, it also contributes to the formation of MEGJs between endothelial and smooth muscle cells. Therefore, there could also be an impairment of smooth muscle to endothelial communication. Unpublished data from our lab has shown a significant increase in perfusion pressure with perivascular nerve stimulation in KO vs HET or WT animals. Increased perfusion pressure indicates muscle contraction and narrowing of the vessel lumen. In this case, we hypothesize that these effects could be due to impaired myoendothelial feedback. This phenomenon occurs when during vasoconstriction, IP_3 moves from smooth muscle to endothelial cells via MEGJs.³⁴⁰ This causes an increase in endothelial cell intracellular Ca^{2+} which activates K_{Ca} channels. This feedback mechanism limits vasoconstriction. Lack of Cx40 can cause impairment of MEGJ formation and communication since it is implicated in their formation and could explain the increased contractile response seen in the KO animals. Further inquiry into the role of Cx40 in myoendothelial feedback could elucidate one of the roles of this Cx in the vasculature.

In conclusion, Cx40 is present in endothelial cells and forms GJs that allow for communication of cells that comprise the vessel wall. More work needs to be done to fully characterize the impact of Cx40 KO on endothelium-dependent vasodilation and cardiovascular function.

4.3 Limitations

It is important to acknowledge that my project has some limitations both due to the nature of the protocols and assays used as well as my experimental design.

My experimental design involved the exposure of HUVECs to 1nM SARS-CoV-2 spike protein. I chose this concentration based on the concentrations used in previous work.^{325,326} However, in addition to reading the literature, time committing, I could have evaluated the effects of various concentrations of the spike protein by evaluating a concentration response curve to determine an optimal concentration of spike protein that elicits an increase in VWF production and/or release for my work. Another limitation of this design is that the SARS-CoV-2 spike protein has mutated with the variants to increase viral survival and transmissibility. The spike protein that I used originates from the original virus. It is possible that mutated spike proteins may elicit a different magnitude of response in endothelial cells; however, using this spike protein still reveals valuable information with regards to the consequences of spike protein exposure in these cells.

Endothelial cells are heterogenous, and their responses to various stimuli may vary based on the organ from which they are obtained.³⁴¹ Additionally, our lab has specifically shown heterogeneity in endothelial cell VWF upregulation and release to hypoxia.¹⁸ Therefore, caution should be taken when translating these results both to other endothelial cell types in culture as well as physiologically. HUVECs can be a good model to confirm whether certain conditions may have an effect on endothelial cells in general; however, they are not organ specific. Furthermore, they

come from large vasculature, while most of the endothelial cells affected by SARS-CoV-2 are in the microvasculature. This emphasizes the importance of completing similar experiments in organ-specific endothelial cells to determine if the effects of the SARS-CoV-2 spike protein persist in these cultures. The nature of cell culture lends itself to limitations. It is a valuable tool in elucidating cell functions and characteristics, but these may not represent what happens physiologically. In the body, organs are made of many different cell types that function together synergistically; this is lacking in cell culture where one cell type is cultured alone in a dish. Physiologically, endothelial cells line the blood vessel, culture reduces this to a 2-dimensional model that removes another characteristic important for their function. Endothelial cells are subject to shear flow which is not present in static cell culture. This could be overcome by culturing cells and subjecting them to laminar or disturbed flow conditions, but even this has its limitations since the cells are still missing integrated signalling sources such as from nerves, the blood, and surrounding tissue. In the context of studying endothelial cells, various vessels from specific organs could be isolated and studied in an organ bath or flow chamber. This allows the cells to operate in a system where other cells are present, but nerve inputs as well as other signalling molecules present in the blood are absent.

The assays I used to detect protein and mRNA expression each come with their own limitations. Measuring mRNA alone using RT-qPCR, while a useful tool to assess changes in transcription, cannot directly correlate to protein levels in the cell.³⁴² mRNA by nature is unstable and may degrade before translation is able to occur. This should be considered while interpreting any changes in mRNA expression, and the difference between mRNA levels and protein levels should be examined. *In situ* hybridization along with immunofluorescence imaging can be used to interpret the relative amounts of mRNA and protein in the cell respectively. immunofluorescence

imaging is a very useful tool to examine protein localization in cells and tissues. Since this is performed on fixed cells, we cannot see protein dynamics, and it is not a measure of protein activity. Using western blots to quantify protein expression in the cell is well established. Using both a western blot and mRNA levels to examine protein expression and/or upregulation or downregulation adds a degree of confidence to my results. Western blots reveal protein expression throughout the cell, not whether those proteins are on the cell surface or the cytoplasm. This becomes relevant when analyzing the expression of proteins that exert their function on the surface of the cell such as ACE2. Thus, examining both the expression of the protein (through immunoblots) as well as its location (through immunofluorescence) is valuable in contributing to the strength of my results.

I confirmed ACE2 expression on HUVECs using both immunoblotting and immunofluorescence imaging. This allowed me to conclude that HUVECs do express ACE2 and that ACE2 is on the surface of the cells. While my western blot did show the expected band at ~97kDa that was expected for ACE2, there were many other bands present on the blot. This could be due to a few reasons. It could be possible that with optimizing certain steps of my protocol for the antibody that I used could improve its specificity as well as adjusting the exposure. Since I only did one blot using an antibody we had not previously used for this experiment, I did not have sufficient time for optimization. It is also possible that this is the protein profile of ACE2 in these cells. This could have been confirmed using the proper positive and negative controls. I did rehybridize one of my blots containing a HEK293 sample in an attempt to use this as a negative control, and while HEK293 does not appear to express ACE2, it is difficult to see clearly in this blot. HEK293 cells overexpressing ACE2 would make a good positive control while HEK293 cells lacking ACE2 would make a good negative control.

ELISA was helpful in determining VWF release from endothelial cells, but this technique cannot reveal if this VWF is sufficient to lead to the formation of platelet aggregates. It additionally cannot evaluate VWF deposition onto the cell membrane; therefore, we cannot measure the complete levels of VWF release from endothelial cells using this assay. Perhaps more important than the VWF concentration is the corresponding formation of platelet aggregates that result in clot formation physiologically. This could be measured by exposing endothelial cells to spike protein for a set amount of time, then submitting the cells to flow with heparinized whole blood as was done by Perico *et al.*³³⁰

Wire myography, despite being a robust *in vitro* method to directly measure various agonist effects in resistance arteries, is limited in that it does not account for the effects of blood flow through the vessels and other endogenous mediators that could influence vascular tone. Additionally, the effect of input from nerves and the brain cannot be measured. This setup can only examine agonist-induced responses, which are only part of what can influence vascular tone. Other setups such as the perfused mesenteric bed, in which some preliminary results indicating an increase in perfusion pressure in KO rats compared to WT and HET animals have been found, retain nerve input, but lack the endogenous mediators in the perfusate. Another limitation of this setup in the context of examining the impact of Cx40 KO is that the wire myograph cannot measure conducted responses such as the spread of EDH along endothelial cells and between endothelial cells and smooth muscle cells in which Cx40 is involved.

The limitations on my work emphasize the need for the use multiple experimental setups to paint a cohesive picture of my results. In addition, these limitations can reveal the need for future experiments to properly clarify the preliminary findings of my project and elucidate the

mechanistic link for ACE2-spike protein interactions leading to VWF release as well as the impact of Cx40 in the rat Cx40 KO.

4.4 Future directions

4.4.1 Further investigating the effects of SARS-CoV-2 spike protein exposure on endothelial cells

In order to further elucidate the consequences of SARS-CoV-2 spike protein exposure on endothelial cells and determine if the spike protein interacts with ACE2 on the surface of endothelial cells, more experiments need to be completed. As mentioned in **Section 4.1**, recent work done by Perico *et al* supports my hypothesis.³³⁰ Using their experiments as a guideline and taking into consideration the limitations of the work I have done so far, I propose the following experiments to further this project.

Since we proposed that the spike protein interacts with ACE2, doing a similar time course experiment as I did but with cells treated with both an ACE2 antibody and the spike protein together would reveal whether the antibody is able to attenuate the effects of the spike protein on VWF release into the media. In addition to completing this experiment in HUVECs, it would also be worth doing in endothelial cells of other organs that are affected by SARS-CoV-2 such as lung microvascular endothelial cells, cardiac, brain, liver, and kidney endothelial cells. We should also examine the impact of spike protein exposure on VWF mRNA levels in these cells.

Visualizing spike protein-ACE2 interactions in culture would be vital to confirming this interaction does happen. A fluorescence resonance energy transfer assay could be used to quantify these interactions.

In addition to measuring VWF released in the media, measuring the hemostatic activity and deposition of VWF onto the luminal side of endothelial cells would be valuable. This could

be done by culturing endothelial cells and then using immunofluorescence imaging to quantify VWF deposition on the cells after they have been exposed to the spike protein. In addition, cells could be cultured and exposed to the spike protein then submitted to flow with heparinized blood and platelet aggregation could be quantified using immunofluorescence imaging as well. Using intact vessels under flow conditions (in a culture myograph for example) could be used to determine the effect of spike protein exposure on VWF release and VWF mRNA in these conditions. We could also examine VWF expression in these vessels using immunohistochemistry. This would provide us with information from an *in vivo* system that more closely mimics what is seen physiologically.

Patients who are older and those who have underlying comorbidities experience more severe symptoms and poorer outcomes from infection with SARS-CoV-2. Therefore, examining the effects of spike protein exposure on endothelial cells in aged cells or in hyperglycemic conditions could reveal a greater upregulation and/or VWF released from endothelial cells. Additionally, we should investigate the effects of ACE2 antibody on VWF expression in spike protein exposure in these cells.

Beyond looking at the consequences of spike protein exposure on VWF in endothelial cells, we should also aim to establish a mechanistic link between ACE2-spike protein interactions and VWF expression. Our lab focusses on the transcriptional regulation of the VWF gene, and so determining if there is a role to play by any of the VWF gene promotor suppressors and/or activators is of particular interest to our group.

4.4.2 Further investigating the impact of Cx40 KO in the vasculature

The effects of Cx40 KO in our rat model beyond agonist-induced responses need to be studied. Since mouse Cx40 KO models have reported changes in the expression levels of other

Cxs such as Cx37,^{312,343} we should evaluate our model for the same changes using immunoblotting. Furthermore, we should also perform immunohistochemistry on fixed blood vessels (specifically resistance arteries) to look at Cx localization in both the endothelium and smooth muscle.

Cx40 is thought to be important in the conduction of responses along a vessel length, since previous experiments in Cx40 mouse KO models have demonstrated an impairment in this response.³¹¹⁻³¹⁴ We should also investigate these responses in our model. Beyond resistance arteries, Cxs are involved in renal autoregulation where vascular conducted responses play an important role in the regulation of tubuloglomerular feedback to regulate the diameter of the afferent arteriole and corresponding glomerular filtration rate.³⁴⁴ Møller *et al* have reported reduced vasoconstriction in the afferent arteriole of Cx40 KO mice.³⁴⁵ Therefore, determining the effects of Cx40 KO in kidney vessel responses in our animal model is of interest.

ED is associated with obesity and diabetes among many other disease states. Investigating the role of Cx40 in early endothelial damage that precedes diabetes could reveal if changes in Cx40 contribute to ED. Similar to previous work done by our collaborators, we are investigating the effects of a non-obese hypercaloric model on vascular function.³⁴⁶ This group also reported changes in Cx expression in aortic rings in rats as a result of this diet. Based on these findings, we could investigate the impact of Cx40 KO on the vascular responses of these animals in addition to characterizing the localization and expression of Cxs in this model.

4.5 Conclusions

The endothelium is an important component of the vascular system, and therefore any damage or inappropriate changes to its function can have severe consequences. Studying the effects of SARS-CoV-2 exposure on cultured endothelial cells revealed that the spike protein was able to induce acute VWF release from HUVECs. I also confirmed that ACE2 is expressed in these

cells which in part supports the hypothesis that these changes in VWF expression are due to spike protein-ACE2 interactions. My experiments in Cx40 KO rats revealed that Cx40 is not essential for ACh-induced vasodilation, but differences in PE-induced vasoconstriction between WT and KO animals suggest that Cx40 may play a role in modulating vasoconstriction. In both projects, further studies will be needed to broaden our understanding in these areas of research.

References

1. Pugsley, M. K. & Tabrizchi, R. The vascular system: An overview of structure and function. *Journal of Pharmacological and Toxicological Methods* **44**, 333–340 (2000).
2. Medical gallery of Blausen Medical 2014. *WikiJournal of Medicine* vol. 1 (2014).
3. Bochenek, M. L. & Schäfer, K. Role of endothelial cells in acute and chronic thrombosis. *Hamostaseologie* **39**, 128–139 (2019).
4. Colburn, P. & Buonassisi, V. Anti-clotting activity of endothelial cell cultures and heparan sulfate proteoglycans. *Biochemical and Biophysical Research Communications* **104**, 220–227 (1982).
5. Marcus, A. J. *et al.* The endothelial cell ecto-ADPase responsible for inhibition of platelet function is CD39. *Journal of Clinical Investigation* **99**, 1351–1360 (1997).
6. Moncada, S., Gryglewski, R., Bunting, S. & Vane, J. R. An enzyme isolated from arteries transforms prostaglandin endoperoxides to an unstable substance that inhibits platelet aggregation. *Nature* **263**, 663–665 (1976).
7. Mellion, B. T. *et al.* Evidence for the inhibitory role of guanosine 3', 5'-monophosphate in ADP-induced human platelet aggregation in the presence of nitric oxide and related vasodilators. *Blood* **57**, 946–55 (1981).
8. Radomski, M. W., Palmer, R. M. J. & Moncada, S. Endogenous nitric oxide inhibits human platelet adhesion to vascular endothelium. *The Lancet* **330**, 1057–1058 (1987).
9. Coughlin, S. R. How the protease thrombin talks to cells. *Proceedings of the National Academy of Sciences* **96**, 11023–11027 (1999).
10. Nieuwdorp, M. *et al.* Loss of endothelial glycocalyx during acute hyperglycemia coincides with endothelial dysfunction and coagulation activation *In vivo*. *Diabetes* **55**, 480–486 (2006).
11. Esmon, C. T., Esmon, N. L. & Harris, K. W. Complex formation between thrombin and thrombomodulin inhibits both thrombin-catalyzed fibrin formation and factor V activation. *Journal of Biological Chemistry* **257**, 7944–7947 (1982).
12. Stearns-Kurosawa, D. J., Kurosawa, S., Mollica, J. S., Ferrell, G. L. & Esmon, C. T. The endothelial cell protein C receptor augments protein C activation by the thrombin-thrombomodulin complex. *Proceedings of the National Academy of Sciences* **93**, 10212–10216 (1996).

13. Moore, K. L., Esmon, C. T. & Esmon, N. L. Tumor necrosis factor leads to the internalization and degradation of thrombomodulin from the surface of bovine aortic endothelial cells in culture. *Blood* **73**, 159–65 (1989).
14. Warn-Cramer, B. J., Almus, F. E. & Rapaport, S. I. Studies of the factor Xa-dependent inhibitor of factor VIIa/tissue factor (extrinsic pathway inhibitor) from cell supernates of cultured human umbilical vein endothelial cells. *Thromb Haemost* **61**, 101–5 (1989).
15. Kohno, M. *et al.* Thrombin stimulates the production of immunoreactive endothelin-1 in cultured human umbilical vein endothelial cells. *Metabolism* **39**, 1003–1005 (1990).
16. Sadler, J. E. Biochemistry and genetics of von Willebrand factor. *Annual Review of Biochemistry* **67**, 395–424 (1998).
17. Poredos, P., Poredos, A. V. & Gregoric, I. Endothelial dysfunction and its clinical implications. *Angiology* **72**, 604–615 (2021).
18. Mojiri, A. *et al.* Endothelial cells of different organs exhibit heterogeneity in von Willebrand factor expression in response to hypoxia. *Atherosclerosis* **282**, 1–10 (2019).
19. Lenting, P. J., Christophe, O. D. & Denis, C. v. von Willebrand factor biosynthesis, secretion, and clearance: connecting the far ends. *Blood* **125**, 2019–2028 (2015).
20. Jaffe, E. A., Hoyer, L. W. & Nachman, R. L. Synthesis of von Willebrand factor by cultured human endothelial cells. *Proceedings of the National Academy of Sciences* **71**, 1906–1909 (1974).
21. Sporn, L. A., Chavin, S. I., Marder, V. J. & Wagner, D. D. Biosynthesis of von Willebrand protein by human megakaryocytes. *Journal of Clinical Investigation* **76**, 1102–1106 (1985).
22. Ginsburg, D. *et al.* Human von Willebrand factor (vWF): Isolation of complementary DNA (cDNA) clones and chromosomal localization. *Science (1979)* **228**, 1401–1406 (1985).
23. Collins, C. J. *et al.* Molecular cloning of the human gene for von Willebrand factor and identification of the transcription initiation site. *Proceedings of the National Academy of Sciences* **84**, 4393–4397 (1987).
24. Titani, K. *et al.* Amino acid sequence of human von Willebrand factor. *Biochemistry* **25**, 3171–3184 (1986).
25. Shapiro, S. E. *et al.* The von Willebrand factor predicted unpaired cysteines are essential for secretion. *Journal of Thrombosis and Haemostasis* **12**, 246–254 (2013).
26. Okhota, S., Melnikov, I., Avtaeva, Y., Kozlov, S. & Gabbasov, Z. Shear stress-induced activation of von Willebrand factor and cardiovascular pathology. *International Journal of Molecular Sciences* **21**, 7804 (2020).

27. Voorberg, J., Fontijn, R., van Mourik, J. A. & Pannekoek, H. Domains involved in multimer assembly of von Willebrand factor (vWF): multimerization is independent of dimerization. *The EMBO Journal* **9**, 797–803 (1990).
28. Katsumi, A., Tuley, E. A., Bodó, I. & Sadler, J. E. Localization of disulfide bonds in the cystine knot domain of human von Willebrand factor. *Journal of Biological Chemistry* **275**, 25585–25594 (2000).
29. Canis, K. *et al.* The plasma von Willebrand factor O-glycome comprises a surprising variety of structures including ABH antigens and disialosyl motifs. *Journal of Thrombosis and Haemostasis* **8**, 137–145 (2010).
30. Canis, K. *et al.* Mapping the N-glycome of human von Willebrand factor. *Biochemical Journal* **447**, 217–228 (2012).
31. Matsushita, T., Meyer, D. & Sadler, J. E. Localization of von Willebrand factor-binding sites for platelet glycoprotein Ib and botrocetin by charged-to-alanine scanning mutagenesis. *Journal of Biological Chemistry* **275**, 11044–11049 (2000).
32. Hoylaerts, M. F. *et al.* von Willebrand factor binds to native collagen VI primarily via its A1 domain. *Biochemical Journal* **324**, 185–191 (1997).
33. Lankhof, H. *et al.* Role of the glycoprotein Ib-binding A1 repeat and the RGD sequence in platelet adhesion to human recombinant von Willebrand factor. *Blood* **86**, 1035–42 (1995).
34. Lankhof, H. *et al.* von Willebrand factor without the A2 domain is resistant to proteolysis. *Thromb Haemost* **77**, 1008–13 (1997).
35. Romijn, R. A. *et al.* Mapping the collagen-binding site in the von Willebrand factor-A3 domain. *Journal of Biological Chemistry* **278**, 15035–15039 (2003).
36. Cruz, M. A., Yuan, H., Lee, J. R., Wise, R. J. & Handin, R. I. Interaction of the von Willebrand factor (vWF) with collagen: Localization of the primary collagen-binding site by analysis of recombinant vWF A domain polypeptides. *Journal of Biological Chemistry* **270**, 10822–10827 (1995).
37. Foster, P. A., Fulcher, C. A., Marti, T., Titani, K. & Zimmerman, T. S. A major factor VIII binding domain resides within the amino-terminal 272 amino acid residues of von Willebrand factor. *The Journal of Biological Chemistry* **262**, 8443–6 (1987).
38. Bryckaert, M., Rosa, J.-P., Denis, C. v. & Lenting, P. J. Of von Willebrand factor and platelets. *Cellular and Molecular Life Sciences* **72**, 307–326 (2015).
39. Wagner, D. D., Olmsted, J. B. & Marder, V. J. Immunolocalization of von Willebrand protein in Weibel-Palade bodies of human endothelial cells. *The Journal of Cell Biology* **95**, 355–360 (1982).

40. Stocksclaeder, M., Schneppenheim, R. & Budde, U. Update on von Willebrand factor multimers: Focus on high-molecular-weight multimers and their role in hemostasis. *Blood Coagulation and Fibrinolysis* **25**, 206–216 (2014).
41. Haberichter, S. L. *et al.* Re-establishment of VWF-dependent Weibel-Palade bodies in VWD endothelial cells. *Blood* **105**, 145–152 (2005).
42. Sporn, L. A., Marder, V. J. & Wagner, D. D. Inducible secretion of large, biologically potent von Willebrand factor multimers. *Cell* **46**, 185–190 (1986).
43. Giblin, J. P., Hewlett, L. J. & Hannah, M. J. Basal secretion of von Willebrand factor from human endothelial cells. *Blood* **112**, 957–964 (2008).
44. Romani de Wit, T., Rondaij, M. G., Hordijk, P. L., Voorberg, J. & van Mourik, J. A. Real-Time imaging of the dynamics and secretory behavior of Weibel-Palade bodies. *Arteriosclerosis, Thrombosis, and Vascular Biology* **23**, 755–761 (2003).
45. Alavi, P., Rathod, A. M. & Jahroudi, N. Age-associated increase in thrombogenicity and its correlation with von Willebrand factor. *Journal of Clinical Medicine* **10**, 4190 (2021).
46. Weiss, H. J., Sussman, I. I. & Hoyer, L. W. Stabilization of factor VIII in plasma by the von Willebrand Factor. *Journal of Clinical Investigation* **60**, 390–404 (1977).
47. Nogami, K. *et al.* A novel mechanism of factor VIII protection by von Willebrand factor from activated protein C–catalyzed inactivation. *Blood* **99**, 3993–3998 (2002).
48. Bierings, R. & Voorberg, J. Up or out: polarity of VWF release. *Blood* **128**, 154–155 (2016).
49. Valentijn, K. M. *et al.* Multigranular exocytosis of Weibel-Palade bodies in vascular endothelial cells. *Vascular Biology* **116**, 1807–1816 (2010).
50. Sporn, L., Marder, V. & Wagner, D. von Willebrand factor released from Weibel-Palade bodies binds more avidly to extracellular matrix than that secreted constitutively. *Blood* **69**, 1531–1534 (1987).
51. Federici, A. B. *et al.* Binding of von Willebrand factor to glycoproteins Ib and IIb/IIIa complex: affinity is related to multimeric size. *British Journal of Haematology* **73**, 93–99 (1989).
52. Ribes, J. A., Francis, C. W. & Wagner, D. D. Fibrin induces release of von Willebrand factor from endothelial cells. *Journal of Clinical Investigation* **79**, 117–123 (1987).
53. Hamilton, K. K. & Sims, P. J. Changes in cytosolic Ca²⁺ associated with von Willebrand factor release in human endothelial cells exposed to histamine. Study of microcarrier cell monolayers using the fluorescent probe indo-1. *Journal of Clinical Investigation* **79**, 600–608 (1987).

54. Levine, J., Harlan, J., Harker, L., Joseph, M. & Counts, R. Thrombin-mediated release of factor VIII antigen from human umbilical vein endothelial cells in culture. *Blood* **60**, 531–534 (1982).
55. Hattori, R., Hamilton, K. K., McEver, R. P. & Sims, P. J. Complement proteins C5b-9 induce secretion of high molecular weight multimers of endothelial von Willebrand factor and translocation of granule membrane protein GMP-140 to the cell surface. *Journal of Biological Chemistry* **264**, 9053–9060 (1989).
56. Ruggeri, Z., Mannucci, P., Lombardi, R., Federici, A. & Zimmerman, T. Multimeric composition of factor VIII/von Willebrand factor following administration of DDAVP: Implications for pathophysiology and therapy of von Willebrand's disease subtypes. *Blood* **59**, 1272–1278 (1982).
57. Pinsky, D. J. *et al.* Hypoxia-induced exocytosis of endothelial cell Weibel-Palade bodies. A mechanism for rapid neutrophil recruitment after cardiac preservation. *Journal of Clinical Investigation* **97**, 493–500 (1996).
58. Schneider, S. W. *et al.* Shear-induced unfolding triggers adhesion of von Willebrand factor fibers. *Proceedings of the National Academy of Sciences* **104**, 7899–7903 (2007).
59. Lancellotti, S., Sacco, M., Basso, M. & Cristofaro, R. de. Mechanochemistry of von Willebrand factor. *Biomolecular Concepts* **10**, 194–208 (2019).
60. Ruggeri, Z. M., Orje, J. N., Habermann, R., Federici, A. B. & Reininger, A. J. Activation-independent platelet adhesion and aggregation under elevated shear stress. *Blood* **108**, 1903–1910 (2006).
61. Savage, B., Saldívar, E. & Ruggeri, Z. M. Initiation of platelet adhesion by arrest onto fibrinogen or translocation on von Willebrand factor. *Cell* **84**, 289–297 (1996).
62. Savage, B., Almus-Jacobs, F. & Ruggeri, Z. M. Specific synergy of multiple substrate–receptor interactions in platelet thrombus formation under flow. *Cell* **94**, 657–666 (1998).
63. Nissinen, L. *et al.* Novel $\alpha 2\beta 1$ integrin inhibitors reveal that integrin binding to collagen under shear stress conditions does not require receptor preactivation. *Journal of Biological Chemistry* **287**, 44694–44702 (2012).
64. Fullard, J. The role of the platelet glycoprotein IIb / IIIa in thrombosis and haemostasis. *Current Pharmaceutical Design* **10**, 1567–1576 (2004).
65. Zhang, C., Kelkar, A. & Neelamegham, S. von Willebrand factor self-association is regulated by the shear-dependent unfolding of the A2 domain. *Blood Advances* **3**, 957–968 (2019).

66. Zheng, Y., Chen, J. & López, J. A. Flow-driven assembly of VWF fibres and webs in vitro microvessels. *Nature Communications* **6**, 7858 (2015).
67. Koupenova, M., Kehrel, B. E., Corkrey, H. A. & Freedman, J. E. Thrombosis and platelets: an update. *European Heart Journal* ehw550 (2016) doi:10.1093/eurheartj/ehw550.
68. Furie, B. & Furie, B. C. Mechanisms of thrombus formation. *New England Journal of Medicine* **359**, 938–949 (2008).
69. Zhang, X., Halvorsen, K., Zhang, C.-Z., Wong, W. P. & Springer, T. A. Mechanoenzymatic cleavage of the ultralarge vascular protein von Willebrand factor. *Science (1979)* **324**, 1330–1334 (2009).
70. Skipwith, C. G., Cao, W. & Zheng, X. L. Factor VIII and platelets synergistically accelerate cleavage of von Willebrand factor by ADAMTS13 under fluid shear stress. *Journal of Biological Chemistry* **285**, 28596–28603 (2010).
71. Shim, K., Anderson, P. J., Tuley, E. A., Wiswall, E. & Evan Sadler, J. Platelet-VWF complexes are preferred substrates of ADAMTS13 under fluid shear stress. *Blood* **111**, 651–657 (2008).
72. Cao, W., Krishnaswamy, S., Camire, R. M., Lenting, P. J. & Zheng, X. L. Factor VIII accelerates proteolytic cleavage of von Willebrand factor by ADAMTS13. *Proceedings of the National Academy of Sciences* **105**, 7416–7421 (2008).
73. Leebeek, F. W. G. & Eikenboom, J. C. J. Von Willebrand's Disease. *New England Journal of Medicine* **375**, 2067–2080 (2016).
74. Yadegari, H. & Oldenburg, J. The current understanding of molecular pathogenesis of quantitative von Willebrand disease, types 1 and 3. *Hämostaseologie* **40**, 105–118 (2020).
75. Sadler, J. E. *et al.* Update on the pathophysiology and classification of von Willebrand disease: a report of the Subcommittee on von Willebrand Factor. *Journal of Thrombosis and Haemostasis* **4**, 2103–2114 (2006).
76. Othman, M. Platelet-Type Von Willebrand Disease: A rare, often misdiagnosed and underdiagnosed bleeding disorder. *Seminars in Thrombosis and Hemostasis* **37**, 464–469 (2011).
77. Shahidi, M. Thrombosis and von Willebrand factor. in *Advances in Experimental Medicine and Biology-Advances in Internal Medicine* vol. 1 285–306 (2016).
78. Furlan, M., Robles, R., Solenthaler, M. & Lämmle, B. Acquired deficiency of von Willebrand factor-cleaving protease in a patient with thrombotic thrombocytopenic purpura. *Blood* **91**, 2839–46 (1998).

79. Mari, D. *et al.* Hemostasis abnormalities in patients with vascular dementia and Alzheimer's disease. *Thrombosis and Haemostasis* **75**, 216–8 (1996).
80. de Oliveira, C. O. *et al.* Plasma von Willebrand factor levels correlate with clinical outcome of severe traumatic brain injury. *Journal of Neurotrauma* **24**, 1331–1338 (2007).
81. Ware, L. B., Eisner, M. D., Thompson, B. T., Parsons, P. E. & Matthay, M. A. Significance of Von Willebrand factor in septic and nonseptic patients with acute lung injury. *American Journal of Respiratory and Critical Care Medicine* **170**, 766–772 (2004).
82. van der Vorm, L. N. *et al.* Circulating active von Willebrand factor levels are increased in chronic kidney disease and end-stage renal disease. *Clinical Kidney Journal* **13**, 72–74 (2020).
83. Goshua, G. *et al.* Endotheliopathy in COVID-19-associated coagulopathy: evidence from a single-centre, cross-sectional study. *The Lancet Haematology* **7**, e575–e582 (2020).
84. Lu, R. *et al.* Genomic characterisation and epidemiology of 2019 novel coronavirus: implications for virus origins and receptor binding. *The Lancet* **395**, 565–574 (2020).
85. Jackson, C. B., Farzan, M., Chen, B. & Choe, H. Mechanisms of SARS-CoV-2 entry into cells. *Nature Reviews Molecular Cell Biology* **23**, 3–20 (2022).
86. Shang, J. *et al.* Structural basis of receptor recognition by SARS-CoV-2. *Nature* **581**, 221–224 (2020).
87. Lan, J. *et al.* Structure of the SARS-CoV-2 spike receptor-binding domain bound to the ACE2 receptor. *Nature* **581**, 215–220 (2020).
88. Wang, Q. *et al.* Structural and functional basis of SARS-CoV-2 entry by using human ACE2. *Cell* **181**, 894–904.e9 (2020).
89. Li, W. *et al.* Angiotensin-converting enzyme 2 is a functional receptor for the SARS coronavirus. *Nature* **426**, 450–454 (2003).
90. Hofmann, H. *et al.* Human coronavirus NL63 employs the severe acute respiratory syndrome coronavirus receptor for cellular entry. *Proceedings of the National Academy of Sciences* **102**, 7988–7993 (2005).
91. Delmas, B. & Laude, H. Assembly of coronavirus spike protein into trimers and its role in epitope expression. *Journal of Virology* **64**, 5367–5375 (1990).
92. Hoffmann, M., Kleine-Weber, H. & Pöhlmann, S. A multibasic cleavage site in the spike protein of SARS-CoV-2 is essential for infection of human lung cells. *Molecular Cell* **78**, 779–784.e5 (2020).

93. Zhang, J., Xiao, T., Cai, Y. & Chen, B. Structure of SARS-CoV-2 spike protein. *Current Opinion in Virology* **50**, 173–182 (2021).
94. Glowacka, I. *et al.* Evidence that TMPRSS2 activates the severe acute respiratory syndrome coronavirus spike protein for membrane fusion and reduces viral control by the humoral immune response. *Journal of Virology* **85**, 4122–4134 (2011).
95. Matsuyama, S. *et al.* Efficient activation of the severe acute respiratory syndrome coronavirus spike protein by the transmembrane protease TMPRSS2. *Journal of Virology* **84**, 12658–12664 (2010).
96. Huang, I. C. *et al.* SARS coronavirus, but not human coronavirus NL63, utilizes cathepsin L to infect ACE2-expressing cells. *Journal of Biological Chemistry* **281**, 3198–3203 (2006).
97. Simmons, G. *et al.* Inhibitors of cathepsin L prevent severe acute respiratory syndrome coronavirus entry. *Proceedings of the National Academy of Sciences* **102**, 11876–11881 (2005).
98. Bayati, A., Kumar, R., Francis, V. & McPherson, P. S. SARS-CoV-2 infects cells after viral entry via clathrin-mediated endocytosis. *Journal of Biological Chemistry* **296**, 100306 (2021).
99. Watanabe, Y., Allen, J. D., Wrapp, D., McLellan, J. S. & Crispin, M. Site-specific glycan analysis of the SARS-CoV-2 spike. *Science (1979)* **369**, 330–333 (2020).
100. Cai, Y. *et al.* Distinct conformational states of SARS-CoV-2 spike protein. *Science (1979)* **369**, 1586–1592 (2020).
101. Liu, L. *et al.* Potent neutralizing antibodies against multiple epitopes on SARS-CoV-2 spike. *Nature* **584**, 450–456 (2020).
102. Chi, X. *et al.* A neutralizing human antibody binds to the N-terminal domain of the Spike protein of SARS-CoV-2. *Science (1979)* **369**, 650–655 (2020).
103. Planas, D. *et al.* Reduced sensitivity of SARS-CoV-2 variant Delta to antibody neutralization. *Nature* **596**, (2021).
104. Wang, P. *et al.* Antibody resistance of SARS-CoV-2 variants B.1.351 and B.1.1.7. *Nature* **593**, (2021).
105. Tong, P. *et al.* Memory B cell repertoire for recognition of evolving SARS-CoV-2 spike. *Cell* **184**, 4969–4980.e15 (2021).
106. Zhang, J. *et al.* Structural impact on SARS-CoV-2 spike protein by D614G substitution. *Science (1979)* **372**, 525–530 (2021).

107. Wrapp, D. *et al.* Cryo-EM structure of the 2019-nCoV spike in the prefusion conformation. *Science (1979)* **367**, 1260–1263 (2020).
108. Walls, A. C. *et al.* Tectonic conformational changes of a coronavirus spike glycoprotein promote membrane fusion. *Proceedings of the National Academy of Sciences* **114**, 11157–11162 (2017).
109. Fan, X., Cao, D., Kong, L. & Zhang, X. Cryo-EM analysis of the post-fusion structure of the SARS-CoV spike glycoprotein. *Nature Communications* **11**, 3618 (2020).
110. Tipnis, S. R. *et al.* A human homolog of angiotensin-converting enzyme: Cloning and functional expression as a captopril-insensitive carboxypeptidase. *Journal of Biological Chemistry* **275**, 33238–33243 (2000).
111. Donoghue, M. *et al.* A novel angiotensin-converting enzyme–related carboxypeptidase (ACE2) converts angiotensin I to angiotensin 1-9. *Circulation Research* **87**, (2000).
112. Hamming, I. *et al.* The emerging role of ACE2 in physiology and disease. *Journal of Pathology J Pathol* **212**, 1–11 (2007).
113. Turner, A. J. & Hooper, N. M. The angiotensin–converting enzyme gene family: genomics and pharmacology. *Trends in Pharmacological Sciences* **23**, 177–183 (2002).
114. Renin–Angiotensin–Aldosterone System Inhibitors in Covid-19. *New England Journal of Medicine* **382**, e92 (2020).
115. Rice, G. I., Thomas, D. A., Grant, P. J., Turner, A. J. & Hooper, N. M. Evaluation of angiotensin-converting enzyme (ACE), its homologue ACE2 and neprilysin in angiotensin peptide metabolism. *Biochemical Journal* **383**, 45–51 (2004).
116. Vickers, C. *et al.* Hydrolysis of biological peptides by human angiotensin-converting enzyme-related carboxypeptidase. *Journal of Biological Chemistry* **277**, 14838–14843 (2002).
117. Zhou, T. *et al.* Cryo-EM structures of SARS-CoV-2 spike without and with ACE2 reveal a pH-dependent switch to mediate endosomal positioning of receptor-binding domains. *Cell Host and Microbe* **28**, 867-879.e5 (2020).
118. Hikmet, F. *et al.* The protein expression profile of ACE2 in human tissues. *Molecular Systems Biology* **16**, (2020).
119. Hamming, I. *et al.* Tissue distribution of ACE2 protein, the functional receptor for SARS coronavirus. A first step in understanding SARS pathogenesis. *Journal of Pathology* **203**, 631–637 (2004).

120. Jia, H. P. *et al.* ACE2 receptor expression and severe acute respiratory syndrome coronavirus infection depend on differentiation of human airway epithelia. *Journal of Virology* **79**, 14614–14621 (2005).
121. Ziegler, C. G. K. *et al.* SARS-CoV-2 receptor ACE2 is an interferon-stimulated gene in human airway epithelial cells and is detected in specific cell subsets across tissues. *Cell* **181**, 1016-1035.e19 (2020).
122. Zou, X. *et al.* Single-cell RNA-seq data analysis on the receptor ACE2 expression reveals the potential risk of different human organs vulnerable to 2019-nCoV infection. *Frontiers of Medicine* **14**, 185–192 (2020).
123. Hou, Y. J. *et al.* SARS-CoV-2 reverse genetics reveals a variable infection gradient in the respiratory tract. *Cell* **182**, 429-446.e14 (2020).
124. Ahn, J. H. *et al.* Nasal ciliated cells are primary targets for SARS-CoV-2 replication in the early stage of COVID-19. *Journal of Clinical Investigation* **131**, (2021).
125. Sungnak, W. *et al.* SARS-CoV-2 entry factors are highly expressed in nasal epithelial cells together with innate immune genes. *Nature Medicine* **26**, 681–687 (2020).
126. Wang, Y. *et al.* A comprehensive investigation of the mRNA and protein level of ACE2, the putative receptor of SARS-CoV-2, in human tissues and blood cells. *International Journal of Medical Sciences* **17**, 1522–1531 (2020).
127. Lindner, D. *et al.* Association of cardiac infection with SARS-CoV-2 in confirmed COVID-19 autopsy cases. *JAMA Cardiology* **5**, 1281 (2020).
128. Zhuang, M. *et al.* Increasing host cellular receptor—angiotensin-converting enzyme 2 expression by coronavirus may facilitate 2019-nCoV (or SARS-CoV-2) infection. *Journal of Medical Virology* **92**, 2693–2701 (2020).
129. Smith, J. C. *et al.* Cigarette smoke exposure and inflammatory signaling increase the expression of the SARS-CoV-2 receptor ACE2 in the respiratory Tract. *Developmental Cell* **53**, 514-529.e3 (2020).
130. Vinayagam, S. & Sattu, K. SARS-CoV-2 and coagulation disorders in different organs. *Life Sciences* **260**, 118431 (2020).
131. Klok, F. A. *et al.* Confirmation of the high cumulative incidence of thrombotic complications in critically ill ICU patients with COVID-19: An updated analysis. *Thrombosis Research* **191**, 148–150 (2020).
132. Lodigiani, C. *et al.* Venous and arterial thromboembolic complications in COVID-19 patients admitted to an academic hospital in Milan, Italy. *Thrombosis Research* **191**, 9–14 (2020).

133. Middeldorp, S. *et al.* Incidence of venous thromboembolism in hospitalized patients with COVID-19. *Journal of Thrombosis and Haemostasis* **18**, 1995–2002 (2020).
134. Nahum, J. *et al.* Venous thrombosis among critically ill patients with coronavirus disease 2019 (COVID-19). *JAMA Network Open* **3**, e2010478 (2020).
135. Levi, M., Thachil, J., Iba, T. & Levy, J. H. Coagulation abnormalities and thrombosis in patients with COVID-19. *The Lancet Haematology* **7**, e438–e440 (2020).
136. Wichmann, D. *et al.* Autopsy findings and venous thromboembolism in patients with COVID-19. *Annals of Internal Medicine* **173**, 268–277 (2020).
137. Ackermann, M. *et al.* Pulmonary vascular endothelialitis, thrombosis, and angiogenesis in COVID-19. *New England Journal of Medicine* **383**, 120–128 (2020).
138. Lippi, G. & Favaloro, E. J. D-dimer is associated with severity of coronavirus disease 2019: A pooled Analysis. *Thrombosis and Haemostasis* **120**, 876–878 (2020).
139. Ranucci, M. *et al.* The procoagulant pattern of patients with COVID-19 acute respiratory distress syndrome. *Journal of Thrombosis and Haemostasis* **18**, 1747–1751 (2020).
140. Angelucci, E., Favaloro, E. J., Henry, B. M. & Lippi, G. Von Willebrand factor and ADAMTS13 in COVID-19 and beyond: A question of balance. *EMJ Hematology* **9**, 55–68 (2021).
141. Marchetti, M. *et al.* Endothelium activation markers in severe hospitalized COVID-19 Patients: Role in mortality risk prediction. *Open* **5**, 253–263 (2021).
142. Tang, N., Li, D., Wang, X. & Sun, Z. Abnormal coagulation parameters are associated with poor prognosis in patients with novel coronavirus pneumonia. *Journal of Thrombosis and Haemostasis* **18**, 844–847 (2020).
143. Al-Ani, F., Chehade, S. & Lazo-Langner, A. Thrombosis risk associated with COVID-19 infection. A scoping review. *Thrombosis Research* **192**, 152–160 (2020).
144. Zhou, F. *et al.* Clinical course and risk factors for mortality of adult inpatients with COVID-19 in Wuhan, China: a retrospective cohort study. *The Lancet* **395**, 1054–1062 (2020).
145. Hu, B., Huang, S. & Yin, L. The cytokine storm and COVID-19. *Journal of Medical Virology* **93**, 250–256 (2021).
146. Zuo, Y. *et al.* Neutrophil extracellular traps and thrombosis in COVID-19. *Journal of Thrombosis and Thrombolysis* **51**, 446–453 (2021).
147. Bonaventura, A. *et al.* Endothelial dysfunction and immunothrombosis as key pathogenic mechanisms in COVID-19. *Nature Reviews Immunology* **21**, 319–329 (2021).

148. Libby, P. & Lüscher, T. COVID-19 is, in the end, an endothelial disease. *European Heart Journal* **41**, 3038–3044 (2020).
149. Ward, S. E. *et al.* Von Willebrand factor propeptide in severe coronavirus disease 2019 (COVID-19): evidence of acute and sustained endothelial cell activation. *British Journal of Haematology* **192**, 714–719 (2021).
150. Escher, R., Breakey, N. & Lämmle, B. Severe COVID-19 infection associated with endothelial activation. *Thrombosis Research* **190**, 62 (2020).
151. Sastry, S., Cuomo, F. & Muthusamy, J. COVID-19 and thrombosis: The role of hemodynamics. *Thrombosis Research* **212**, 51–57 (2022).
152. Monteil, V. *et al.* Inhibition of SARS-CoV-2 infections in engineered human tissues using clinical-grade soluble human ACE2. *Cell* **181**, 905-913.e7 (2020).
153. Liu, F. *et al.* SARS-CoV-2 infects endothelial cells in vivo and in vitro. *Frontiers in Cellular and Infection Microbiology* **11**, (2021).
154. Ma, Z., Yang, K. Y., Huang, Y. & Lui, K. O. Endothelial contribution to COVID-19: an update on mechanisms and therapeutic implications. *Journal of Molecular and Cellular Cardiology* **164**, 69–82 (2022).
155. Schimmel, L. *et al.* Endothelial cells are not productively infected by SARS-CoV-2. *Clinical & Translational Immunology* **10**, (2021).
156. Nascimento Conde, J., Schutt, W. R., Gorbunova, E. E. & Mackow, E. R. Recombinant ACE2 expression is required for SARS-CoV-2 to infect primary human endothelial cells and induce inflammatory and procoagulative responses. *mBio* **11**, (2020).
157. Deinhardt-Emmer, S. *et al.* SARS-CoV-2 causes severe epithelial inflammation and barrier dysfunction. *Journal of Virology* **95**, 110–131 (2021).
158. Wang, P. *et al.* A cross-talk between epithelium and endothelium mediates human alveolar–capillary injury during SARS-CoV-2 infection. *Cell Death & Disease* **11**, 1042 (2020).
159. Helms, J. *et al.* High risk of thrombosis in patients with severe SARS-CoV-2 infection: a multicenter prospective cohort study. *Intensive Care Medicine* **46**, 1089–1098 (2020).
160. Goshua, G. *et al.* Endotheliopathy in COVID-19-associated coagulopathy: evidence from a single-centre, cross-sectional study. *The Lancet Haematology* **7**, e575–e582 (2020).
161. Ward, S. E. *et al.* ADAMTS13 regulation of VWF multimer distribution in severe COVID-19. *Journal of Thrombosis and Haemostasis* **19**, 1914–1921 (2021).

162. Mulvany, M. J. & Aalkjaer, C. Structure and function of small arteries. *Physiological Reviews* **70**, 921–961 (1990).
163. Kenner, T. Arterial blood pressure and its measurement. *Basic Research in Cardiology* **83**, 107–121 (1988).
164. Touyz, R. M. *et al.* Vascular smooth muscle contraction in hypertension. *Cardiovascular Research* **114**, 529–539 (2018).
165. Jensen, L. J., Salomonsson, M., Jensen, B. L. & Holstein-Rathlou, N.-H. Depolarization-induced calcium influx in rat mesenteric small arterioles is mediated exclusively via mibefradil-sensitive calcium channels. *British Journal of Pharmacology* **142**, 709–718 (2004).
166. VanBavel, E., Sorop, O., Andreasen, D., Pfaffendorf, M. & Jensen, B. L. Role of T-type calcium channels in myogenic tone of skeletal muscle resistance arteries. *American Journal of Physiology-Heart and Circulatory Physiology* **283**, H2239–H2243 (2002).
167. Braunstein, T. H. *et al.* The role of L- and T-type calcium channels in local and remote calcium responses in rat mesenteric terminal arterioles. *Journal of Vascular Research* **46**, 138–151 (2009).
168. Bean, B. P., Sturek, M., Puga, A. & Hermsmeyer, K. Calcium channels in muscle cells isolated from rat mesenteric arteries: modulation by dihydropyridine drugs. *Circulation Research* **59**, 229–235 (1986).
169. Phan, T. X. *et al.* TRPV1 expressed throughout the arterial circulation regulates vasoconstriction and blood pressure. *The Journal of Physiology* **598**, 5639–5659 (2020).
170. Pórszász, R. *et al.* Capsaicin-induced nonneural vasoconstriction in canine mesenteric arteries. *European Journal of Pharmacology* **441**, 173–175 (2002).
171. Zheng, Y.-M. *et al.* Heterogeneous gene expression and functional activity of ryanodine receptors in resistance and conduit pulmonary as well as mesenteric artery smooth muscle cells. *Journal of Vascular Research* **45**, 469–479 (2008).
172. Kobayashi, S., Kitazawa, T., Somlyo, A. v & Somlyo, A. P. Cytosolic heparin inhibits muscarinic and α -adrenergic Ca^{2+} release in smooth muscle. *Journal of Biological Chemistry* **264**, 17997–18004 (1989).
173. Bao, J. X., Eriksson, I. E. & Stjärne, L. Neurotransmitters and pre- and post-junctional receptors involved in the vasoconstrictor response to sympathetic nerve stimulation in rat tail artery. *Acta Physiologica Scandinavica* **140**, 467–479 (1990).

174. Bradley, E., Law, A., Bell, D. & Johnson, C. D. Effects of varying impulse number on cotransmitter contributions to sympathetic vasoconstriction in rat tail artery. *American Journal of Physiology-Heart and Circulatory Physiology* **284**, H2007–H2014 (2003).
175. Docherty, J. R. The pharmacology of α 1-adrenoceptor subtypes. *European Journal of Pharmacology* **855**, 305–320 (2019).
176. Minneman, K. P. Alpha 1-adrenergic receptor subtypes, inositol phosphates, and sources of cell Ca^{2+} . *Pharmacological Reviews* **40**, 87–119 (1988).
177. Mahoney, J. P. & Sunahara, R. K. Mechanistic insights into GPCR–G protein interactions. *Current Opinion in Structural Biology* **41**, 247–254 (2016).
178. Kobilka, B. K. G protein coupled receptor structure and activation. *Biochimica et Biophysica Acta (BBA) - Biomembranes* **1768**, 794–807 (2007).
179. Hepler, J. R. & Gilman, A. G. G proteins. *Trends in Biochemical Sciences* **17**, 383–387 (1992).
180. Wu, D., Lee, C. H., Rhee, S. G. & Simon, M. I. Activation of phospholipase C by the alpha subunits of the Gq and G11 proteins in transfected Cos-7 cells. *Journal of Biological Chemistry* **267**, 1811–1817 (1992).
181. Tykocki, N. R., Boerman, E. M. & Jackson, W. F. Smooth muscle ion channels and regulation of vascular tone in resistance arteries and arterioles. *Comprehensive Physiology* **7**, 485–581 (2017).
182. Keef, K. D., Hume, J. R. & Zhong, J. Regulation of cardiac and smooth muscle Ca^{2+} channels ($\text{Ca}_v 1.2a,b$) by protein kinases. *American Journal of Physiology-Cell Physiology* **281**, C1743–C1756 (2001).
183. Leprêtre, N., Mironneau, J. & Morel, J. L. Both alpha 1A- and alpha 2A-adrenoreceptor subtypes stimulate voltage-operated L-type calcium channels in rat portal vein myocytes. Evidence for two distinct transduction pathways. *Journal of Biological Chemistry* **269**, 29546–29552 (1994).
184. Mironneau, J. & Macrez-Leprêtre, N. Modulation of Ca^{2+} channels by α 2A- and α 2A-adrenoceptors in vascular myocytes: Involvement of different transduction pathways. *Cellular Signalling* **7**, 471–479 (1995).
185. Povstyan, O. v, Harhun, M. I. & Gordienko, D. v. Ca^{2+} entry following P2X receptor activation induces IP_3 receptor-mediated Ca^{2+} release in myocytes from small renal arteries. *British Journal of Pharmacology* **162**, 1618–1638 (2011).
186. Benham, C. D. & Tsien, R. W. A novel receptor-operated Ca^{2+} -permeable channel activated by ATP in smooth muscle. *Nature* **328**, 275–278 (1987).

187. Gonzalez-Montelongo, M. del C. & Fountain, S. J. Neuropeptide Y facilitates P2X1 receptor-dependent vasoconstriction via Y1 receptor activation in small mesenteric arteries during sympathetic neurogenic responses. *Vascular Pharmacology* **136**, 106810 (2021).
188. Allen, B. G. & Walsh, M. P. The biochemical basis of the regulation of smooth-muscle contraction. *Trends in Biochemical Sciences* **19**, 362–368 (1994).
189. Walsh, M. P. Vascular smooth muscle myosin light chain diphosphorylation: Mechanism, function, and pathological implications. *IUBMB Life* **63**, 987–1000 (2011).
190. Chacko, S., Conti, M. A. & Adelstein, R. S. Effect of phosphorylation of smooth muscle myosin on actin activation and Ca^{2+} regulation. *Proceedings of the National Academy of Sciences* **74**, 129–133 (1977).
191. Ikebe, M. & Hartshorne, D. J. Phosphorylation of smooth muscle myosin at two distinct sites by myosin light chain kinase. *Journal of Biological Chemistry* **260**, 10027–10031 (1985).
192. Weber, L. P., Lierop, J. E. & Walsh, M. P. Ca^{2+} -independent phosphorylation of myosin in rat caudal artery and chicken gizzard myofilaments. *The Journal of Physiology* **516**, 805–824 (1999).
193. Ti Deng, J., van Lierop, J. E., Sutherland, C. & Walsh, M. P. Ca^{2+} -independent smooth muscle contraction: A novel function for integrin-linked kinase. *Journal of Biological Chemistry* **276**, 16365–16373 (2001).
194. Niiro, N. & Ikebe, M. Zipper-interacting protein kinase induces Ca^{2+} -free smooth muscle contraction via myosin light chain phosphorylation. *Journal of Biological Chemistry* **276**, 29567–29574 (2001).
195. Sutherland, C. & Walsh, M. P. Myosin regulatory light chain diphosphorylation slows relaxation of arterial smooth muscle. *Journal of Biological Chemistry* **287**, 24064–24076 (2012).
196. Wu, X., Clack, B. A., Zhi, G., Stull, J. T. & Cremo, C. R. Phosphorylation-dependent structural changes in the regulatory light chain domain of smooth muscle heavy meromyosin. *Journal of Biological Chemistry* **274**, 20328–20335 (1999).
197. Walsh, M. P. Calcium-dependent mechanisms of regulation of smooth muscle contraction. *Biochemistry and Cell Biology* **69**, 771–800 (1991).
198. Butler, T., Paul, J., Europe-Finner, N., Smith, R. & Chan, E.-C. Role of serine-threonine phosphoprotein phosphatases in smooth muscle contractility. *American Journal of Physiology-Cell Physiology* **304**, C485–C504 (2013).

199. Ratz, P. H. & Miner, A. S. Role of protein kinase C ζ and calcium entry in KCl-Induced vascular smooth muscle calcium sensitization and feedback control of cellular calcium levels. *Journal of Pharmacology and Experimental Therapeutics* **328**, 399–408 (2009).
200. Johnson, R. P. *et al.* Ca²⁺ sensitization via phosphorylation of myosin phosphatase targeting subunit at threonine-855 by Rho kinase contributes to the arterial myogenic response. *The Journal of Physiology* **587**, 2537–2553 (2009).
201. Mizutani, T., Kawabata, K., Koyama, Y., Takahashi, M. & Haga, H. Regulation of cellular contractile force in response to mechanical stretch by diphosphorylation of myosin regulatory light chain via RhoA signaling cascade. *Cell Motility and the Cytoskeleton* **66**, 389–397 (2009).
202. Emmert, D. A. *et al.* Rho-kinase-mediated Ca²⁺-independent contraction in rat embryo fibroblasts. *American Journal of Physiology-Cell Physiology* **286**, C8–C21 (2004).
203. Wilson, D. P., Susnjar, M., Kiss, E., Sutherland, C. & Walsh, M. P. Thromboxane A₂-induced contraction of rat caudal arterial smooth muscle involves activation of Ca²⁺ entry and Ca²⁺ sensitization: Rho-associated kinase-mediated phosphorylation of MYPT1 at Thr-855, but not Thr-697. *Biochemical Journal* **389**, 763–774 (2005).
204. Wei, R. Investigation of the functional role of endothelial K_{Ca} channels in regulation of resistance artery diameter. (University of Alberta, 2018).
205. Floyd, R. & Wray, S. Calcium transporters and signalling in smooth muscles. *Cell Calcium* **42**, 467–476 (2007).
206. Vanhoutte, P. M., Shimokawa, H., Feletou, M. & Tang, E. H. C. Endothelial dysfunction and vascular disease - a 30th anniversary update. *Acta Physiologica* **219**, 22–96 (2017).
207. Portilla, D., Morrissey, J. & Morrison, A. R. Bradykinin-activated membrane-associated phospholipase C in Madin-Darby canine kidney cells. *Journal of Clinical Investigation* **81**, 1896–1902 (1988).
208. Gerwins, P. & Fredholm, B. B. Stimulation of adenosine A₁ receptors and bradykinin receptors, which act via different G proteins, synergistically raises inositol 1,4,5-trisphosphate and intracellular free calcium in DDT1 MF-2 smooth muscle cells. *Proceedings of the National Academy of Sciences* **89**, 7330–7334 (1992).
209. Joannides, R. *et al.* Nitric oxide is responsible for flow-dependent dilatation of human peripheral conduit arteries in vivo. *Circulation* **91**, 1314–1319 (1995).
210. Grabowski, E. F., Jaffe, E. A. & Weksler, B. B. Prostacyclin production by cultured endothelial cell monolayers exposed to step increases in shear stress. *The Journal of Laboratory and Clinical Medicine* **105**, 36–43 (1985).

211. Bubolz, A. H. *et al.* Activation of endothelial TRPV4 channels mediates flow-induced dilation in human coronary arterioles: role of Ca²⁺ entry and mitochondrial ROS signaling. *American Journal of Physiology-Heart and Circulatory Physiology* **302**, H634–H642 (2012).
212. Ballermann, B. J., Dardik, A., Eng, E. & Liu, A. Shear stress and the endothelium. *Kidney International* **54**, S100–S108 (1998).
213. Watanabe, H. *et al.* Anandamide and arachidonic acid use epoxyeicosatrienoic acids to activate TRPV4 channels. *Nature* **424**, 434–438 (2003).
214. Mendoza, S. A. *et al.* TRPV4-mediated endothelial Ca²⁺ influx and vasodilation in response to shear stress. *American Journal of Physiology-Heart and Circulatory Physiology* **298**, H466–H476 (2010).
215. Sukumaran, S. v. *et al.* TRPV4 channel activation leads to endothelium-dependent relaxation mediated by nitric oxide and endothelium-derived hyperpolarizing factor in rat pulmonary artery. *Pharmacological Research* **78**, 18–27 (2013).
216. Hellermann, G. R. & Solomonson, L. P. Calmodulin promotes dimerization of the oxygenase domain of human endothelial nitric-oxide synthase. *Journal of Biological Chemistry* **272**, 12030–12034 (1997).
217. Shu, X. *et al.* Endothelial nitric oxide synthase in the microcirculation. *Cellular and Molecular Life Sciences* **72**, 4561–4575 (2015).
218. Forstermann, U. & Sessa, W. C. Nitric oxide synthases: regulation and function. *European Heart Journal* **33**, 829–837 (2012).
219. Crane, B. R. *et al.* Structure of Nitric Oxide Synthase Oxygenase Dimer with Pterin and Substrate. *Science (1979)* **279**, 2121–2126 (1998).
220. Hemmens, B., Goessler, W., Schmidt, K. & Mayer, B. Role of bound zinc in dimer stabilization but not enzyme activity of neuronal nitric-oxide synthase. *Journal of Biological Chemistry* **275**, 35786–35791 (2000).
221. Li, H. *et al.* Crystal structures of zinc-free and -bound heme domain of human inducible nitric-oxide synthase. *Journal of Biological Chemistry* **274**, 21276–21284 (1999).
222. Stuehr, D. J., Cho, H. J., Kwon, N. S., Weise, M. F. & Nathan, C. F. Purification and characterization of the cytokine-induced macrophage nitric oxide synthase: an FAD- and FMN-containing flavoprotein. *Proceedings of the National Academy of Sciences* **88**, 7773–7777 (1991).
223. Marletta, M. A. Nitric oxide synthase structure and mechanism. *Journal of Biological Chemistry* **268**, 12231–12234 (1993).

224. Stuehr, D., Pou, S. & Rosen, G. M. Oxygen reduction by nitric-oxide synthases. *Journal of Biological Chemistry* **276**, 14533–14536 (2001).
225. Aoyagi, M., Arvai, A. S., Tainer, J. A. & Getzoff, E. D. Structural basis for endothelial nitric oxide synthase binding to calmodulin. *EMBO J* **22**, 766–75 (2003).
226. Volkmann, N. *et al.* Holoenzyme structures of endothelial nitric oxide synthase – An allosteric role for calmodulin in pivoting the FMN domain for electron transfer. *Journal of Structural Biology* **188**, 46–54 (2014).
227. Ju, H., Zou, R., Venema, V. J. & Venema, R. C. Direct interaction of endothelial nitric-oxide synthase and caveolin-1 Inhibits synthase activity. *Journal of Biological Chemistry* **272**, 18522–18525 (1997).
228. Dedio, J. *et al.* NOSIP, a novel modulator of endothelial nitric oxide synthase activity. *The FASEB Journal* **15**, 79–89 (2001).
229. Straub, A. C. *et al.* Hemoglobin α /eNOS coupling at myoendothelial junctions is required for nitric oxide scavenging during vasoconstriction. *Arteriosclerosis, Thrombosis, and Vascular Biology* **34**, 2594–2600 (2014).
230. Kondrikov, D. *et al.* β -Actin association with endothelial nitric-oxide synthase modulates nitric oxide and superoxide generation from the enzyme. *Journal of Biological Chemistry* **285**, 4319–4327 (2010).
231. Xu, H. *et al.* A heat shock protein 90 binding domain in endothelial nitric-oxide synthase influences enzyme function. *Journal of Biological Chemistry* **282**, 37567–37574 (2007).
232. Rees, D. D., Palmer, R. M. J., Schulz, R., Hodson, H. F. & Moncada, S. Characterization of three inhibitors of endothelial nitric oxide synthase in vitro and in vivo. *British Journal of Pharmacology* **101**, 746–752 (1990).
233. Moore, P. K., Al-Swayeh, O. A., Chong, N. W. S., Evans, R. A. & Gibson, A. L-NG-nitro arginine (L-NOARG), a novel, L-arginine-reversible inhibitor of endothelium-dependent vasodilatation in vitro. *British Journal of Pharmacology* **99**, 408–412 (1990).
234. Palmer, R. M. J., Ferrige, A. G. & Moncada, S. Nitric oxide release accounts for the biological activity of endothelium-derived relaxing factor. *Nature* **327**, 524–526 (1987).
235. Underbakke, E. S. *et al.* Nitric oxide-induced conformational changes in soluble guanylate cyclase. *Structure* **22**, 602–611 (2014).
236. Denninger, J. W. & Marletta, M. A. Guanylate cyclase and the \cdot NO/cGMP signaling pathway. *Biochimica et Biophysica Acta (BBA) - Bioenergetics* **1411**, 334–350 (1999).

237. Tsai, E. J. & Kass, D. A. Cyclic GMP signaling in cardiovascular pathophysiology and therapeutics. *Pharmacology & Therapeutics* **122**, 216–238 (2009).
238. James, P., Inui, M., Tada, M., Chiesi, M. & Carafoli, E. Nature and site of phospholamban regulation of the Ca²⁺ pump of sarcoplasmic reticulum. *Nature* **342**, 90–92 (1989).
239. Schlossmann, J. *et al.* Regulation of intracellular calcium by a signalling complex of IRAG, IP3 receptor and cGMP kinase I β . *Nature* **404**, 197–201 (2000).
240. Raeymaekers, L., Hofmann, F. & Casteels, R. Cyclic GMP-dependent protein kinase phosphorylates phospholamban in isolated sarcoplasmic reticulum from cardiac and smooth muscle. *Biochemical Journal* **252**, 269–273 (1988).
241. Peng, W., Hoidal, J. R. & Farrukh, I. S. Regulation of Ca²⁺-activated K⁺ channels in pulmonary vascular smooth muscle cells: role of nitric oxide. *Journal of Applied Physiology* **81**, 1264–1272 (1996).
242. Nakamura, M. *et al.* Effects of the phosphorylation of myosin phosphatase by cyclic GMP-dependent protein kinase. *Cellular Signalling* **11**, 671–676 (1999).
243. Edwards, G., Dora, K. A., Gardener, M. J., Garland, C. J. & Weston, A. H. K⁺ is an endothelium-derived hyperpolarizing factor in rat arteries. *Nature* **396**, 269–272 (1998).
244. Brown, B. M., Shim, H., Christophersen, P. & Wulff, H. Pharmacology of small- and intermediate-conductance calcium-activated potassium channels. *Annual Review of Pharmacology and Toxicology* **60**, 219–240 (2020).
245. Xia, X.-M. *et al.* Mechanism of calcium gating in small-conductance calcium-activated potassium channels. *Nature* **395**, 503–507 (1998).
246. Fanger, C. M. *et al.* Calmodulin mediates calcium-dependent activation of the intermediate conductance K_{Ca} Channel, IK_{Ca1}. *Journal of Biological Chemistry* **274**, 5746–5754 (1999).
247. Christophersen, P. & Wulff, H. Pharmacological gating modulation of small- and intermediate-conductance Ca²⁺-activated K⁺ channels (K_{Ca} 2.x and K_{Ca} 3.1). *Channels* **9**, 336–343 (2015).
248. Sandow, S. L., Neylon, C. B., Chen, M. X. & Garland, C. J. Spatial separation of endothelial small- and intermediate-conductance calcium-activated potassium channels (K_{Ca}) and connexins: possible relationship to vasodilator function? *Journal of Anatomy* **209**, 689–698 (2006).
249. Ledoux, J. *et al.* Functional architecture of inositol 1,4,5-trisphosphate signaling in restricted spaces of myoendothelial projections. *Proceedings of the National Academy of Sciences* **105**, 9627–9632 (2008).

250. Saliez, J. *et al.* Role of caveolar compartmentation in endothelium-derived hyperpolarizing factor-mediated relaxation. *Circulation* **117**, 1065–1074 (2008).
251. Tran, C. H. T. *et al.* Endothelial Ca²⁺ wavelets and the induction of myoendothelial feedback. *American Journal of Physiology-Cell Physiology* **302**, C1226–C1242 (2012).
252. Kerr, P. M. *et al.* Activation of endothelial IK_{Ca} channels underlies NO-dependent myoendothelial feedback. *Vascular Pharmacology* **74**, 130–138 (2015).
253. Lamy, C. *et al.* Allosteric block of KCa2 channels by apamin. *Journal of Biological Chemistry* **285**, 27067–27077 (2010).
254. Wulff, H. *et al.* Design of a potent and selective inhibitor of the intermediate-conductance Ca²⁺-activated K⁺ channel, *IKCa1*: A potential immunosuppressant. *Proceedings of the National Academy of Sciences* **97**, 8151–8156 (2000).
255. Kanno, Y. & Loewenstein, W. R. Cell-to-cell passage of large molecules. *Nature* **212**, 629–30 (1966).
256. Sheridan, J. D. Electrophysiological evidence for low-resistance intercellular junctions in the early chick embryo. *Journal of Cell Biology* **37**, 650–659 (1968).
257. Hautefort, A., Pfenniger, A. & Kwak, B. R. Endothelial connexins in vascular function. *Vascular Biology* **1**, H117–H124 (2019).
258. Molica, F., Figueroa, X., Kwak, B., Isakson, B. & Gibbins, J. Connexins and pannexins in vascular function and disease. *International Journal of Molecular Sciences* **19**, 1663 (2018).
259. Laird, D. W. & Lampe, P. D. Therapeutic strategies targeting connexins. *Nature Reviews Drug Discovery* **17**, 905–921 (2018).
260. Molica, F., Meens, M. J. P., Morel, S. & Kwak, B. R. Mutations in cardiovascular connexin genes. *Biology of the Cell* **106**, 269–293 (2014).
261. Söhl, G. & Willecke, K. Gap junctions and the connexin protein family. *Cardiovascular Research* **62**, 228–32 (2004).
262. Koval, M. Pathways and control of connexin oligomerization. *Trends in Cell Biology* **16**, 159–166 (2006).
263. Beyer, E. C. *et al.* Heteromeric mixing of connexins: Compatibility of partners and functional consequences. *Cell Communication and Adhesion* **8**, 199–204 (2001).
264. Jiang, J. X. & Goodenough, D. A. Heteromeric connexons in lens gap junction channels. *Proceedings of the National Academy of Sciences* **93**, 1287–1291 (1996).

265. Stauffer, K. A. The gap junction proteins β 1-connexin (connexin-32) and β 2-connexin (connexin-26) can form heteromeric hemichannels. *Journal of Biological Chemistry* **270**, 6768–6772 (1995).
266. Laird, D. W. Life cycle of connexins in health and disease. *Biochemical Journal* **394**, 527–543 (2006).
267. Veenstra, R. D. *et al.* Selectivity of connexin-specific gap junctions does not correlate with channel conductance. *Circulation Research* **77**, 1156–1165 (1995).
268. Elfgang, C. *et al.* Specific permeability and selective formation of gap junction channels in connexin-transfected HeLa cells. *The Journal of Cell Biology* **129**, 805–17 (1995).
269. Bai, D., Yue, B. & Aoyama, H. Crucial motifs and residues in the extracellular loops influence the formation and specificity of connexin docking. *Biochimica et Biophysica Acta (BBA) - Biomembranes* **1860**, 9–21 (2018).
270. Harris, A. L. Connexin channel permeability to cytoplasmic molecules. *Progress in Biophysics and Molecular Biology* **94**, 120–143 (2007).
271. Barrio, L. C. *et al.* Gap junctions formed by connexins 26 and 32 alone and in combination are differently affected by applied voltage. *Proceedings of the National Academy of Sciences* **88**, 8410–8414 (1991).
272. Bevans, C. G., Kordel, M., Rhee, S. K. & Harris, A. L. Isoform composition of connexin channels determines selectivity among second messengers and uncharged molecules. *Journal of Biological Chemistry* **273**, 2808–2816 (1998).
273. Solan, J. L. & Lampe, P. D. Spatio-temporal regulation of connexin43 phosphorylation and gap junction dynamics. *Biochimica et Biophysica Acta (BBA) - Biomembranes* **1860**, 83–90 (2018).
274. Gaietta, G. *et al.* Multicolor and electron microscopic imaging of connexin trafficking. *Science (1979)* **296**, 503–507 (2002).
275. Wu, J.-I. & Wang, L.-H. Emerging roles of gap junction proteins connexins in cancer metastasis, chemoresistance and clinical application. *Journal of Biomedical Science* **26**, 8 (2019).
276. Pogoda, K., Kameritsch, P., Mannell, H. & Pohl, U. Connexins in the control of vasomotor function. *Acta Physiologica* **225**, e13108 (2019).
277. Retamal, M. A. *et al.* Extracellular cysteine in connexins: Role as redox sensors. *Frontiers in Physiology* **7**, 1 (2016).

278. Oshima, A., Tani, K., Hiroaki, Y., Fujiyoshi, Y. & Sosinsky, G. E. Projection structure of a N-terminal deletion mutant of connexin 26 channel with decreased central pore density. *Cell Communication & Adhesion* **15**, 85–93 (2008).
279. Oh, S., Verselis, V. K. & Bargiello, T. A. Charges dispersed over the permeation pathway determine the charge selectivity and conductance of a Cx32 chimeric hemichannel. *The Journal of Physiology* **586**, 2445–2461 (2008).
280. Harris, A. L. Emerging issues of connexin channels: biophysics fills the gap. *Quarterly Reviews of Biophysics* **34**, 325–472 (2001).
281. Kyle, J. W. *et al.* An intact connexin N-terminus is required for function but not gap junction formation. *Journal of Cell Science* **121**, 2744–2750 (2008).
282. Xu, Q. *et al.* Gating of connexin 43 gap junctions by a cytoplasmic loop calmodulin binding domain. *American Journal of Physiology-Cell Physiology* **302**, C1548–C1556 (2012).
283. Mitropoulou, G. & Bruzzone, R. Modulation of perch connexin35 hemi-channels by cyclic AMP requires a protein kinase A phosphorylation site. *Journal of Neuroscience Research* **72**, 147–157 (2003).
284. Johnstone, S. R., Billaud, M., Lohman, A. W., Taddeo, E. P. & Isakson, B. E. Posttranslational modifications in connexins and pannexins. *The Journal of Membrane Biology* **245**, 319–332 (2012).
285. Spagnol, G. *et al.* Secondary structural analysis of the carboxyl-terminal domain from different connexin isoforms. *Biopolymers* **105**, 143–162 (2016).
286. Moreno, A. P., Sáez, J. C., Fishman, G. I. & Spray, D. C. Human connexin43 gap junction channels. Regulation of unitary conductances by phosphorylation. *Circulation Research* **74**, 1050–1057 (1994).
287. Straub, A. C. *et al.* Site-specific connexin phosphorylation is associated with reduced heterocellular communication between smooth muscle and endothelium. *Journal of Vascular Research* **47**, 277–286 (2010).
288. Cottrell, G. T., Lin, R., Warn-Cramer, B. J., Lau, A. F. & Burt, J. M. Mechanism of v-Src- and mitogen-activated protein kinase-induced reduction of gap junction communication. *American Journal of Physiology-Cell Physiology* **284**, C511–C520 (2003).
289. Solan, J. L. & Lampe, P. D. Connexin43 in LA-25 cells with active v-src is phosphorylated on Y247, Y265, S262, S279/282, and S368 via multiple signaling pathways. *Cell Communication & Adhesion* **15**, 75–84 (2008).
290. Solan, J. L. & Lampe, P. D. Connexin43 phosphorylation: structural changes and biological effects. *Biochemical Journal* **419**, 261–272 (2009).

291. Retamal, M. A., Cortés, C. J., Reuss, L., Bennett, M. V. L. & Sáez, J. C. S-nitrosylation and permeation through connexin 43 hemichannels in astrocytes: Induction by oxidant stress and reversal by reducing agents. *Proceedings of the National Academy of Sciences* **103**, 4475–4480 (2006).
292. Straub, A. C. *et al.* Compartmentalized connexin 43 S-nitrosylation/denitrosylation regulates heterocellular communication in the vessel wall. *Arteriosclerosis, Thrombosis, and Vascular Biology* **31**, 399–407 (2011).
293. Colussi, C. *et al.* N^ε-lysine acetylation determines dissociation from GAP junctions and lateralization of connexin 43 in normal and dystrophic heart. *Proceedings of the National Academy of Sciences* **108**, 2795–2800 (2011).
294. D'hondt, C. *et al.* Regulation of connexin- and pannexin-based channels by post-translational modifications. *Biology of the Cell* **105**, 373–398 (2013).
295. Laing, J. G. & Beyer, E. C. The gap junction protein connexin43 is degraded via the ubiquitin proteasome pathway. *Journal of Biological Chemistry* **270**, 26399–26403 (1995).
296. Jacobsen, N. L. *et al.* Regulation of Cx37 channel and growth suppressive properties by phosphorylation. *Journal of Cell Science* (2017) doi:10.1242/jcs.202572.
297. Dukic, A. R. *et al.* A protein kinase A-ezrin complex regulates connexin 43 gap junction communication in liver epithelial cells. *Cellular Signalling* **32**, 1–11 (2017).
298. Thévenin, A. F., Margraf, R. A., Fisher, C. G., Kells-Andrews, R. M. & Falk, M. M. Phosphorylation regulates connexin43/ZO-1 binding and release, an important step in gap junction turnover. *Molecular Biology of the Cell* **28**, 3595–3608 (2017).
299. Ek-Vitorin, J. F., King, T. J., Heyman, N. S., Lampe, P. D. & Burt, J. M. Selectivity of connexin 43 channels is regulated through protein kinase C-dependent phosphorylation. *Circulation Research* **98**, 1498–1505 (2006).
300. Park, D. J. *et al.* Akt phosphorylates connexin43 on Ser373, a “mode-1” binding site for 14-3-3. *Cell Communication & Adhesion* **14**, 211–226 (2007).
301. Kwak, B. R., Mulhaupt, F., Veillard, N., Gros, D. B. & Mach, F. Altered pattern of vascular connexin expression in atherosclerotic plaques. *Arteriosclerosis, Thrombosis, and Vascular Biology* **22**, 225–230 (2002).
302. Yeh, H. *et al.* Reduced expression of endothelial connexins 43 and 37 in hypertensive rats is rectified after 7-day carvedilol treatment. *American Journal of Hypertension* **19**, 129–135 (2006).

303. Hakim, C. H., Jackson, W. F. & Segal, S. S. Connexin isoform expression in smooth muscle cells and endothelial cells of hamster cheek pouch arterioles and retractor feed arteries. *Microcirculation* **15**, 503–514 (2008).
304. Severs, N. J. *et al.* Immunocytochemical analysis of connexin expression in the healthy and diseased cardiovascular system. *Microscopy Research and Technique* **52**, 301–322 (2001).
305. Pogoda, K. & Kameritsch, P. Molecular regulation of myoendothelial gap junctions. *Current Opinion in Pharmacology* **45**, 16–22 (2019).
306. Matchkov, V. v. *et al.* Analysis of effects of connexin-mimetic peptides in rat mesenteric small arteries. *American Journal of Physiology-Heart and Circulatory Physiology* **291**, H357–H367 (2006).
307. Boettcher, M. & de Wit, C. Distinct endothelium-derived hyperpolarizing factors emerge in vitro and in vivo and are mediated in part via connexin 40–dependent myoendothelial coupling. *Hypertension* **57**, 802–808 (2011).
308. Figueroa, X. F., Lillo, M. A., Gaete, P. S., Riquelme, M. A. & Sáez, J. C. Diffusion of nitric oxide across cell membranes of the vascular wall requires specific connexin-based channels. *Neuropharmacology* **75**, 471–478 (2013).
309. de Wit, C. & Griffith, T. M. Connexins and gap junctions in the EDHF phenomenon and conducted vasomotor responses. *Pflügers Archiv - European Journal of Physiology* **459**, 897–914 (2010).
310. de Wit, C., Roos, F., Bolz, S.-S. & Pohl, U. Lack of vascular connexin 40 is associated with hypertension and irregular arteriolar vasomotion. *Physiological Genomics* **13**, 169–177 (2003).
311. de Wit, C. *et al.* Impaired conduction of vasodilation along arterioles in connexin40-deficient mice. *Circulation Research* **86**, 649–655 (2000).
312. Jobs, A. *et al.* Defective Cx40 maintains Cx37 expression but intact Cx40 is crucial for conducted dilations irrespective of hypertension. *Hypertension* **60**, 1422–1429 (2012).
313. Figueroa, X. F. & Duling, B. R. Dissection of two Cx37-independent conducted vasodilator mechanisms by deletion of Cx40: electrotonic versus regenerative conduction. *American Journal of Physiology-Heart and Circulatory Physiology* **295**, H2001–H2007 (2008).
314. Wölfle, S. E. *et al.* Connexin45 cannot replace the function of connexin40 in conducting endothelium-dependent dilations along arterioles. *Circulation Research* **101**, 1292–1299 (2007).

315. Rummery, N. M., McKenzie, K. U. S., Whitworth, J. A. & Hill, C. E. Decreased endothelial size and connexin expression in rat caudal arteries during hypertension. *Journal of Hypertension* **20**, 247–253 (2002).
316. Brisset, A. C., Isakson, B. E. & Kwak, B. R. Connexins in vascular physiology and pathology. *Antioxidants & Redox Signaling* **11**, 267–282 (2009).
317. Polacek, D., Bech, F., McKinsey, J. F. & Davies, P. F. Connexin43 gene expression in the rabbit arterial wall: Effects of hypercholesterolemia, balloon injury and their combination. *Journal of Vascular Research* **34**, 19–30 (1997).
318. Blackburn, J. P. *et al.* Upregulation of connexin43 gap junctions during early stages of human coronary atherosclerosis. *Arteriosclerosis, Thrombosis, and Vascular Biology* **15**, 1219–1228 (1995).
319. DePaola, N. *et al.* Spatial and temporal regulation of gap junction connexin43 in vascular endothelial cells exposed to controlled disturbed flows *in vitro*. *Proceedings of the National Academy of Sciences* **96**, 3154–3159 (1999).
320. Gabriels, J. E. & Paul, D. L. Connexin43 is highly localized to sites of disturbed flow in rat aortic endothelium but connexin37 and connexin40 are more uniformly distributed. *Circulation Research* **83**, 636–643 (1998).
321. Ebong, E. E., Kim, S. & DePaola, N. Flow regulates intercellular communication in HAEC by assembling functional Cx40 and Cx37 gap junctional channels. *American Journal of Physiology-Heart and Circulatory Physiology* **290**, H2015–H2023 (2006).
322. Vorderwülbecke, B. J. *et al.* Regulation of endothelial connexin40 expression by shear stress. *Am J Physiol Heart Circ Physiol* **302**, 143–152 (2012).
323. Grundy, D. Principles and standards for reporting animal experiments in The Journal of Physiology and Experimental Physiology. *Experimental Physiology* **100**, 755–758 (2015).
324. Haile, Y. *et al.* Reprogramming of HUVECs into induced pluripotent stem cells (HiPSCs), generation and characterization of HiPSC-derived neurons and astrocytes. *PLOS ONE* **10**, e0119617 (2015).
325. Buzhdygan, T. P. *et al.* The SARS-CoV-2 spike protein alters barrier function in 2D static and 3D microfluidic in-vitro models of the human blood–brain barrier. *Neurobiology of Disease* **146**, (2020).
326. Raghavan, S., Kenchappa, D. B. & Leo, M. D. SARS-CoV-2 spike protein induces degradation of junctional proteins that maintain endothelial barrier integrity. *Frontiers in Cardiovascular Medicine* **8**, (2021).

327. Jilma, B. *et al.* Effects of desmopressin on circulating P-selectin. *British Journal of Haematology* **93**, 432–436 (1996).
328. Varga, Z. *et al.* Endothelial cell infection and endotheliitis in COVID-19. *The Lancet* **395**, 1417–1418 (2020).
329. Mojiri, A. *et al.* Hypoxia results in upregulation and de novo activation of von Willebrand factor expression in lung endothelial cells. *Arteriosclerosis, Thrombosis, and Vascular Biology* **33**, 1329–1338 (2013).
330. Perico, L. *et al.* SARS-CoV-2 spike protein 1 activates microvascular endothelial cells and complement system leading to platelet aggregation. *Frontiers in Immunology* **13**, (2022).
331. Birch, K. A., Pober, J. S., Zavoico, G. B., Means, A. R. & Ewenstein, B. M. Calcium/calmodulin transduces thrombin-stimulated secretion: studies in intact and minimally permeabilized human umbilical vein endothelial cells. *Journal of Cell Biology* **118**, 1501–1510 (1992).
332. Kaufmann, J. E. *et al.* Vasopressin-induced von Willebrand factor secretion from endothelial cells involves V2 receptors and cAMP. *Journal of Clinical Investigation* **106**, 107–116 (2000).
333. Vischer, U. M., Lang, U. & Wollheim, C. B. Autocrine regulation of endothelial exocytosis: von Willebrand factor release is induced by prostacyclin in cultured endothelial cells. *FEBS Letters* **424**, 211–215 (1998).
334. Vischer, U. M. & Wollheim, C. B. Purine nucleotides induce regulated secretion of von Willebrand factor: involvement of cytosolic Ca²⁺ and cyclic adenosine monophosphate-dependent signaling in endothelial exocytosis. *Blood* **91**, 118–27 (1998).
335. Bigdelou, B. *et al.* COVID-19 and preexisting comorbidities: Risks, synergies, and clinical outcomes. *Frontiers in Immunology* **13**, (2022).
336. Wilson, C., Lee, M. D. & Mccarron, J. G. Acetylcholine released by endothelial cells facilitates flow-mediated dilatation. *The Journal of Physiology* **594**, 7267–7307 (2016).
337. Bennett, J. A. *et al.* Acetylcholine inhibits platelet activation. *Journal of Pharmacology and Experimental Therapeutics* **369**, 182–187 (2019).
338. Alonso, F., Boittin, F.-X., Bény, J.-L. & Haefliger, J.-A. Loss of connexin40 is associated with decreased endothelium-dependent relaxations and eNOS levels in the mouse aorta. *Am J Physiol Heart Circ Physiol* **299**, 1365–1373 (2010).
339. Verselis, V. K. & Srinivas, M. Connexin channel modulators and their mechanisms of action. *Neuropharmacology* **75**, 517–524 (2013).

340. Lemmey, H. A. L., Garland, C. J. & Dora, K. A. Intrinsic regulation of microvascular tone by myoendothelial feedback circuits. in *Current Topics in Membranes* vol. 85 327–355 (Academic Press, 2020).
341. Gifre-Renom, L., Daems, M., Luttun, A. & Jones, E. A. V. Organ-specific endothelial cell differentiation and impact of microenvironmental cues on endothelial heterogeneity. *International Journal of Molecular Sciences* **23**, (2022).
342. Liu, Y., Beyer, A. & Aebersold, R. On the dependency of cellular protein levels on mRNA abundance. *Cell* **165**, 535–550 (2016).
343. Simon, A. M. & McWhorter, A. R. Decreased intercellular dye-transfer and downregulation of non-ablated connexins in aortic endothelium deficient in connexin37 or connexin40. *Journal of Cell Science* **116**, 2223–2236 (2003).
344. Carlström, M., Wilcox, C. S. & Arendshorst, W. J. Renal autoregulation in health and disease. *Physiological Reviews* **95**, 405–511 (2015).
345. Møller, S., Jacobsen, J. C. B., Holstein-Rathlou, N. H. & Sorensen, C. M. Lack of connexins 40 and 45 reduces local and conducted vasoconstrictor responses in the murine afferent arterioles. *Frontiers in Physiology* **11**, (2020).
346. Alaaeddine, R. *et al.* Impaired endothelium-dependent hyperpolarization underlies endothelial dysfunction during early metabolic challenge: Increased ROS generation and possible interference with NO function. *Journal of Pharmacology and Experimental Therapeutics* **371**, 567–582 (2019).